LUND UNIVERSITY

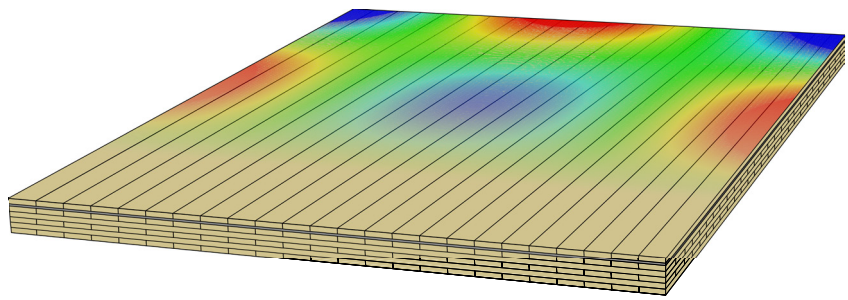

IMPROVING VIBRATION PERFORMANCE OF CROSS-LAMINATED TIMBER PANELS
A computational investigation

ANNIE BOHMAN

Structural Mechanics

Licentiate Dissertation

DEPARTMENT OF CONSTRUCTION SCIENCES
DIVISION OF STRUCTURAL MECHANICS

ISRN LUTVDG/TVSM--26/3084--SE (1-88) | ISSN 0281-6679
ISBN 978-91-8104-945-9 (Print) | 978-91-8104-946-6 (Pdf)
LICENTIATE DISSERTATION

IMPROVING VIBRATION PERFORMANCE OF CROSS-LAMINATED TIMBER PANELS

A computational investigation

ANNIE BOHMAN

Printed by V-husets tryckeri LTH, Lund, Sweden, March 2026 *(Pl)*.

For information, address:
Div. of Structural Mechanics,
Faculty of Engineering LTH, Lund University, Box 118, SE-221 00 Lund, Sweden.
Homepage: www.byggmek.lth.se

Acknowledgements

The work presented in this dissertation has been carried out at the Division of Structural Mechanics at Lund University.

I would like to thank my main supervisor Dr. Peter Persson, and co-supervisors Prof. Kent Persson and Dr. Linus Andersson for their support and guidance over the course of the project. I would also like to thank Prof. Fredrik Ljunggren at Luleå University of Technology for sharing experimental data and giving a perspective from the acoustical side. Additionally, I would like to thank the rest of my colleagues at the Division of Structural Mechanics for creating an inspiring workplace.

Last but not least, I would like to thank my family and friends, especially my parents, Anette and Tony, and my sister, Tilda for their continued support during my life.

Lund, March 2026
Annie Bohman

Abstract

Construction with timber is becoming increasingly popular. Using timber for construction can be more environmentally friendly compared to the more conventional reinforced concrete, and since the emittance of carbon dioxide from the construction sector needs to be reduced, utilising more timber can be part of a possible solution.

The development of mass timber products such as cross-laminated timber (CLT) has contributed to the increased attractiveness of timber construction. CLT panels are typically constructed of 3, 5 or 7 spruce layers, oriented perpendicularly to its adjacent layers. CLT panels can be used for various structural elements, such as floors or walls. The crosswise orientation of the layers contributes to a high in-plane stiffness and strength. This, in turn, makes CLT panels suitable for e.g. long-span floors or walls regarding static loading.

From a structural dynamic perspective, the combination of low mass (compared to concrete and steel) and high stiffness can lead to challenges regarding vibrations and sound propagation, especially in the low-frequency range. This, in turn, affects occupants of timber buildings. Commonly reported annoyances are disturbing sound and vibrations from neighbours walking and talking. Sound and vibrations can be propagated in two main ways in buildings: direct transmission through a separating element such as a wall, or by flanking transmission, where vibrations can propagate through the structure, and hence cause problems with disturbing vibrations and sounds in rooms far away from the source. For reducing flanking transmissions in timber buildings, elastomers are commonly introduced in junctions between structural elements.

To mitigate disturbing vibrations and sound propagation in timber buildings, commonly add-on solutions such as floating floors or suspended ceilings are built to create an acoustically insulating space that separates the CLT panels from the non-loadbearing parts. Additionally, it is common to increase the mass of the panels by adding e.g. concrete (which also increases the stiffness).

The aim of the dissertation is to analyse how the vibration response of CLT panels can be mitigated by modifying the panels themselves, and hence reducing the need for add-ons. For the investigations, finite element models were utilised, and

frequency response functions were evaluated using free–free displacement boundary conditions. Timber and elastomer material properties were calibrated and verified using experimental data.

For the studies, two main methods of panel modification have been analysed. Firstly, by exchanging the timber lamination material in the CLT panel from the typical spruce to the denser and stiffer birch, oak or compressed spruce, or by integrating concrete layers or lamellae into the panel. Secondly, by integrating an elastomer layer into the CLT panel, hence adding significant energy dissipation to the panel. Both investigated methods showed significant potential.

By changing from spruce to a heavier and stiffer timber lamination material, mobility root mean square (RMS) values in the range of 70–50% of the mobility RMS value of a reference spruce panel can be reached. By integrating a concrete layer corresponding to 6% of the panel volume into a spruce CLT panel, a mobility RMS value of approximately 80% of the mobility RMS value of a reference spruce panel can be reached. Additionally, by integrating an elastomer layer of the same dimensions as the concrete layer, a mobility RMS value of approximately 80% of the mobility RMS value of the reference panel can be reached. Furthermore, by combining the effect of changing timber lamination material with the integration of concrete or elastomer into the CLT panel, reductions of mobility RMS values in the range of 60–50% compared to the mobility RMS value of a spruce panel can be reached by using a concrete or elastomer layer.

Contents

Paper A
Vibration reduction in cross-laminated timber panels by using individual concrete lamellae.
Khuong An Ung, Annie Bohman, Linus Andersson, Peter Persson, Sam Johansson and Lars Vabbersgaard Andersen.
In proceedings of SEMC 2025, 9:th International Conference on Structural Engineering, Mechanics and Computation, Cape Town, South Africa, 2025.

Paper B
Vibration reduction in cross-laminated timber panels by using integrated elastomer layers.
Annie Bohman, Linus Andersson, Kent Persson and Peter Persson.
In proceedings of SEMC 2025, 9:th International Conference on Structural Engineering, Mechanics and Computation, Cape Town, South Africa, 2025.

Paper C
Vibration reduction in cross-laminated timber panels using various lamination materials and integrated elastomer layers.
Annie Bohman, Linus Andersson, Kent Persson, Fredrik Ljunggren and Peter Persson.
Journal of Building Engineering, Volume 118, 2026, 115037.

Part I

Introduction and overview

1 Introduction

In recent times, construction with timber has become increasingly popular. Construction using timber can have many benefits, e.g. less environmental impact, less energy usage, less water usage and a more time-efficient construction process compared to conventional construction [1]. Mass timber, such as cross-laminated timber (CLT) [2] has arisen as an alternative construction material to reinforced concrete for multi-storey buildings. CLT panels are built up by an odd number of layers, most commonly 3, 5 or 7 layers. These are glued together perpendicularly to the adjacent layers, see Figure 1.1. CLT panels are produced in factories, with a high degree of prefabrication – e.g., with openings for doors, windows, and installations – and can then be transported to the construction site for assembly. CLT panels are suitable as structural elements for both floors and walls.

However, constructing buildings using lightweight materials, such as timber, also has its drawbacks. Challenges regarding disturbing vibrations and noise for occupants of the buildings can arise. These challenges can be caused by e.g. walking, talking and vibrating machines from inside the building, or road- and railway traffic from outside the building.

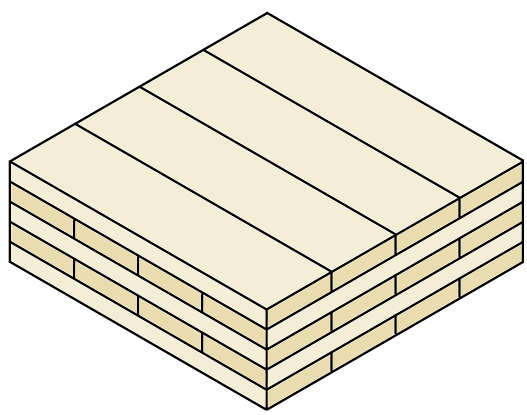

Figure 1.1: A schematic of a five-layer CLT panel.

Hence, to reduce problems regarding vibrations and sound radiation in CLT panels, the design of the panels themselves could be improved. To evaluate how different design choices of affects the dynamic response, measurements can be conducted. However, conducting measurements are time consuming and expensive. Hence, another way of evaluating the design choices is using numerical models, calibrated to measured data. For this purpose, the finite element (FE) method can be utilised.

1.1 AIM OF RESEARCH

The overarching aim is to mitigate disturbing vibrations and noise in order to improve the comfort of occupants of timber buildings. In turn, this could reduce the need for add-on solutions and enable longer spans. Specifically, focus is on CLT floor and wall panels, and how the panels themselves can be modified to mitigate vibrations and noise radiation. The impact on vibration levels in CLT panels was evaluated for two design modification methods. Firstly, by making the panel denser and stiffer, by changing the typical spruce to birch, oak or compressed spruce, or by integrating concrete into the panel. Secondly, by adding more energy dissipation to the panel by integrating an elastomer layer. The effect on vibration levels by modifying the panels was evaluated numerically using FE modelling.

1.2 OUTLINE

The dissertation is divided into two parts.

Part I consists of an introduction and overview, organised into seven chapters. In Chapter 2, timber buildings and their problems regarding vibrations and sound radiation are presented. In Chapter 3, governing theory on structural dynamics and FE modelling is introduced. In Chapter 4, methods to calibrate numerical models to measured data are presented. In Chapter 5, strategies on how to mitigate vibrations in timber panels by panel modification are presented. Chapter 6 consists of summaries of the appended papers and author contributions. Lastly, Chapter 7 contains the concluding remarks of the dissertation.

Part II includes three appended papers. In Paper A, the effect on the vibration levels by exchanging certain lamellae in a CLT panel with concrete was investigated. In Paper B, CLT panels of spruce, oak and a combination of the two – both with and without an integrated elastomer layer – were analysed with respect to vibration levels. In Paper C, numerical models were calibrated to measurements, and vibration levels were evaluated for CLT panels made of spruce, birch and compressed spruce, both with and without an elastomer layer.

2 Vibrations in CLT panels

In present times, when greenhouse gas emissions need to be reduced, research has shown that the building sector (including both construction and operation) accounted for 34% of global carbon dioxide emissions in year 2023 [3]. Thus, the emissions from the building industry need to be reduced. Studies have shown that compared to reinforced concrete, timber can be a more environmentally friendly material [4–6]. Trees bind carbon dioxide when they grow, which remains after the trees are cut and made into structural timber, leading to a potential environmental benefit when the timber is used to construct buildings [7,8]. Hence, increased usage of timber can be part of a solution to reducing emissions.

2.1 STRUCTURAL TIMBER

Approximately 70% of Sweden's land area is covered by forest. The most common tree species are pine and spruce, followed by birch, with 40%, 39% and 13% of the total growing stock, respectively [9]. Moreover, 35% of Europe was reported to be covered by forest in 2020, with the most common tree species being pine, spruce, beech and oak, with 30%, 23%, 12% and 10% of the total growing stock, respectively [10]. Trees can be divided into softwoods and hardwoods. Examples of softwoods are spruce and pine, and examples of hardwoods are birch, oak and beech.

Trees adapt to the climate in which they grow, causing the material properties to vary depending on fibre direction. For wood, three directions can be identified; the longitudinal (L) direction which is parallel with the fibre direction, the radial (R) direction which is perpendicular to the growth rings and the transversal (T) direction which is parallel with the growth rings.

To increase the mechanical properties of lower quality timber, and hence make it more attractive for construction, lamellae can be densified. Densification is often conducted as a combination of heat, moisture and pressure, in the radial direction of the lamellae [11,12]. Compression of wood can be divided into bulk densification

and surface densification, where bulk densification means that the whole lamellae is densified, and surface densification indicates that one or more surfaces are densified, thus leading to a less time-consuming process, and less reduced wood volume [12].

Wood has been used for construction for a very long time [13]. However, in Sweden, severe fire incidents led to a ban on construction of timber buildings of more than two storeys in year 1874. This ban was lifted in tear 1994, and from then on, construction of multi-storey timber buildings has rapidly increased in Sweden, with roughly 37 000 apartments in timber buildings existing in year 2023 [14]. Of the total amount of apartments in multi-storey buildings constructed in year 2024, 17% were constructed using mainly timber [15]. In analysing buildings of all sizes, the share of timber construction was for example 80% in Canada, 70% in Scandinavia, 65% in USA, 50% in Germany, 45% in Austria and 40% in England in year 2020 [13].

Regarding timber construction, CLT has become a competitive alternative to the more commonly used reinforced concrete. Typically, CLT is produced using strength class graded softwoods, such as spruce, in Sweden. However, also hardwoods and compressed timber have been investigated for use for CLT panels, see [16–19] and [20, 21], respectively. Various combinations of lamination materials have also been evaluated in [22].

CLT has high in-plane stiffness and strength, making it beneficial for loadbearing walls and long-span floors considering static loading. However, from a structural dynamic perspective, the combination of the low mass (in comparison to concrete and steel) and high stiffness can lead to problems regarding disturbing vibrations and sound radiation [23–25].

2.2 VIBRATIONS AND SOUND RADIATION

Timber buildings have extensive challenges regarding acoustic insulation compared to concrete buildings, especially for low frequencies (here regarded as maximum 500 Hz). For floors, disturbing vibrations and sound radiation can be problematic, while sound radiation can be problematic for walls.

Sound propagation can be divided into airborne and structure-borne sound transmission, see Figure 2.1. Airborne sound is propagated from, e.g., a loudspeaker or talking, while structure-borne sound is initiated by the structure being excited from, e.g., footsteps or a vibrating machine. For both propagation types, the sound can be propagated both through direct- and flanking transmission paths; the paths being shown in Figure 2.1. Flanking transmission leads to the risk of vibrations propagating long distances through the structure, and thus disturbing vibrations and noise can be emitted in spaces far away from the source. To reduce problems with flanking transmission in multi-storey timber buildings, elastomers are

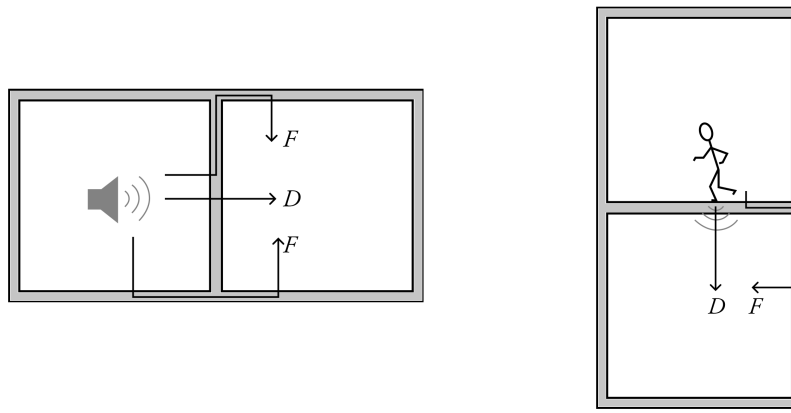

(a) Airborne sound.

(b) Structure-borne sound.

Figure 2.1: Direct (D)- and flanking (F) transmission paths.

commonly introduced in junctions between structural elements.

Both vibrations and sound radiation can be disturbing for occupants of timber buildings. Humans are sensitive to whole-body vibrations, typically below 80–100 Hz, which can – depending on amplitude and frequency – lead to discomfort, disturbed activities, impaired health and motion sickness [26, 27]. Also noise impacts health, and can lead to, e.g., sleep disorders, stress, hearing loss, fatigue, cardiovascular diseases, increased blood pressure, anxiety and depression [28]. For occupants of multi-storey timber buildings, annoyance due to neighbours is most commonly reported, with the most common annoyances relating to impact noise from upstairs neighbours walking and noise from neighbours talking and daily living [29]. Impact noise from walking, so-called footfall loading, contains low-frequency content, and has been reported to be the most common annoyance in timber buildings [30].

Building regulations regarding sound insulation have been developed with regards to concrete buildings, and when utilising these standards for timber buildings, buildings which fulfil the requirements can still be perceived as having insufficient sound insulation to occupants [30]. Regarding vibrations, deflection limits can be used for evaluation, which has been found to be insufficient for mass timber floor systems [31]. Currently, there are two applicable European standards regarding design of timber structures, [32] and [33], for which the methods for determining the vibration criteria differ. In the older standard [32], the evaluation is based on fundamental frequency, deflections due to a static load, and velocity response due to a unit impulse load. In the newer standard [33], vibrations are assessed using a more performance based method, where e.g. the response due to footfall loading can be evaluated. Here, various performance based criteria are introduced, where

designers can choose performance level.

To increase the acoustic insulation for floor CLT panels, the loadbearing part of the floor system is often separated from the ceiling or floor, i.e. the non-loadbearing part [24]. Examples of such methods are floating floors [34, 35] and suspended ceilings [35]. However, these add-on solutions are mostly effective for higher frequencies [23]. Casting concrete on the timber panel, hybrid concrete–CLT, is also a method of increasing the mass and stiffness, and hence mitigating the disturbing vibrations [36, 37].

3 Structural dynamic analysis

In this chapter, a theoretical background to computational structural dynamic analysis is presented. Central concepts, including free vibration and harmonic excitation for structures, are introduced. Additionally, various damping models are presented, and the concept of frequency response functions (FRFs) is introduced. The theory is based on the assumption of linearity, which is reasonable for analyses of comfort vibrations, since the strain amplitudes are low.

Differential equations can be used to describe various engineering problems. Since these often cannot be solved analytically, numerical methods can be employed. An example of such a method is the FE method.

For further reading on structural dynamics and the finite element method, see e.g. [38, 39] and [40], respectively.

3.1 EQUATION OF MOTION

Single degree of freedom system

The simplest way of modelling a structure is by employing a single degree of freedom (SDOF) system, see Figure 3.1a. This system consists of a mass m, a spring with stiffness k and a viscous damper with damping coefficient c. The mass moves frictionlessly in its degree of freedom (DOF), displaced $u(t)$ from its static equilibrium position due to excitation by the time dependent load $p(t)$. A free body diagram of the SDOF system is shown in Figure 3.1b.

Using Newton's second law, $\Sigma F = ma$, where ΣF is the sum of the forces and a is the acceleration, on the system in Figure 3.1 results in

$$p(t) - ku(t) - c\dot{u}(t) = m\ddot{u}(t), \tag{3.1}$$

where $\dot{u}(t)$ is the velocity and $\ddot{u}(t)$ is the acceleration.

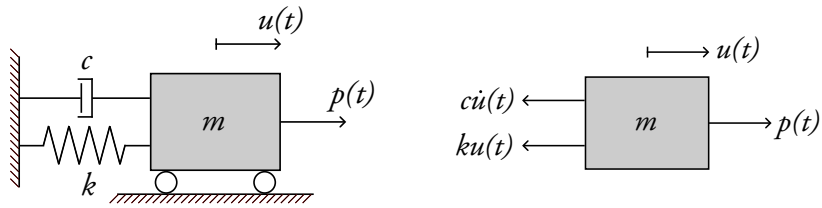

(a) SDOF system.

(b) Free body diagram of SDOF system.

Figure 3.1: SDOF system.

Equation (3.1) can be rearranged as

$$m\ddot{u}(t) + c\dot{u}(t) + ku(t) = p(t), \tag{3.2}$$

which is the equation of motion for an SDOF system.

Multi degree of freedom system

Structures can require more than one DOF to be analysed accurately. Then, multi degree of freedom (MDOF) systems can be used, see e.g. Figure 3.2. Equation (3.2) can be extended to MDOF systems as

$$\mathbf{M}\ddot{\mathbf{u}}(t) + \mathbf{C}\dot{\mathbf{u}}(t) + \mathbf{K}\mathbf{u}(t) = \mathbf{p}(t), \tag{3.3}$$

where $\mathbf{M}$, $\mathbf{C}$ and $\mathbf{K}$ are the mass, damping and stiffness matrices, respectively, while $\ddot{\mathbf{u}}(t)$, $\dot{\mathbf{u}}(t)$, $\mathbf{u}(t)$ and $\mathbf{p}(t)$ are the acceleration, velocity, displacement and load vectors, respectively.

3.2 EIGENFREQUENCIES AND EIGENMODES

A structure has specific eigenfrequencies for which large vibration amplitudes in certain vibration patterns occur. These can be determined using the assumption of free vibration, i.e. the response is due to initial displacements and velocities. Here, the damping can be disregarded if a lightly damped structure is considered.

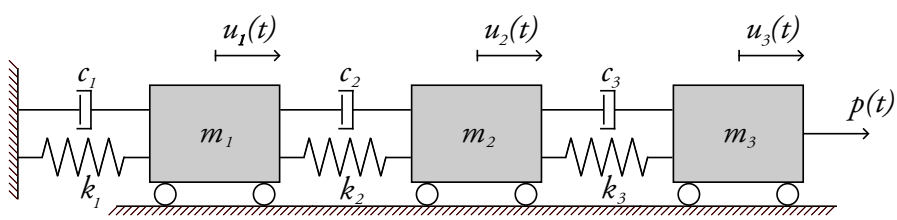

Figure 3.2: MDOF system.

Single degree of freedom system

For an SDOF system, the eigenfrequency can be determined starting from Eq.(3.2), with the assumptions $p(t) = 0$ and $c = 0$ as

$$m\ddot{u}(t) + ku(t) = 0. \tag{3.4}$$

Employing a trial solution

$$u(t) = \hat{U}\mathrm{e}^{\mathrm{i}\omega t} \quad \rightarrow \quad \ddot{u}(t) = -\omega^2\hat{U}\mathrm{e}^{\mathrm{i}\omega t}, \tag{3.5}$$

where $\hat{U}$ is the amplitude, e is Euler's number, the imaginary unit $\mathrm{i} = \sqrt{-1}$ and ω is the angular forcing frequency. Inserting the trial solution into Eq. (3.4),

$$(-\omega^2 m + k)\hat{U}\mathrm{e}^{\mathrm{i}\omega t} = 0 \tag{3.6}$$

is obtained. The solution should be independent of $\hat{U}\mathrm{e}^{\mathrm{i}\omega t}$, and thus

$$-\omega^2 m + k = 0 \quad \rightarrow \quad \omega^2 = k/m. \tag{3.7}$$

Here, the angular eigenfrequency for a SDOF system, $\omega_n = \sqrt{k/m}$ is introduced. This can be translated into the cyclic eigenfrequency as $f_n = \omega_n/2\pi$.

Multi degree of freedom system

For MDOF systems, the eigenfrequencies can be derived in a similar way as for SDOF systems. With the assumption of $\mathbf{p}(t) = \mathbf{0}$ and $\mathbf{C} = \mathbf{0}$,

$$\mathbf{M}\ddot{\mathbf{u}}(t) + \mathbf{K}\mathbf{u}(t) = \mathbf{0} \tag{3.8}$$

is obtained. A solution is employed on the form

$$\mathbf{u}(t) = \hat{U}\mathrm{e}^{\mathrm{i}\omega t}\boldsymbol{\phi} \quad \rightarrow \quad \ddot{\mathbf{u}}(t) = -\omega^2\hat{U}\mathrm{e}^{\mathrm{i}\omega t}\boldsymbol{\phi}, \tag{3.9}$$

where $\boldsymbol{\phi}$ is the eigenmode vectors.

Inserting the trial solution into Eq. (3.8), the equation becomes

$$(-\omega^2\mathbf{M} + \mathbf{K})\boldsymbol{\phi} = \mathbf{0}, \tag{3.10}$$

which can be solved as

$$\det(-\omega_n^2\mathbf{M} + \mathbf{K}) = 0, \tag{3.11}$$

where the angular eigenfrequencies $\omega_n = \omega_1, \omega_2, ..., \omega_N$ can be determined for an N-DOF system. Additionally, by inserting the angular eigenfrequencies into Eq. (3.10), the corresponding eigenmodes can be determined.

When a structure is excited close to an eigenfrequency, resonance will occur, and for an undamped case, the amplitude will approach infinity. In practice, however, all structures have damping, and thus, the vibration amplitudes will be bounded.

The displacement $\mathbf{u}(t)$, can be reformulated using modal expansion

$$\mathbf{u}(t) = \sum_{n=1}^{N} \boldsymbol{\phi}_n q_n(t) = \boldsymbol{\Phi}\mathbf{q}, \tag{3.12}$$

where $q_n(t) = \hat{q}_n \mathrm{e}^{\mathrm{i}\omega t}$ is the modal coordinate of the nth eigenmode.

Often, the dynamic behaviour of the system can be described sufficiently without including all modes. Hence, $J < N$ modes can be utilised as

$$\mathbf{u}(t) \approx \sum_{j=1}^{J} \boldsymbol{\phi}_j q_j(t) = \boldsymbol{\Phi}_J \mathbf{q}_J, \tag{3.13}$$

where $q_j(t) = \hat{q}_j \mathrm{e}^{\mathrm{i}\omega t}$ is the modal coordinate of the jth eigenmode. This is known as modal truncation.

3.3 HARMONIC EXCITATION

Single degree of freedom system

When a damped system is excited by a harmonic load, it will – after an initial transient part – respond by oscillating with the same frequency as the excitation. Focusing on the steady-state response, i.e. disregarding the initial transient response, Eq. (3.2) can be solved by employing the solution

$$u(t) = \hat{u}\mathrm{e}^{\mathrm{i}\omega t} \quad \rightarrow \quad \dot{u}(t) = \mathrm{i}\omega\hat{u}\mathrm{e}^{\mathrm{i}\omega t} \quad \rightarrow \quad \ddot{u}(t) = -\omega^2\hat{u}\mathrm{e}^{\mathrm{i}\omega t} \tag{3.14}$$

and

$$p(t) = \hat{p}\mathrm{e}^{\mathrm{i}\omega t}, \tag{3.15}$$

where $\hat{u}$ is the complex displacement amplitude and $\hat{p}$ is the complex load amplitude.

Inserting this into Eq. (3.2), the formulation becomes

$$(-\omega^2 m + \mathrm{i}\omega c + k)\hat{u} = \hat{p}, \tag{3.16}$$

for which the displacement amplitude can be solved for as

$$\hat{u} = \frac{\hat{p}}{-\omega^2 m + \mathrm{i}\omega c + k}. \tag{3.17}$$

Multi degree of freedom system

Harmonic excitation of an MDOF system is solved similarly to an SDOF system. A trial solution is employed,

$$\mathbf{u}(t) = \hat{\mathbf{u}}\mathrm{e}^{\mathrm{i}\omega t} \quad \rightarrow \quad \dot{\mathbf{u}}(t) = \mathrm{i}\omega\hat{\mathbf{u}}\mathrm{e}^{\mathrm{i}\omega t} \quad \rightarrow \quad \ddot{\mathbf{u}}(t) = -\omega^2\hat{\mathbf{u}}\mathrm{e}^{\mathrm{i}\omega t} \tag{3.18}$$

and

$$\mathbf{p}(t) = \hat{\mathbf{p}}\mathrm{e}^{\mathrm{i}\omega t}, \tag{3.19}$$

where $\hat{\mathbf{u}}$ is the complex displacement amplitude vector and $\hat{\mathbf{p}}$ is the complex load amplitude vector.

Inserting these into Eq. (3.3), the frequency domain equation of motion for an MDOF system is obtained,

$$(-\omega^2\mathbf{M} + \mathrm{i}\omega\mathbf{C} + \mathbf{K})\hat{\mathbf{u}} = \hat{\mathbf{p}}. \tag{3.20}$$

Here, $\mathbf{D}(\omega) = -\omega^2\mathbf{M} + \mathrm{i}\omega\mathbf{C} + \mathbf{K}$ is the dynamic stiffness matrix, and thus the response can be rewritten as $\mathbf{D}(\omega)\hat{\mathbf{u}} = \hat{\mathbf{p}}$.

The complex displacement amplitudes can be solved directly as

$$\hat{\mathbf{u}} = \mathbf{D}(\omega)^{-1}\hat{\mathbf{p}}. \tag{3.21}$$

This method is applicable for systems with frequency-dependent material properties, however, becomes computationally heavy for large systems.

For systems with frequency-independent material properties, the displacement response can be determined using the eigenmodes. By utilising the formulation in Eq. (3.13), and approximating the modal coordinates as

$$\mathbf{q}_J(t) = \hat{\mathbf{q}}_J\mathrm{e}^{\mathrm{i}\omega t} \quad \rightarrow \quad \dot{\mathbf{q}}_J(t) = \mathrm{i}\omega\hat{\mathbf{q}}_J\mathrm{e}^{\mathrm{i}\omega t} \quad \rightarrow \quad \ddot{\mathbf{q}}_J(t) = -\omega^2\hat{\mathbf{q}}_J\mathrm{e}^{\mathrm{i}\omega t}, \tag{3.22}$$

where $\hat{\mathbf{q}}_J$ is the modal coordinate amplitude vector, the equation of motion in Eq. (3.3) can be diagonalised as

$$(-\omega^2\boldsymbol{\Phi}_J^{\mathrm{T}}\mathbf{M}\boldsymbol{\Phi}_J + \mathrm{i}\omega\boldsymbol{\Phi}_J^{\mathrm{T}}\mathbf{C}\boldsymbol{\Phi}_J + \boldsymbol{\Phi}_J^{\mathrm{T}}\mathbf{K}\boldsymbol{\Phi}_J)\hat{\mathbf{q}}_J = \boldsymbol{\Phi}_J^{\mathrm{T}}\hat{\mathbf{p}}, \tag{3.23}$$

where proportional damping is assumed (see further Section 3.4).

This equation can be reformulated as

$$(-\omega^2\mathbf{M}_J + \mathrm{i}\omega\mathbf{C}_J + \mathbf{K}_J)\hat{\mathbf{q}}_J = \hat{\mathbf{p}}_J, \tag{3.24}$$

where

$$\begin{gathered}\mathbf{M}_J = \boldsymbol{\Phi}_J^{\mathrm{T}}\mathbf{M}\boldsymbol{\Phi}_J = \mathrm{diag}(M_j), \quad \mathbf{C}_J = \boldsymbol{\Phi}_J^{\mathrm{T}}\mathbf{C}\boldsymbol{\Phi}_J = \mathrm{diag}(C_j), \\ \mathbf{K}_J = \boldsymbol{\Phi}_J^{\mathrm{T}}\mathbf{K}\boldsymbol{\Phi}_J = \mathrm{diag}(K_j), \quad \hat{\mathbf{p}}_J = \boldsymbol{\Phi}_J^{\mathrm{T}}\hat{\mathbf{p}}\end{gathered} \tag{3.25}$$

and M_j, C_j and K_j are the modal mass, -damping and -stiffness for mode j.

This equation can be solved as

$$\hat{\mathbf{q}}_J = (-\omega^2 \mathbf{M}_J + \mathrm{i}\omega \mathbf{C}_J + \mathbf{K}_J)^{-1} \hat{\mathbf{p}}_J, \tag{3.26}$$

which is similar to Eq. (3.21), however, this system is diagonal, and thus the computational power needed to solve this is reduced.

From Eq. (3.26), the solution can be transformed from modal coordinates to physical coordinates via Eq. (3.13).

3.4 DAMPING

In reality, all structures have damping. Damping refers to a dissipation of mechanical energy into heat, and thus the vibration amplitude is reduced, and does not approach infinity during resonance. Various phenomena lead to energy losses, e.g., on the material level due to internal friction or on the structure level due to friction.

Structural damping

If the level of damping is not varying considerably with frequency, rate-independent damping can be appropriate to employ. This way of employing damping can e.g. be used in analysing timber panels. Rate-independent means that the damping is constant over the frequency span. This damping model can be applied by using a loss factor, η – which at resonance is $\eta = 2\zeta$ and where ζ is the modal damping ratio. The damping matrix can then be expressed as

$$\mathbf{C} = \frac{\eta}{\omega} \mathbf{K}, \tag{3.27}$$

so that Eq. (3.20) becomes

$$(-\omega^2 \mathbf{M} + \mathbf{K}(1 + \mathrm{i}\eta))\hat{\mathbf{u}} = \hat{\mathbf{p}}. \tag{3.28}$$

The dynamic stiffness matrix can, thus, be reformulated as $\mathbf{D}(\omega) = -\omega^2 \mathbf{M} + \mathbf{K}(1 + \mathrm{i}\eta)$.

Modal damping

Another method of taking damping into account is to use modal damping. Then, the mode shape $\boldsymbol{\phi}_n$ is paired with its modal damping ratio ζ_n. Additionally, the

eigenfrequency can be considered independent of damping for damping ratios $\zeta_n < 0.20$, thus, $\omega_d = \omega_n\sqrt{1-\zeta_n^2} \approx \omega_n$, where ω_d is the damped eigenfrequency. For MDOF systems, damping ratios can be used in analyses of modally truncated systems (cf. Eq. (3.25)). Hence, the damping formulation is

$$C_j = 2\zeta_j\omega_j M_j. \tag{3.29}$$

3.5 FREQUENCY RESPONSE FUNCTIONS

An FRF describes the relation between input and output for a system. Common FRFs are compliance (displacement/load), mobility (velocity/load) and accelerance (acceleration/load). These FRF matrices can be determined as

$$\mathbf{H_u}(\omega) = \mathbf{D}(\omega)^{-1}, \quad \mathbf{H_v}(\omega) = \mathrm{i}\omega\mathbf{H_u}(\omega) \quad \text{and} \quad \mathbf{H_a}(\omega) = -\omega^2\mathbf{H_u}(\omega), \tag{3.30}$$

respectively.

FRFs can be measured and computed. In experimental testing, the input (load) and output (e.g. acceleration) are measured, and thus the FRF can be determined. For computations, steady-state analyses of structures loaded with a unit load gives the FRFs directly.

An FRF matrix for a structure with N evaluation points is structured as

$$\mathbf{H}(\omega) = \begin{bmatrix} h_{11}(\omega) & h_{12}(\omega) & \dots & h_{1N}(\omega) \\ h_{21}(\omega) & h_{22}(\omega) & \dots & h_{2N}(\omega) \\ \vdots & \vdots & \ddots & \vdots \\ h_{N1}(\omega) & h_{N2}(\omega) & \dots & h_{NN}(\omega) \end{bmatrix}, \tag{3.31}$$

where

$$h_{ij}(\omega) = \frac{\hat{x}_i(\omega)}{\hat{p}_j(\omega)} = \frac{\text{Response in point } i}{\text{Excitation in point } j}. \tag{3.32}$$

FRF matrices are symmetric, and thus $h_{ij}(\omega) = h_{ji}(\omega)$. This is due to the transfer function between two evaluation points being the same independently of at which position the load is applied and at which position the response is evaluated. This is known as reciprocity.

Depending on what is of interest regarding vibration response, various FRFs can be appropriate for result evaluation. Humans are sensitive to accelerations, and hence, accelerance FRFs could be an appropriate metric [27]. On the other hand, sound radiation from vibrating structures is related to velocity, and hence mobility FRFs could be appropriate to evaluate.

3.6 FINITE ELEMENT MODELLING

Even though some simple problems can be solved analytically, larger, more complicated problems require numerical solution methods. Hence, the FE method can be suitable. The following derivations are based on formulations in [40, 41]

Strong formulation

The derivation of the FE formulation is initiated by the differential equations of motion for a deformed body V with surface boundary S,

$$\tilde{\boldsymbol{\nabla}}^{\mathrm{T}}\boldsymbol{\sigma} + \mathbf{b} = \rho\ddot{\mathbf{u}}, \tag{3.33}$$

where

$$\tilde{\boldsymbol{\nabla}}^{\mathrm{T}} = \begin{bmatrix} \frac{\partial}{\partial x} & 0 & 0 & \frac{\partial}{\partial y} & \frac{\partial}{\partial z} & 0 \\ 0 & \frac{\partial}{\partial y} & 0 & \frac{\partial}{\partial x} & 0 & \frac{\partial}{\partial z} \\ 0 & 0 & \frac{\partial}{\partial z} & 0 & \frac{\partial}{\partial x} & \frac{\partial}{\partial y} \end{bmatrix}, \quad \boldsymbol{\sigma} = \begin{bmatrix} \sigma_{xx} \\ \sigma_{yy} \\ \sigma_{zz} \\ \sigma_{xy} \\ \sigma_{xz} \\ \sigma_{yz} \end{bmatrix} \quad \text{and} \quad \mathbf{b} = \begin{bmatrix} b_x \\ b_y \\ b_z \end{bmatrix}. \tag{3.34}$$

Here, $\tilde{\boldsymbol{\nabla}}$ is a matrix differential operator, $\boldsymbol{\sigma}$ is the stress vector, $\mathbf{b}$ is the body force vector, ρ is the mass density and $\ddot{\mathbf{u}}$ is the acceleration vector determined as $\ddot{\mathbf{u}} = \frac{\partial^2 \mathbf{u}}{\partial t^2}$ were $\mathbf{u} = [u_x \; u_y \; u_z]^{\mathrm{T}}$ is the displacement vector.

Boundary conditions can be assigned at S, regarding the displacements (essential) and forces (natural). The initial displacement and velocity at time $t = 0$ can be written as $\mathbf{u}(t = 0) = \mathbf{u_0}$ and $\dot{\mathbf{u}}(t = 0) = \dot{\mathbf{u}}_\mathbf{0}$.

Weak formulation

The weak formulation is derived from Eq. (3.33). This equation is premultiplied with a vector of arbitrary weight functions $\mathbf{v} = [v_x \; v_y \; v_z]^{\mathrm{T}}$, and integrated over the volume V,

$$\int_V \mathbf{v}^{\mathrm{T}}(\tilde{\boldsymbol{\nabla}}^{\mathrm{T}}\boldsymbol{\sigma} + \mathbf{b} - \rho\ddot{\mathbf{u}}) \, \mathrm{d}V = \mathbf{0}. \tag{3.35}$$

The first term of Eq. (3.35) is integrated by parts using Green–Gauss theorem as

$$\int_V \mathbf{v}^{\mathrm{T}}\tilde{\boldsymbol{\nabla}}^{\mathrm{T}}\boldsymbol{\sigma} \, \mathrm{d}V = \int_S \mathbf{v}^{\mathrm{T}}\mathbf{t} \, \mathrm{d}S - \int_V (\tilde{\boldsymbol{\nabla}}\mathbf{v})^{\mathrm{T}}\boldsymbol{\sigma} \, \mathrm{d}V, \tag{3.36}$$

where $\mathbf{t}$ is the traction vector.

Inserting Eq. (3.36) into Eq. (3.35) gives

$$\int_V \mathbf{v}^{\mathrm{T}} \rho \ddot{\mathbf{u}} \, \mathrm{d}V + \int_V (\tilde{\boldsymbol{\nabla}} \mathbf{v})^{\mathrm{T}} \boldsymbol{\sigma} \, \mathrm{d}V = \int_V \mathbf{v}^{\mathrm{T}} \mathbf{b} \, \mathrm{d}V + \int_S \mathbf{v}^{\mathrm{T}} \mathbf{t} \, \mathrm{d}S, \tag{3.37}$$

which is the weak formulation of Eq. (3.33). This formulation is independent of constitutive relation.

Finite element formulation

The FE equations of three-dimensional elasticity can be derived from Eq. (3.37). The displacement vector can be approximated by

$$\mathbf{u} = \mathbf{N}\mathbf{a}, \tag{3.38}$$

where the matrix $\mathbf{N}$ contains the global shape functions used to determine the displacement field by interpolating the nodal displacements $\mathbf{a}$.

Adopting the Galerkin method, the weight vector is chosen as

$$\mathbf{v} = \mathbf{N}\mathbf{c}, \tag{3.39}$$

where $\mathbf{c}$ is an arbitrary constant vector.

A linear elastic orthotropic constitutive model can be adopted, where the strains are assumed to be small,

$$\boldsymbol{\sigma} = \mathbf{D}\boldsymbol{\varepsilon} = \mathbf{D}\tilde{\boldsymbol{\nabla}}\mathbf{u} = \mathbf{D}\tilde{\boldsymbol{\nabla}}\mathbf{N}\mathbf{a}, \tag{3.40}$$

where

$$\mathbf{D} = \begin{bmatrix} D_{11} & D_{12} & D_{13} & 0 & 0 & 0 \\ D_{21} & D_{22} & D_{23} & 0 & 0 & 0 \\ D_{31} & D_{32} & D_{33} & 0 & 0 & 0 \\ 0 & 0 & 0 & D_{44} & 0 & 0 \\ 0 & 0 & 0 & 0 & D_{55} & 0 \\ 0 & 0 & 0 & 0 & 0 & D_{66} \end{bmatrix} \quad \text{and} \quad \boldsymbol{\varepsilon} = \begin{bmatrix} \varepsilon_{xx} \\ \varepsilon_{yy} \\ \varepsilon_{zz} \\ \varepsilon_{xy} \\ \varepsilon_{xz} \\ \varepsilon_{yz} \end{bmatrix}. \tag{3.41}$$

Here, $\mathbf{D}$ is the constitutive matrix for an orthotropic material and $\boldsymbol{\varepsilon}$ represents the strains.

By renaming $\tilde{\nabla}\mathbf{N} = \mathbf{B}$ and inserting Eqs. (3.38)–(3.40) into Eq. (3.37), the formulation becomes

$$\left(\int_V \mathbf{N}^{\mathrm{T}} \rho \mathbf{N} \, \mathrm{d}V \right) \ddot{\mathbf{a}} + \left(\int_V \mathbf{B}^{\mathrm{T}} \mathbf{D} \mathbf{B} \, \mathrm{d}V \right) \mathbf{a} = \int_V \mathbf{N}^{\mathrm{T}} \mathbf{b} \, \mathrm{d}V + \int_S \mathbf{N}^{\mathrm{T}} \mathbf{t} \, \mathrm{d}S, \tag{3.42}$$

which can be reformulated as

$$\mathbf{M\ddot{a}} + \mathbf{Ka} = \mathbf{p}, \tag{3.43}$$

with

$$\begin{gathered}\mathbf{M} = \int_V \mathbf{N}^{\mathrm{T}} \rho \mathbf{N} \, \mathrm{d}V, \quad \mathbf{K} = \int_V \mathbf{B}^{\mathrm{T}} \mathbf{D} \mathbf{B} \, \mathrm{d}V \quad \text{and} \\ \mathbf{p} = \int_V \mathbf{N}^{\mathrm{T}} \mathbf{b} \, \mathrm{d}V + \int_S \mathbf{N}^{\mathrm{T}} \mathbf{t} \, \mathrm{d}S,\end{gathered} \tag{3.44}$$

where $\mathbf{M}$ is the mass matrix, $\mathbf{K}$ is the stiffness matrix and $\mathbf{p}$ is the force vector.

Introducing the damping matrix $\mathbf{C}$, the formulation becomes

$$\mathbf{M\ddot{a}} + \mathbf{C\dot{a}} + \mathbf{Ka} = \mathbf{p}. \tag{3.45}$$

3.7 MODELLING OF ELASTOMERS

Elastomers are, as previously mentioned, commonly used in junctions between structural elements in timber buildings. Elastomers are viscoelastic materials, meaning that they possess a combination of viscous and elastic behaviour under deformation. Hence, the material behaviour is frequency dependent. The following derivations are based on [42]. In considering linear viscoelasticity, which is applicable for cases with small strains, such as comfort vibration analyses, the stress of the elastomer becomes

$$\sigma^* = E^*(\omega)\varepsilon^*, \tag{3.46}$$

where $E^*(\omega)$ is the complex Young's modulus and ε^* is the harmonic strain. Here, notation * indicates a complex number. The formulation of E^* can be expanded as

$$E^* = \frac{\sigma^*}{\varepsilon^*} = \frac{\sigma_0 \mathrm{e}^{\mathrm{i}(\omega t + \delta)}}{\varepsilon_0 \mathrm{e}^{\mathrm{i}\omega t}} = \frac{\sigma_0}{\varepsilon_0}\mathrm{e}^{\mathrm{i}\delta} = E_{dyn}\mathrm{e}^{\mathrm{i}\delta}, \tag{3.47}$$

where σ_0 is the stress amplitude, ε_0 is the strain amplitude, $\delta = \arg(E^*)$ is the phase angle and E_{dyn} is the dynamic Young's modulus.

Equation (3.47) can be rewritten using rectangular form as

$$E^* = E_{dyn}(\cos\delta + \mathrm{i}\sin\delta) = E_s + \mathrm{i}E_l, \tag{3.48}$$

where E_s is the storage modulus and E_l is the loss modulus. Here, the storage modulus represents the elastic response, and the loss modulus represents the energy dissipation of the system.

This can also be rewritten as

$$E^* = E_{dyn}\cos\delta\left(1 + \mathrm{i}\frac{\sin\delta}{\cos\delta}\right) = E_s(1 + \mathrm{i}\tan\delta) = E_s(1 + \mathrm{i}\eta), \tag{3.49}$$

where η is the loss factor. For sufficiently low damping, it can be approximated that $\eta \approx \delta$.

Assuming an isotropic elastomer, the shear and bulk moduli – which describe a material's response to shear stress, and to uniform pressure, respectively – can be determined as

$$G_0 = \frac{E_0}{2(1+\nu_0)} \quad \text{and} \quad K_0 = \frac{E_0}{3(1-2\nu_0)}, \tag{3.50}$$

where ν_0 is Poisson's ratio.

Moreover, the shear and bulk moduli can be divided into storage and loss parts, as

$$G^* = G_s + \mathrm{i}G_l \quad \text{and} \quad K^* = K_s + \mathrm{i}K_l. \tag{3.51}$$

A method of determining material properties of elastomers using experimental data, manufacturer data sheets and FE modelling was developed in [42] and further verified in [43]. To include the material properties of the elastomer in an FE analysis, the storage and loss parts of the shear and bulk moduli need to be determined. This can be done by introducing a scale factor, $\alpha(\omega)$, determined as $\alpha(\omega) = \frac{E_{dyn}(\omega)}{E_0}$. Then, $G_{dyn}(\omega) = \alpha(\omega)G_0$ and $K_{dyn}(\omega) = \alpha(\omega)K_0$ can also be determined. The storage and loss parts of the moduli can then be determined as

$$\begin{aligned} G_s = G_{dyn}\cos\delta, \quad G_l = G_{dyn}\sin\delta \\ K_s = K_{dyn}\cos\delta \quad \text{and} \quad K_l = K_{dyn}\sin\delta. \end{aligned} \tag{3.52}$$

4 Model calibration

Numerical models can be validated to experimental data, to increase the accuracy. Wood inherently has large variations regarding material properties [44–46]. Hence, results from an experimental campaign can be used to calibrate and validate the numerical model, for example regarding material properties.

4.1 EXPERIMENTAL TESTING

By use of experimental campaigns, structures' dynamic behaviours can be determined. In an experimental campaign, the structure can be excited using a a shaker or impact hammer, and the response obtained by use of accelerometers. For obtaining the response, piezoelectric accelerometers can be used. These consist of a seismic mass and a piezoelectric material. When the accelerometer base is subjected to vibrations, the piezoelectric material is mechanically stressed and generates an electric charge which is proportional to the applied force. The acceleration can be determined from the force by use of Newton's second law [47]. Electrodynamic shakers consist of an electric coil in a magnetic field, and are used to excite the structure in a point using, e.g., a random- or sine signal. Impulse hammers are used to generate impulses onto multiple points of the structure [48].

When conducting measurements, the data (e.g. load and acceleration) is measured in the time domain. By utilising a fast Fourier transform (FFT), the results can be transformed to the frequency domain, and hence, FRFs can be determined. Utilising the FRFs and various algorithms, the eigenfrequencies, modal damping ratios and mode shapes can be determined. For the measurements, either one or more shakers in combination with a number of accelerometers or a number of hammer impulses in combination with one or more accelerometers can be used to determine the FRFs [48]. Prior to conducting measurements, it is important to analyse the structure to determine appropriate positions of the shaker, hammer impulses and accelerometers, e.g. so the structure is not excited in a node in a mode.

When measuring on structures in a laboratory setting, free–free displacements boundary conditions are convenient, meaning that no displacements are prescribed. Physically, this can be accomplished by use of soft springs, either with the panel resting on or hanging from them. Additionally, free–free boundary conditions are simple to implement in numerical models [48].

4.2 CALIBRATING NUMERICAL MODELS

As mentioned above, experimental campaigns can be used to collect data of the dynamic behaviour of structures. However, using experimental campaigns for analysing the behaviour of structures can be quite extensive. Hence, a more efficient method of analysing the dynamic behaviour of a structure is using a combination of experimental data and numerical results. By doing this, the numerical models can be calibrated and validated against experimental data and then be used to analyse the structure's behaviour extensively.

Regarding comfort vibrations, timber can be modelled as an orthotropic, linear elastic material. For modelling, a rectangular coordinate system can be defined, see Figure 4.1, where L, R and T denote the longitudinal, radial and transversal directions, respectively. Due to this modelling assumption, 10 material properties can be defined; the density ρ, Young's modulus in the longitudinal, radial and transversal directions (E_{L}, E_{R} and E_{T}), shear moduli (G_{LR}, G_{LT} and G_{RT}) as well as Poisson's ratios (ν_{LR}, ν_{LT} and ν_{RT}).

Calibration of material properties can be important when analysing timber structures numerically, due to the variability of the material properties. In Figure 4.2, an experimentally obtained FRF is compared to an FRF computed using material parameters found in the literature (G_{RT} from [46], Poisson's ratios from [17] and the density, Young's moduli and the remaining shear moduli from [49]), as well as computed using calibrated material properties.

To evaluate the vibration response over a frequency span, the root mean square (RMS) value can be utilised. The RMS value is defined as

$$\tilde{x} = \sqrt{\frac{1}{N}\sum_{n=1}^{N} x_n^2}, \tag{4.1}$$

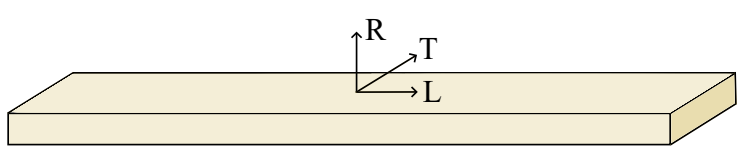

Figure 4.1: A lamella with the rectangular coordinate system.

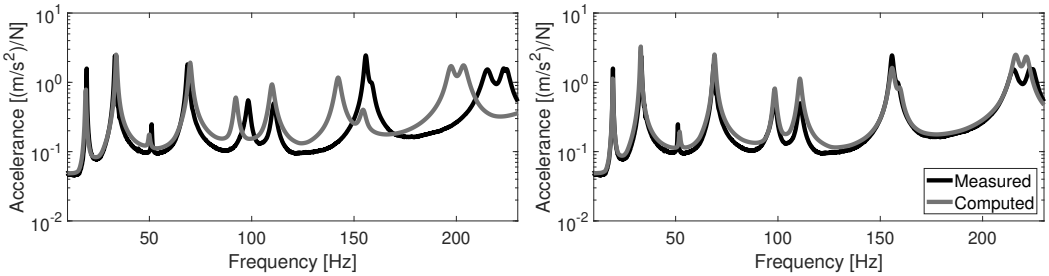

(a) Material properties from literature. **(b)** Calibrated material properties.

Figure 4.2: Comparison of computed and experimentally obtained accelerance FRFs. The legend is valid for both figures.

where N is the number of frequency increments and x_n is the response for increment n. Here, x is considered as the amplitude of the complex magnitude of accelerance or mobility. The spatially averaged response of a surface can be represented as

$$x_n = \frac{1}{M} \sum_{m=1}^{M} x_m, \tag{4.2}$$

for each frequency increment n. Here, M is the number of evaluation positions and x_m is the response in position m.

To evaluate how similar mode shapes are, the modal assurance criterion (MAC) [50], defined as

$$\text{MAC} = \frac{|(\boldsymbol{\phi}_{i,A})^T(\boldsymbol{\phi}_{j,B})|^2}{(\boldsymbol{\phi}_{i,A})^T(\boldsymbol{\phi}_{i,A})(\boldsymbol{\phi}_{j,B})^T(\boldsymbol{\phi}_{j,B})}, \tag{4.3}$$

can be used. Here, $\boldsymbol{\phi}_{i,A}$ and $\boldsymbol{\phi}_{j,B}$ are the mode shapes of numbers i and j of models A and B, respectively. The MAC value can be between 0 and 1, where a perfect match between $\boldsymbol{\phi}_{i,A}$ and $\boldsymbol{\phi}_{j,B}$ leads to $\text{MAC}(i,j) = 1$. Once confirmed that the modes are the same, their eigenfrequencies can be compared using a normalised relative frequency difference (NRFD), which can be defined as

$$\text{NRFD} = \frac{f_{i,A} - f_{j,B}}{f_{j,B}}, \tag{4.4}$$

in which $f_{i,A}$ and $f_{j,B}$ are eigenfrequencies number i and j for models A and B.

Sensitivity analysis

To analyse which material properties influence the vibration response, a sensitivity analysis can be conducted. As an example, a three-layer CLT panel of dimensions 4 m × 0.5 m was analysed regarding eigenfrequencies and eigenmodes. All layers

have a thickness of 20 mm. The panel was analysed using free–free displacement boundary conditions and solid shell finite elements of size 25 mm were used. The 10 lowest eigenfrequencies and eigenmodes were evaluated, see Figure 4.3.

For conducting a sensitivity analysis, each material property can be individually varied between a lower- and upper limit, while the other properties are kept constant. Here, five equally spaced values were used for each material property. The lower and upper limits, as well as the reference material properties from the literature are presented in Table 4.1.

Figure 4.4 exemplifies how the eigenfrequencies are affected when one material parameter at a time is changed, using NRFD values. MAC values were used to ensure that the compared eigenfrequencies correspond to the same eigenmodes in the subfigures. Bi and Tj stand for bending mode i and torsion mode j, respectively. From Figure 4.4, it can be observed that the material properties that affect the eigenfrequencies significantly are ρ, E_{L}, G_{LT} and G_{RT}, where ρ and G_{RT} affect

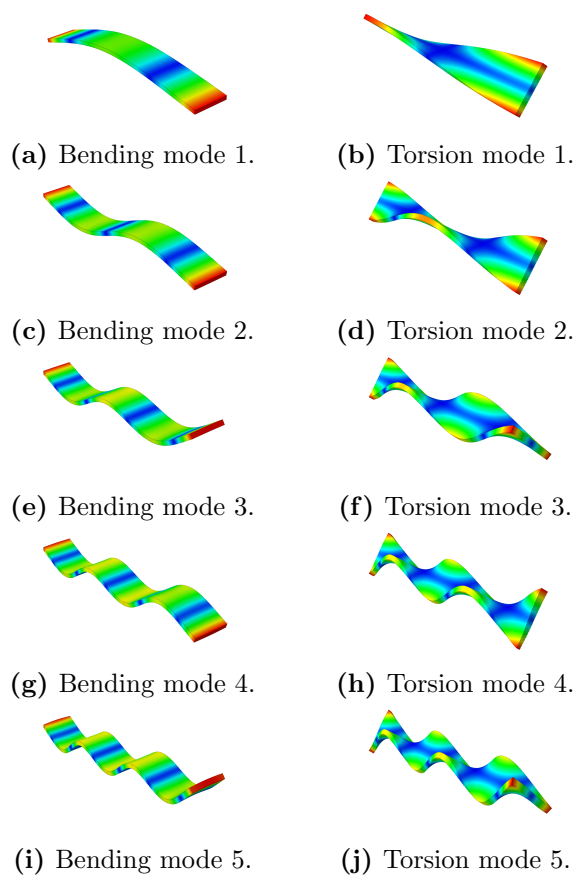

(a) Bending mode 1. **(b)** Torsion mode 1.

(c) Bending mode 2. **(d)** Torsion mode 2.

(e) Bending mode 3. **(f)** Torsion mode 3.

(g) Bending mode 4. **(h)** Torsion mode 4.

(i) Bending mode 5. **(j)** Torsion mode 5.

Figure 4.3: Mode shapes corresponding to the 10 lowest eigenfrequencies.

Table 4.1: Lower and upper limits as well as reference material properties [17, 46, 49] for spruce. The unit of the density is kg/m^3, the moduli MPa and Poisson's ratios are dimensionless.

	ρ	E_L	E_R	E_T	G_LR	G_LT	G_RT	ν_LR	ν_LT	ν_RT
Reference	420	11 000	370	370	690	690	49	0.45	0.45	0.28
Lower	350	7 000	200	200	400	400	30	0.35	0.35	0.25
Upper	900	16 000	600	600	1 000	1 000	100	0.50	0.50	0.40

all modes, while E_L mostly affects the bending modes and G_LT the torsion modes. Subsequently, if a calibration is to be conducted, these properties would be relevant to modify.

Calibration procedures

For conducting a calibration, e.g. Newton optimisation can be used. For further information on Newton optimisation and various other optimisation procedures, see e.g. [51]. For calibrating material properties for a CLT panel, the following procedure can be be used.

The minimum of a function $g = \sum_{i=1}^{N} \left(\frac{f_{calc.,i} - f_{exp.,i}}{f_{exp.,i}} \right)^2$ is sought.

Using Taylor expansion around the current point $\mathbf{x}_k$, a quadratic approximation of the function is acquired (neglecting higher order terms),

$$g(\mathbf{x}) \approx g(\mathbf{x}_k) + \mathbf{g}_k^\mathrm{T}(\mathbf{x} - \mathbf{x}_k) + \frac{1}{2}(\mathbf{x} - \mathbf{x}_k)^\mathrm{T}\mathbf{H}_k(\mathbf{x} - \mathbf{x}_k), \tag{4.5}$$

where $\mathbf{g}_k = \nabla g(\mathbf{x}_k)$ and $\mathbf{H}_k = \nabla^2 g(\mathbf{x}_k)$ are the gradient and Hessian matrix, respectively, evaluated in $\mathbf{x} = \mathbf{x}_k$.

Differentiating the approximation with respect to $\mathbf{x}$,

$$\mathbf{g}_k + \mathbf{H}_k(\mathbf{x} - \mathbf{x}_k) = \mathbf{0}, \tag{4.6}$$

is obtained. If the Hessian matrix is positive definite, $\mathbf{H}_k > 0$, the function will have a minimum at

$$\mathbf{x}_{k+1} = \mathbf{x}_k - \mathbf{H}_k^{-1}\mathbf{g}_k. \tag{4.7}$$

The algorithm continues until the step length is less than the set tolerance.

Another way of conducting a calibration of material properties is by varying a material property and comparing the computed and experimentally obtained FRFs using various metrics, such as RMS values, MAC values and NRFD values as well

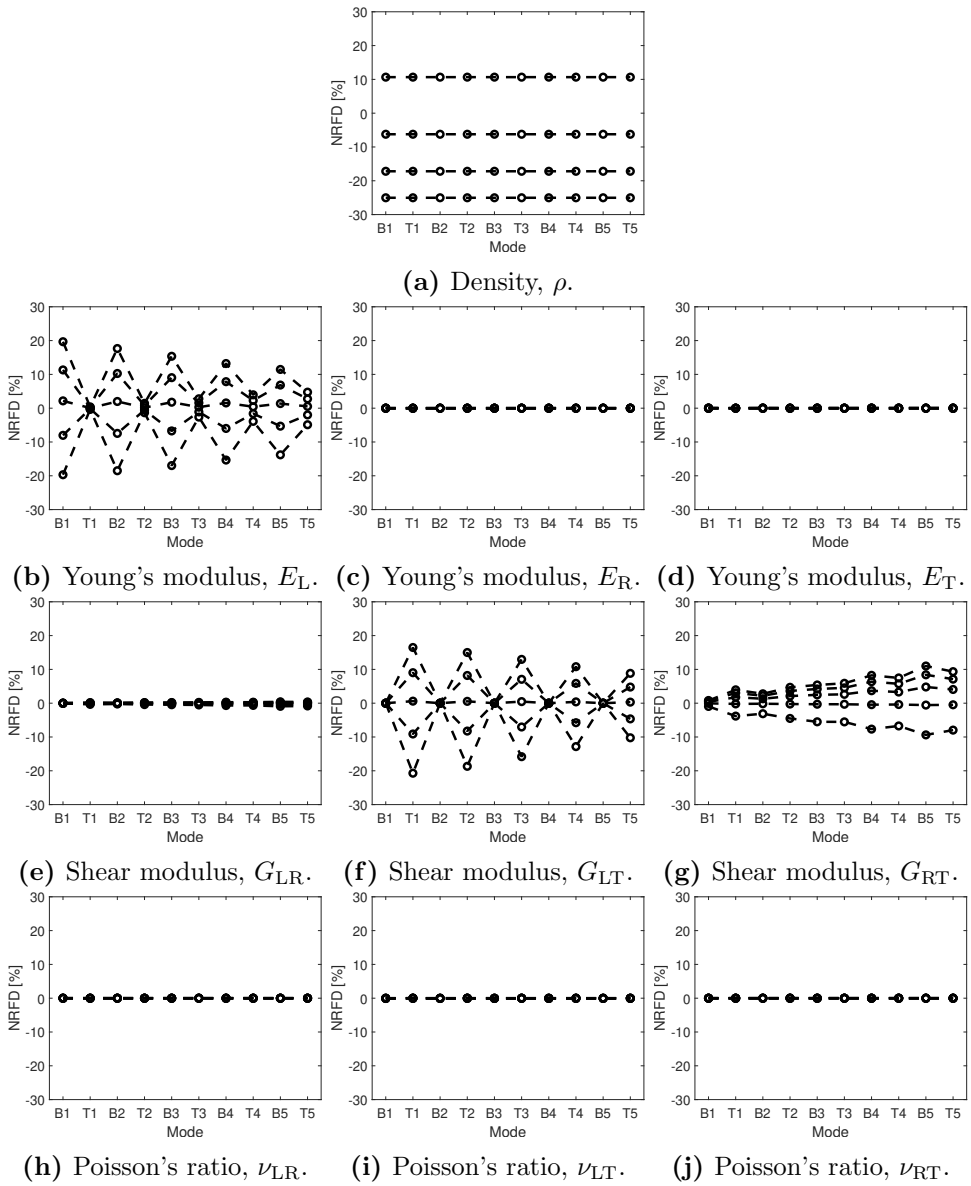

(a) Density, ρ.

(b) Young's modulus, E_{L}. **(c)** Young's modulus, E_{R}. **(d)** Young's modulus, E_{T}.

(e) Shear modulus, G_{LR}. **(f)** Shear modulus, G_{LT}. **(g)** Shear modulus, G_{RT}.

(h) Poisson's ratio, ν_{LR}. **(i)** Poisson's ratio, ν_{LT}. **(j)** Poisson's ratio, ν_{RT}.

Figure 4.4: Analyses showing how the eigenfrequencies are affected when various material properties are varied. Bi and Tj stand for bending mode i and torsion mode j, respectively.

as vibration amplitudes. When computed FRFs resembles measured FRFs within decided tolerances for the various metrics, the calibration is concluded.

Once one or several numerical models are calibrated and verified using measurement data, these can be used for further analyses; which may be faster and less expensive than conducting additional measurements.

5 Vibration reduction strategies

Two main methods of CLT panel modification for vibration reduction have been investigated in the dissertation. Firstly, using a denser and stiffer lamination material in the panel, and secondly, inserting an elastomer layer with high energy dissipation properties and low stiffness (in comparison to the timber) into the panel. Previous studies have shown promising results regarding reduction of vibration levels by utilising these methods. Using hardwoods or compressed spruce instead of spruce was investigated in [16, 17, 20] and [20], respectively. Additionally, in [20], integrating an elastomer layer into CLT panels was investigated.

In the appended papers, vibration mitigation by panel modification has been investigated. In **Paper A**, how the vibration levels were affected by exchanging spruce lamellae with concrete was explored. In **Paper B**, the effect on vibration response by using oak or a combination of spruce and oak, as well as integrating an elastomer layer into a CLT panel was studied. In **Paper C**, the effect on vibration response by using birch or compressed spruce, as well as integrating an elastomer layer into the CLT panels was analysed. In the studies in the appended papers, CLT panels of various sizes have been used and the vibration responses were evaluated using various frequency ranges. Hence, to summarise and compare the evaluated methods of panel modifications, a case study was conducted, and will hereafter be described.

To compare the mentioned methods of vibration reduction by panel modification, two different CLT panels of dimensions 4 m $\times$ 3 m were utilised. The first panel is made of purely timber, and has five layers of 25 mm thick lamellae, see Figure 5.1a. The second panel consists of two additional layers, one 10 mm layer and one 25 mm layer on top of the five-layer panel, see Figure 5.1b. FE models were used to study the effect of the various modifications on the vibration levels of the panels. Free–free displacement boundary conditions were used, and the panel was loaded with a unit load in one corner of the top surface. Solid shell elements of size 25 mm were utilised. The response was evaluated using spatially averaged mobility FRFs between 10 and 200 Hz on the surface on the same side of the panel as the load.

The material properties of spruce, birch and compressed spruce were taken from

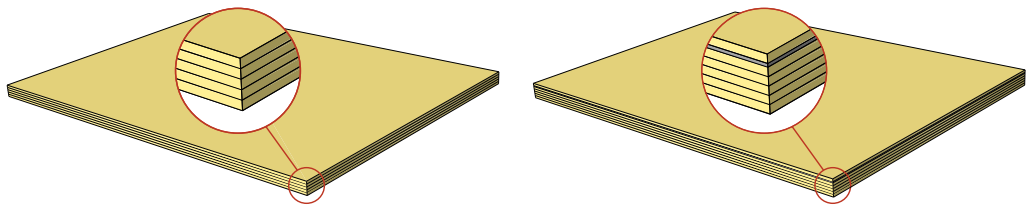

(a) Five-layer panel.

(b) Five-layer panel with two additional layers.

Figure 5.1: CLT panels that were used for the case studies, 4 m × 3 m. The yellow colour indicates timber and the grey colour concrete or elastomer.

[52], and oak from [53]. For all lamination materials, however, Poisson's ratios were $\nu_{LR} = \nu_{LT} = 0.45$ and $\nu_{RT} = 0.28$, since these have been shown to not affect the vibration response (cf. Figure 4.4). The same loss factor was used for all timber lamination materials, $\eta = 0.02$, to easier evaluate how various other material properties affect the vibrational behaviour. The timber material properties used in the case study are presented in Table 5.1.

For the 10 mm layer, concrete or elastomer were used. The concrete was modelled as isotropic and linear elastic with density $\rho = 2\ 400$ kg/m^3, Young's modulus $E = 31\ 000$ MPa, Poisson's ratio $\nu = 0.20$ [54] and loss factor $\eta = 0.02$. The elastomer layer was modelled as isotropic and viscoelastic utilising the material model determined in [42] with material properties from [52]: the density is $\rho = 1\ 150$ kg/m^3, Young's modulus $E = 11$ MPa, Poisson's ratio $\nu = 0.43$ and the frequency-dependent storage and loss shear and bulk moduli are presented in Figure 5.2.

5.1 CHANGING LAMINATION MATERIAL

The vibrational effect of changing timber lamination material in a CLT panel was explored in **Paper B**. The use of oak was compared to using spruce, and in **Paper**

Table 5.1: Material properties for the various lamination materials. The unit of the density is kg/m^3 and the moduli are MPa.

	ρ	E_L	E_R	E_T	G_{LR}	G_{LT}	G_{RT}
Spruce	429	12 043	370	370	690	576	79
Birch	608	14 486	1 185	640	850	784	155
Oak	637	13 988	733	733	1 392	1 392	460
Compressed spruce	787	14 354	679	679	1 267	1 939	101

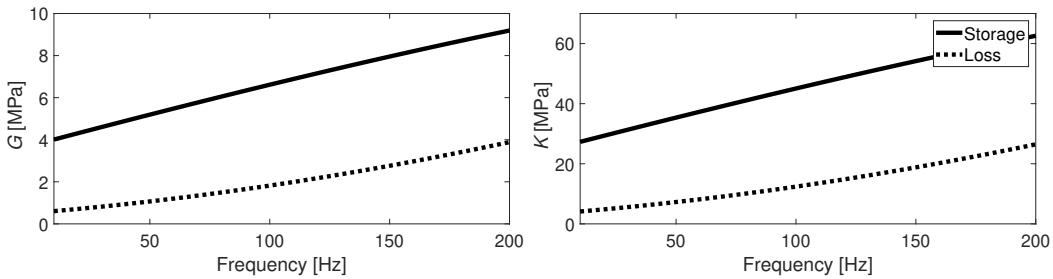

(a) Shear modulus. **(b)** Bulk modulus.

Figure 5.2: The shear and bulk moduli of the used elastomer, separated into storage and loss components. The legend is valid for both figures.

C, utilisation of birch and compressed spruce, respectively, were compared to the use of spruce.

To evaluate how the timber lamination material affects the vibrational response, the five-layer panel in Figure 5.1a was used, using spruce (reference), birch, oak and compressed spruce. In Figure 5.3, the spatially averaged mobility FRFs are presented. The mobility RMS values, normalised against the mobility RMS value of the spruce panel are presented in Figure 5.4. As can be observed, by exchanging the spruce to one of the other lamination materials, the vibrational response is decreased compared to the reference spruce panel. Here, by using compressed spruce, the mobility RMS value is approximately 50% of the mobility RMS value of the reference panel, while by using the various hardwoods, the response can be reduced to approximately 70–55% of the mobility RMS value of the spruce panel.

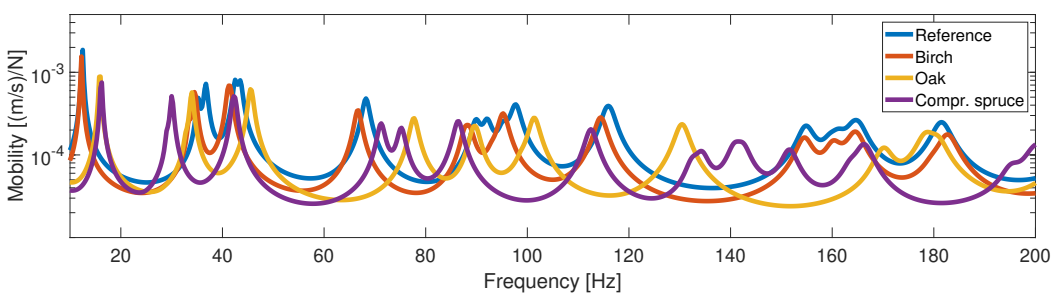

Figure 5.3: Spatially averaged mobility FRFs of spruce (reference), birch, oak and compressed spruce CLT panels.

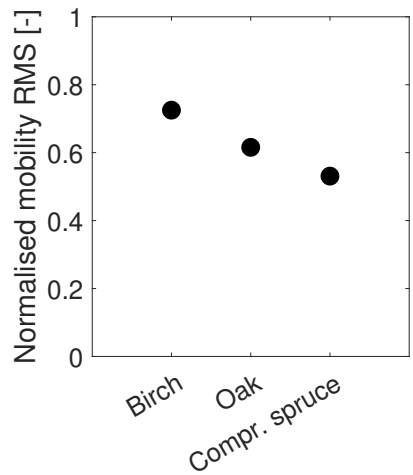

Figure 5.4: Mobility RMS values for five-layer panels of various lamination materials, normalised to the mobility RMS value of the spruce panel.

5.2 INTEGRATING A LAYER OF DIFFERENT MATERIAL

The vibrational effect of exchanging spruce lamellae with concrete lamellae was explored in **Paper A**, while the effect on integrating an elastomer layer into a CLT panel was analysed in **Papers B** and **C**.

To evaluate how integrating a material with differing material properties than timber into the panel affects the response, the panel in Figure 5.1b was used. For these analyses the reference panel has the same build-up, but the 10 mm layer is spruce oriented perpendicularly to the two adjacent layers. In Figure 5.5, spatially averaged mobility FRFs are presented for three panels; the reference panel, a panel with a concrete layer and a panel with an elastomer layer. By using a concrete layer, the panel stiffness is increased more than the mass, and hence, the resonance frequencies increase. Using an elastomer layer leads to a heavier and weaker panel, and thus the resonance frequencies are reduced. For both types of modified panels, the resonance amplitudes are reduced in comparison to the reference spruce panel. Additionally, the high damping of the elastomer leads to the resonance peaks becoming broader and less pronounced than for the two other panels, especially for higher frequencies.

5.3 COMBINATION OF BOTH METHODS

The vibration levels can be further reduced by combining the two panel modification methods. Panels made from alternative lamination materials with an integ-

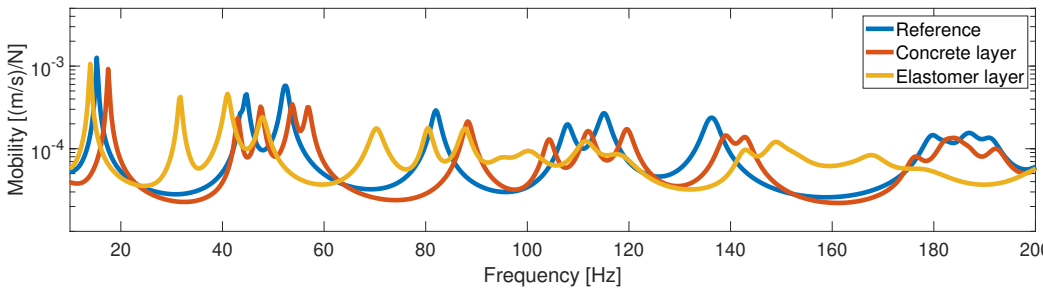

Figure 5.5: Spatially averaged mobility FRFs of spruce CLT panels with an integrated layer of spruce, concrete or elastomer.

rated concrete- or elastomer layer were studied for this purpose. The normalised mobility RMS values for panels of spruce, birch, oak and compressed spruce with a concrete layer are presented in Figure 5.6a. Here, a mobility RMS level of between 80% and 50% of the mobility RMS value of the reference spruce panel can be reached, depending on lamination material. In Figure 5.6b, the normalised mobility RMS values for panels with an integrated elastomer layer are shown. Here, a mobility RMS level of between 85–45% of the RMS value of the reference panel can be reached.

From Figure 5.6, the same trend can be observed; by inserting either a layer of concrete or a layer of elastomer, the mobility RMS values are reduced compared to the reference model. By combining a heavier and stiffer lamination material with a

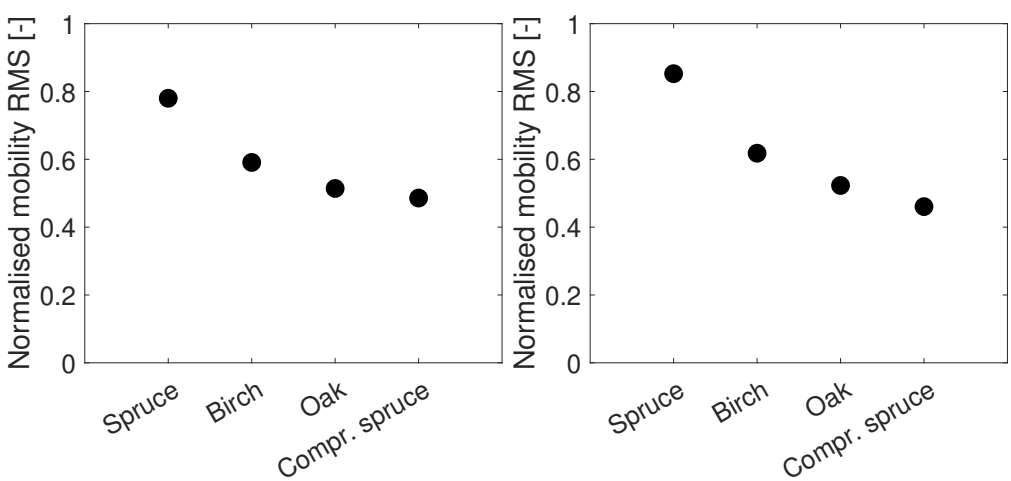

(a) Concrete layer. **(b)** Elastomer layer.

Figure 5.6: Mobility RMS values for modified panels of spruce, birch, oak and compressed spruce with an integrated layer, normalised to the mobility RMS value of the spruce panel.

layer of either concrete or elastomer, a larger reduction of the response is reached.

6 Appended papers: abstracts and author contributions

PAPER A

Khuong An Ung, Annie Bohman, Linus Andersson, Peter Persson, Sam Johansson and Lars Vabbersgaard Andersen. *Vibration reduction in cross-laminated timber panels by using individual concrete lamellae.* In proceedings of SEMC 2025, 9:th International Conference on Structural Engineering, Mechanics and Computation, Cape Town, South Africa, 2025.

The use and significance of timber structures are on the rise, especially thanks to cross-laminated timber (CLT). This engineered wood product is manufactured by stacking multiple layers of wood lamellae, each oriented perpendicularly to the one below it, and then bonding them with adhesives to form a floor or wall panel. Timber, as a building material, presents potential environmental benefits over traditional materials like concrete. However, timber constructions often exhibit greater sensitivity to dynamic loads, which underscores the importance of enhancing the design of these structural elements to mitigate vibrations and reduce low-frequency structure-borne sound. This study explores the vibrational performance of panels where lamellae of conventional spruce are partially replaced by concrete. The panel vibrations were calculated by using the finite element method. The material parameters for spruce were obtained by calibrating the finite element model to measurement data from experimental modal analysis. It was seen that appreciable reduction in the level of vibration can be achieved by replacing individual spruce lamellae with concrete. By replacing only a few percent of the lamellae, more than a halving of the vibration level of the frequency response function could be seen for a free—free panel, considering all resonance frequencies below 500 Hz.

Contributions by Annie Bohman

She advised in formulating the problem statement and determine the methodology, solution procedures and scrutinised the results as well as the conclusions. Moreover, she proofread the paper and gave feedback on the writing and presentation of the results.

PAPER B

Annie Bohman, Linus Andersson, Kent Persson and Peter Persson. *Vibration reduction in cross-laminated timber panels by using integrated elastomer layers.* In proceedings of SEMC 2025, 9:th International Conference on Structural Engineering, Mechanics and Computation, Cape Town, South Africa, 2025.

Construction with timber is becoming increasingly popular, partially due to its environmental benefits in comparison to steel and concrete. This is especially true for cross-laminated timber (CLT) panels — an engineered wood product consisting of stacked timber lamellae oriented perpendicularly to each other. CLT panels have high stiffness in comparison to its mass, which leads to a sensitivity to dynamic loads, such as footfall loading, and is thus prone to vibro-acoustic problems. Enhancing the design of these panels is therefore of importance in order to mitigate low-frequency vibrations and structure-borne noise. This study aims at numerically investigating the possibility of mitigating the vibration response of CLT panels by introducing elastomer layers in-between the timber layers, as well as by exchanging the timber material from the typical spruce to oak. Numerical simulations of the panels were performed by use of the finite element method. Frequency-dependent material properties were used for the elastomer layers. It was shown that by changing the wood species and integrating elastomer layers in CLT panels, the vibration response can be reduced in the frequency range 1–120 Hz.

Contributions by Annie Bohman

Main author of the paper and wrote the manuscript. Formulated research aims, developed the FE models, performed the calculations and drew the conclusions that were presented.

PAPER C

Annie Bohman, Linus Andersson, Kent Persson, Fredrik Ljunggren and Peter Persson. *Vibration reduction in cross-laminated timber panels using various lamination materials and integrated elastomer layers.* Journal of Building Engineering, Volume 118, 2026, 115037.

Cross-laminated timber (CLT) is increasingly used for construction of multi-storey buildings. However, ensuring satisfactory vibro-acoustic performance, particularly in the low-frequency range (typically below 200 Hz), remains a significant challenge, often necessitating add-on solutions such as floating floors. In this study, the aim was to investigate how vibration levels for CLT panels can be reduced by using various lamination materials as well as integrated elastomer layers. Finite element (FE) models were developed, calibrated and validated based on experimental modal analysis of CLT panels with and without elastomer layers. Specifically, elastic moduli of spruce, birch and compressed spruce were calibrated to experimentally obtained eigenfrequencies and mode shapes. Moreover, calibrated FE models of selected panels were used to determine and calibrate a viscoelastic material model for the elastomer layer using frequency-dependent stiffnesses and damping. Using the material model for the numerical simulations, the deviations in accelerance root mean square values were less than 1 dB compared to the experimental data. Finally, it was shown that by using birch or compressed spruce instead of spruce the vibration response could be reduced by 30% and 50%, respectively, for a realistic floor panel size. By integrating a 12 mm elastomer layer into the panels, the vibration response could be reduced by an additional 40%, compared to a panel without an elastomer layer.

Contributions by Annie Bohman

Main author of the paper and wrote the manuscript. Formulated research aims, developed the FE models, performed the calculations and drew the conclusions that were presented.

7 Concluding remarks

7.1 CONCLUSIONS

The studies have demonstrated the potential to reduce vibration levels in CLT panels by modifying the panels themselves. Throughout the studies, the low-frequency region has been the focus. Material properties serving as input data to FE models were calibrated for various timber materials and an elastomer layer. By utilising the calibrated material properties in the FE models of the CLT panels, the resulting FRFs closely resembled the experimentally obtained FRFs. In the studies, both accelerance and mobility FRFs have been used to evaluate the vibration response of the modified CLT panels. Additionally, the vibration response has been evaluated for various low-frequency ranges.

By changing the timber lamination material in the CLT panel to a denser and stiffer timber material than spruce, it was found that a mobility RMS level of between 70% and 50% of the mobility RMS value of a reference spruce panel can be reached by using birch, oak or compressed spruce.

By exchanging approximately 6% of the panel volume from spruce to concrete, a mobility RMS level of 80% of the mobility RMS level of a reference spruce panel can be reached. By integrating the concrete layer, the mass and stiffness of the CLT panel are increased, however, the stiffness is increased more than the mass, and hence the resonance frequencies are higher than for the reference spruce panel. Additionally, it was found that the positioning of the concrete affects the vibration response significantly; for a CLT panel with 5% of the timber volume exchanged for concrete lamellae, accelerance RMS values of up to 20% of the accelerance RMS value for a reference spruce panel could be reached.

By integrating an elastomer layer constituting 6% of the total panel volume into a spruce CLT panel, a mobility RMS level of approximately 80% of the mobility RMS level of a reference spruce panel can be reached. Evaluating accelerance RMS values, a CLT panel with approximately 7% of the panel volume of elastomer can reach 40% of the accelerance RMS level of a reference spruce panel. This elastomer

adds significant damping to the panel, and hence the resonance peaks are lowered. The stiffness becomes less than for the spruce panel, while the mass is increased, and hence the resonance frequencies are reduced. Additionally, when increasing the thickness of the elastomer layer, the vibration response is further reduced.

By combining the effect of creating a CLT panel of a heavier and denser timber lamination material than spruce with integrating a layer of concrete or elastomer, the response can be additionally reduced. When combining birch, oak or compressed spruce with an integrated layer of concrete, a mobility RMS value of 60–50% of the mobility RMS value of a reference spruce panel can be reached. If an elastomer layer is integrated into CLT panels of the alternative lamination materials, a mobility RMS value of between 60% and 50% of the mobility RMS value of the reference spruce panel can be reached.

Considering all CLT panel modification methods evaluated in the dissertation, it can be concluded that vibration reduction through panel modification shows significant potential. However, the investigations have also shown that e.g. panel geometry, material properties and position of elastomer or concrete layers influence the vibration response. Hence, further investigations are required to draw more definitive conclusions.

7.2 FURTHER RESEARCH

In the dissertation, the dynamic behaviour of CLT panels, altered using various modification methods, has been analysed. All panels have been analysed using free–free displacement boundary conditions and throughout the investigations, FRFs have been computed to evaluate how the modified panels perform in comparison to reference spruce panels.

To further align the research to the practical implementation of the modified panels in the construction industry, evaluating realistic displacement boundary conditions relevant for both floors and walls would be relevant. Furthermore, larger-scale analyses of inter-connected panels with non-loadbearing walls would also be relevant to study. When using realistic displacement boundary conditions and connecting multiple CLT panels, it would also be relevant to evaluate realistic loading situations, such as the dynamic response due to excitation from footfall loading. Here, also static analyses of deflection and springiness should be evaluated to verify whether floor panels fulfil such requirements. Additionally, investigating the dynamic behaviour of the modified panels at higher frequencies (up to 3 150 Hz), as well as couple the panels with air to evaluate the effects of fluid structure interaction and sound pressure in a room due to various load situations would be relevant to study.

References

[1] Abed, J., Rayburg, S., Rodwell, J., Neave, M. (2022), A Review of the Performance and Benefits of Mass Timber as an Alternative to Concrete and Steel for Improving the Sustainability of Structures, *Sustainability* **14**, 5570.

[2] Schickhofer, G. (1994), Starrer und nachgiebiger Verbund bei geschichteten, flächenhaften Holzstrukturen, Ph.D. thesis, TU Graz, Austria.

[3] United Nations Environment Programme (2025), *Global Status Report for Buildings and Construction 2024/2025: Not just another brick in the wall - The solutions exist. Scaling them will build on progress and cut emissions fast.*

[4] Oh, J.W., Park, K.S., Kim, H.S., Kim, I., Pang, S.J., Ahn, K.S., Oh, J.K. (2023), Comparative CO_2 emissions of concrete and timber slabs with equivalent structural performance, *Energy and Buildings* **281**, 112768.

[5] Younis, A., Dodoo, A. (2022), Cross-laminated timber for building construction: A life-cycle-assessment overview, *Journal of Building Engineering* **52**, 104482.

[6] Skullestad, J.L., Bohne, R.A., Lohne, J. (2016), High-rise Timber Buildings as a Climate Change Mitigation Measure – A Comparative LCA of Structural System Alternatives, *Energy Procedia* **96**, 112–123.

[7] Churkina, G., Organschi, A., Reyer, C.P.O., Ruff, A., Vinke, K., Liu, Z. Reck, B.K., Graedel, T.E., Schellnhuber, H.J. (2020), Buildings as a global carbon sink, *Nature Sustainability* **3**, 269–276.

[8] Mishra, A., Humpenöder, F., Churkina, G., Reyer, C.P.O., Beier, F., Bodirsky, B.L., Schellnhuber, H.J., Lotze-Campen, H., Popp, A. (2022), Land use change and carbon emissions of a transformation to timber cities, *Nature Communications* **13**, 4889.

[9] SLU Riksskogstaxeringen (2024), *Skogsdata 2024: Aktuella uppgifter om de svenska skogarna från SLU Riksskogstaxeringen. Tema: arter.*

[10] Forest Europe (2020), *State of Europe's Forests 2020*.

[11] Cabral, J.P., Kafle, B., Subhani, M., Reiner, J., Ashraf, M. (2022), Densification of timber: a review on the process, material properties, and application, *Journal of Wood Science* **68**, 20.

[12] Luan, Y., Fang, C.H., Ma, Y.F., Fei, B.H. (2022), Wood mechanical densification: a review on processing, *Materials and Manufacturing Processes* **37(4)**, 359–371.

[13] Švajlenka, J., Pošiváková, T. (2025), *Optimizing Construction Management: Sustainable Technologies, Waste Reduction, and Solutions for Wood-based Agricultural Structures*, chap. Construction Systems Based on Wood, Springer Nature, ISBN 978-3-031-84327-3.

[14] Jarnerö, K., Johansson, M. (2025), *Kartläggning av brandincidenter i flervåningshus med trästomme 1996–2023*.

[15] TMF – Trä- och möbelföretagen (2024), *Andel Trä Flerbostadshus 2024*.

[16] Jonasson, J., Persson, P., Danielsson, H. (2024), Mitigating footfall-induced vibrations in cross-laminated timber floor-panels by using beech or birch, *Journal of Building Engineering* **86**, 108751.

[17] Persson, P., Flodén, O., Danielsson, H., Peplow, A., Vabbersgaard Andersen, L. (2021), Improved low-frequency performance of cross-laminated timber floor panels by informed material selection, *Applied Acoustics* **179**, 108017.

[18] Liang, Y., Taoum, A., Kotlarewski, N., Chan, A., Holloway, D. (2024), Investigating Vibration Characteristics of Cross-Laminated Timber Panels Made from Fast-Grown Plantation Eucalyptus nitens under Different Support Conditions, *Buildings* **14(3)**, 831.

[19] Cheng, C.C., Haviarova, E. (2026), Mechanical performance of thin-layer hardwood cross-laminated timber panels from yellow-poplar and black walnut for interior applications, *Journal of Building Engineering* **117**, 114833.

[20] Ljunggren, F. (2023), Innovative solutions to improved sound insulation of CLT floors, *Developments in the Built Environment* **13**, 100117.

[21] Pradhan, S., Mohammadabadi, M., Entsminger, E.D., Ragon, K. (2024), Influence of Densification on Structural Performance and Failure Mode of Cross-laminated Timber under Bending Load, *BioResources* **19(2)**, 2342–2352.

[22] Satir, E., Adhikari, S., Hindman, D.P. (2024), Evaluation of bending and shear properties of mixed softwood & hardwood cross-laminated timbers, *Journal of Building Engineering* **96**, 110646.

[23] Gibson, B., Nguyen, T., Sinaie, S., Heath, D., Ngo, T. (2022), The low frequency structure-borne sound problem in multi-storey timber buildings and potential of acoustic metamaterials: A review, *Building and Environment* **224**, 109531.

[24] Bazli, M., Heitzmann, M., Ashrafi, H. (2022), Long-span timber flooring systems: A systematic review from structural performance and design considerations to constructability and sustainability aspects, *Journal of Building Engineering* **48**, 103981.

[25] Faircloth, A., Karampour, H., Hamm, P., Müller, T., Pavic, A., Reynolds, P., Gilbert, B.P., Schoenwald, S., Huang, H., Gronquist, P., Ruf, J., Brancheriau, L., Kumar, C. (2025), Global state of knowledge on human-induced sound and vibration events: defining future research directions for mass timber products, *Journal of Wood Science* **71**, 71.

[26] ISO 2631 (2003), *International standard ISO 2631-2:2003. Mechanical vibration and shock – Evaluation of human exposure to whole-body vibration - Part 2: Vibration in buildings (1 Hz to 80 Hz).*

[27] Griffin, M.J. (1996), *Handbook of Human Vibration*, Elsevier Science, ISBN 978-0-12-303041-2.

[28] Araújo Alves, J., Neto Paiva, F., Torres Silva, L., Remoaldo, P. (2020), Low-Frequency Noise and Its Main Effects on Human Health—A Review of the Literature between 2016 and 2019, *Applied Sciences* **10**, 5205.

[29] Vardaxis, N.G., Bard, D., Persson Waye, K. (2018), Review of acoustic comfort evaluation in dwellings—part I: Associations of acoustic field data to subjective responses from building surveys, *Building Acoustics* **25(2)**, 151–170.

[30] Ljunggren, F., Simmons, C., Hagberg, K. (2014), Correlation between sound insulation and occupants' perception – Proposal of alternative single number rating of impact sound, *Applied Acoustics* **85**, 57–68.

[31] Zhang, S., Zhou, J., Chui, Y.H. (2025), Deflection criteria for controlling timber floor vibrations: A 200-year evolution, *Engineering Structures* **326**, 119370.

[32] EN 1995 (2004), *European standard EN 1995-1-1:2004. Eurocode 5 – Design of timber structures – Part 1-1: General rules and rules for buildings.*

[33] EN 1995 (2025), *European standard EN 1995-1-1:2025. Eurocode 5 – Design of timber structures – Part 1-1: General rules and rules for buildings.*

[34] Caniato, M., Bettarello, F., Granzotto, N., Marzi, A., Gasparella, A. (2024), Modelling the impact sound reduction of floating floors applied on cross-laminated timber floors, *Journal of Building Engineering* **91**, 109679.

[35] Vardaxis, N.G., Bard Hagberg, D., Dahlström, J. (2022), Evaluating Laboratory Measurements for Sound Insulation of Cross-Laminated Timber (CLT) Floors: Configurations in Lightweight Buildings, *Applied Sciences* **12(15)**, 7642.

[36] Zhang, X., Hu, X., Gong, H., Zhang, J., Lv, Z., Hong, W. (2020), Experimental study on the impact sound insulation of cross laminated timber and timber-concrete composite floors, *Applied Acoustics* **161**, 107173.

[37] Guo, C., Zhou, J., Chui, Y.H. (2025), Experimental and numerical investigations on vibration performance of mass timber slab floors with floating concrete toppings, *Engineering Structures* **330**, 119919.

[38] Craig, R.R., Kurdila, A.J. (2007), *Fundamentals of Structural Dynamics*, John Wiley & Sons, Inc., 2 edn., ISBN 978-0-471-43044-5.

[39] Chopra, A.K. (2020), *Dynamics of Structures: Theory and Application to Earthquake Engineering*, Pearson Education Ltd., 5 edn., ISBN 978-1-29-224918-6.

[40] Bathe, K.J. (2006), *Finite Element Procedures*, Pearson Education Ltd., ISBN 978-0-9790049-0-2.

[41] Ottosen, N., Petersson, H. (1992), *Introduction to the Finite Element Method*, Pearson Education Ltd., ISBN 978-0-13-473877-2.

[42] Negreira, J., Austrell, P.E., Flodén, O., Bard, D. (2014), Characterisation of an Elastomer for Noise and Vibration Insulation in Lightweight Timber Buildings, *Building Acoustics* **21(4)**, 251–276.

[43] Paolini, A., Kollmannsberger, S., Winter, C., Buchschmid, M., Müller, G., Rabold, A., Mecking, S., Schanda, U., Rank, E. (2017), A high-order finite element model for vibration analysis of cross-laminated timber assemblies, *Building Acoustics* **24(3)**, 135–158.

[44] Milojević, M., Racic, V., Nefovska-Danilović, M. (2025), Uncertainty analysis of CLT floor vibrations due to inherent variability in structural properties, *Journal of Building Engineering* **113**, 113725.

[45] Persson, P., Flodén, O. (2019), Effect of material parameter variability on vibroacoustic response in wood floors, *Applied Acoustics* **146**, 38–49.

[46] Dahl, K.B. (2009), Mechanical properties of clear wood from Norway spruce, Ph.D. thesis, Norwegian University of Science and Technology.

[47] Brüel & Kjær, *Piezoelectric Accelerometers for Vibration Measurements*.

[48] Brandt, A. (2023), *Noise and vibration analysis: Signal analysis and experimental procedures*, John Wiley & Sons Ltd., 2 edn., ISBN 978-1-118-96218-3.

[49] EN 338 (2016), *European standard EN 338:2016. Structural timber – Strength classes.*

[50] Allemang, R.J., Brown, D.L. (1982), A Correlation Coefficient for Modal Vector Analysis, In: *Proceedings of the 1st International Modal Analysis Conference (IMAC I)*, 110–116.

[51] Antoniou, A., Lu, W.S. (2007), *Practical Optimization: Algorithms and Engineering Applications*, Springer, ISBN 978-0-387-71107-2.

[52] Bohman, A., Andersson, L., Persson, K., Ljunggren, F., Persson, P. (2026), Vibration reduction in cross-laminated timber panels using various lamination materials and integrated elastomer layers, *Journal of Building Engineering* **118**, 115037.

[53] Bohman, A., Andersson, L., Persson, K., Persson, P. (2025), Vibration reduction in cross-laminated timber panels by using integrated elastomer layers, In: *Proceedings of SEMC 2025, 9:th International Conference on Structural Engineering, Mechanics and Computation.*, 96–101.

[54] EN 1992 (2005), *European standard EN 1992-1-1:2005. Eurocode 2: Design of concrete structures – Part 1-1: General rules and rules for buildings.*

Part II

Appended publications

Paper A

Engineering Materials, Structures, Systems and Methods for a More Sustainable Future – Zingoni (Ed.)

Vibration reduction in cross-laminated timber panels by using individual concrete lamellae

K.A. Ung, A. Bohman, L. Andersson & P. Persson
Department of Construction Sciences, Lund University, Lund, Sweden

S. Johansson
Sweco AB, Malmö, Sweden

L.V. Andersen
Department of Civil and Architectural Engineering, Aarhus University, Aarhus, Denmark

ABSTRACT: The use and significance of timber structures are on the rise, especially thanks to cross-laminated timber (CLT). This engineered wood product is manufactured by stacking multiple layers of wood lamellae, each oriented perpendicularly to the one below it, and then bonding them with adhesives to form a floor or wall panel. Timber, as a building material, presents potential environmental benefits over traditional materials like concrete. However, timber constructions often exhibit greater sensitivity to dynamic loads, which underscores the importance of enhancing the design of these structural elements to mitigate vibrations and reduce low-frequency structure-borne sound. This study explores the vibrational performance of panels where lamellae of conventional spruce are partially replaced by concrete. The panel vibrations were calculated by using the finite element method. The material parameters for spruce were obtained by calibrating the finite element model to measurement data from experimental modal analysis. It was seen that appreciable reduction in the level of vibration can be achieved by replacing individual spruce lamellae with concrete. By replacing only a few percent of the lamellae, more than a halving of the vibration level of the frequency response function could be seen for a free–free panel, considering all resonance frequencies below 500 Hz.

1 INTRODUCTION

Timber structures are gaining importance due to environmental benefits and sustainability aspects (Brandner 2013). Specifically, the usage of cross-laminated timber (CLT) panels in multistory buildings have risen in popularity over the recent decades. Introduced in the 1990s, CLT panels offer significant structural advantages. Even in cases where a CLT panel will be used as a single-span floor slab, for example, the cross-lamination provides significantly improved mechanical and hygromechanical performances compared to glulam or construction wood that offer very limited bending stiffness and capacity in the transverse direction and suffer from a poor form stability in environments with changing humidity.

Because of timber's high stiffness-to-mass ratio, timber buildings are sensitive to dynamic loading, such as footfalls, which can cause annoyance and discomfort to residents. Due to, for example, noise and vibration issues, bare CLT panels are not used as finalized floor and/or wall elements today. Improving the design of CLT panels may allow for the use of bare panels without any add-on structures such as floating floors or a layer of cast concrete.

Efforts have been made to develop solutions that can improve the vibroacoustic performance of CLT panels. The use of an integrated soft elastomer layer in CLT panels has shown promise to reduce panel vibrations (Bohman *et al.* 2025, Ljunggren 2023). Ljunggren (2023) also showed that use of the stiffer and heavier wood species birch can mitigate the vibration response. Moreover, CLT panels comprised of spruce lamellae which had been compressed to about half their height, thus approximately doubling their density, were also shown to reduce the panel vibrations appreciably. Other studies have shown that using the stiffer and heavier wood species beech, in addition to birch, in constructing the panels can significantly decrease their vibration levels (Jonasson *et al.* 2024, Persson *et al.* 2021). Further, a concrete layer cast on top of the panel could also be used to mitigate vibrations caused by foot steps (Yeoh *et al.* 2011), but may not be a materially effective measure. According to Andersen *et al.* (2022b), based on a computational framework developed by the same authors Andersen *et al.* (2022a), adding a top-layer of

DOI: 10.1201/9781003677895-12

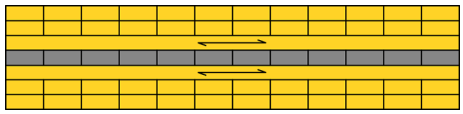

Figure 1. A spruce (yellow color) CLT panel, where the mid-layer is made of concrete (gray color).

concrete on the CLT slabs has no significant mitigation effect regarding the vibrations transmitted over longer distances within a large building.

The present paper uses the reported benefits of using lamellae that are stiffer and heavier than the standard species spruce, together with the advantages of concrete layer for mitigating step sound, as motivation to explore the vibroacoustic performance of spruce panels with some or several integrated concrete lamellae. As an example, see Figure 1, which shows a panel with the mid-layer changed to concrete. The panel vibrations were calculated using finite element (FE) models calibrated to experimental testing. The vibroacoustic performance is quantified in the paper as accelerance, involving the response of all modes below the one-third octave band center frequency 500 Hz. This ensures that the problematic frequency regions for timber structures are covered (Gibson *et al.* 2022). Early preliminary results were reported in Johansson and Ung (2024).

2 NUMERICAL ANALYSIS

In order to investigate the effects of using concrete lamellae in CLT panels, FE models have been used. In order to obtain complex frequency response functions (FRFs), the equation of motion,

$$\mathbf{M}\ddot{\mathbf{u}}(t) + \mathbf{C}\dot{\mathbf{u}}(t) + \mathbf{K}\mathbf{u}(t) = \mathbf{p}(t), \qquad (1)$$

was solved, where **M**, **C**, and **K** are the mass, stiffness, and damping matrices, respectively. The displacement and load vectors are denoted **u**(t) and **p**(t), respectively, and the dot indicates the derivative with respect to time t.

2.1 *Steady-state analyses*

Steady-state analyses were conducted using the FE models in order to calculate the accelerance FRFs:

$$\mathbf{A}(\omega) = -\omega^2 \frac{\mathbf{U}(\omega)}{\mathbf{P}(\omega)} = \omega^2(\omega^2\mathbf{M} - \mathrm{i}\omega\mathbf{C} - \mathbf{K})^{-1}, \quad (2)$$

where ω is the angular frequency in radians per second, while $\mathbf{U}(\omega)$ and $\mathbf{P}(\omega)$ are the complex-valued amplitudes of the harmonic displacements and loads, respectively.

The panels were excited under free–free conditions by a unit point load (1 N) in one of the corners, and the acceleration was evaluated in the opposite corner (cf. Figure 2) for the frequency range below 562 Hz. A frequency step of 0.3 Hz was utilised to ensure an adequte accuracy in determining the position of resonance peaks in the accelerance. The upper frequency was selected to cover the one-third octave band with the center frequency 500 Hz. The lowest one-third octave band has its center frequency at 8 Hz, so that the quasi-static region is mostly omitted.

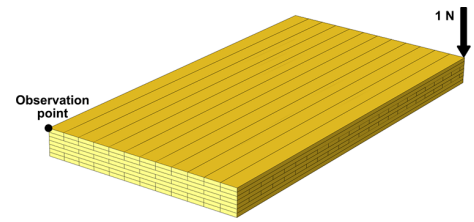

Figure 2. Positions of the load and the observation point on the FE models.

Because a unit load was used, accelerance is directly obtained as acceleration. The load and evaluation points were located on the same panel surface. Modal analysis was utilised to reduce the computational cost. All modes occurring below twice the upper frequency limit, i.e. below 1124 Hz, were used as the modal basis.

2.2 *Finite element modeling of the CLT slabs*

A three-dimensional geometry was used to allow for change in material properties of each individual lamella. Full interaction between the lamellae was used, i.e. no relative motion was allowed. Linear continuum shell elements were utilised, having eight nodes with three degrees of freedom (d.o.f.) each. One element was used in the thickness direction of each lamella, and four elements were used for each lamellae width.

The commercial software Abaqus (Dassault-Systemes 2023) was employed for developing the FE models used in the investigation. A cartesian coordinate system was employed, assuming that the radial direction of the timber lamellae aligns with the vertical axis.

3 MODEL CALIBRATION

3.1 *Experimental testing data*

A measurement campaign using experimental modal analysis was carried out on 16 nominally identical 4 m long CLT panels of the standard strength class C24 (Ljunggren 2023). The panels were excited by a shaker in a fixed position, and the vibration response was recorded by

27 accelerometers evenly distributed over the panel surface. In the study, the modal parameters in terms of natural frequencies, mode shapes, and modal damping ratios were determined for the first five free–free modes.

The damping ratio used in the present study, 0.7%, was determined as an average over all measured damping ratios, i.e. averaging over 16 panels and 5 modes. Moreover, a frequency-independent loss factor, which invokes damping in the equation of motion as a complex part of the stiffness matrix, was used as two times the damping ratio. The mean density of the weighted panels was 428 kg/m^3, and this density was applied in all the models.

The average natural frequencies of the five modes are: Mode 1, 19.7 Hz; Mode 2, 32.4 Hz; Mode 3, 52.1 Hz; Mode 4, 67.0 Hz; and Mode 5, 98.7 Hz. Modes 1, 3, and 5 are the first, second and third bending modes, respectively. Modes 2 and 4, are the first and second torsion modes, respectively.

3.2 *Calibration of elastic moduli of timber*

The measured data was employed to validate the FE modeling approach used in the study and to obtain realistic mechanical properties of the material. The elastic moduli that influence the eigenfrequencies were determined through a sensitivity analysis of the effect of each elastic modulus on the eigenfrequencies and mode shapes. One elastic modulus was varied at the time while the others were kept constant. The sensitivity analysis revealed that the elastic modulus in the longitudinal direction (E_L) significantly influenced the natural frequencies of the bending modes. The shear modulus (G_{LT}) notably affected the torsional modes, while the rolling shear modulus (G_{RT}) impacted both bending and torsional modes. The other moduli, i.e. (E_T, E_R, and G_{LR}), had negligible effects on the natural frequencies and were therefore not included in the calibration process. The values of E_T and E_R were kept to their reference C24 values, whilst G_{LR} was set equal to the calibrated G_{LT}, since the orientation of the annual rings of the lamellae is more or less arbitrary. Also, the Poisson ratios had insignificant influence. It should be noted that the tuning of the material properties did not lead to any changes in the mode order for the considered CLT panel configuration.

Moreover, to determine proper values of the elastic moduli that were deemed important in the sensitivity analysis, a Newton optimization routine (Antoniou and Lu 2007) was used to calibrate the moduli. In the calibration process, the eigenfrequencies and mode shapes resulting from the tested elastic moduli were compared to the measured averaged natural frequencies for each mode in Ljunggren (2023), targeting the lowest relative difference in measured and computed natural frequencies. In the calibration process, the objective function to be minimized, $g(f)$, was defined as the sum of the n squared frequency differences for the numerically (subscript `num') and experimentally (supscript 'exp') determined natural frequencies for the five measured modes as:

$$g = \sum_{n=1}^{N} \left(\frac{f_{n,\text{num}} - f_{n,\text{exp}}}{f_{n,\text{exp}}} \right)^2 . \tag{3}$$

The calibrated elastic moduli of spruce, as modeled in the paper, are: E_L = 12 000 MPa, E_T = E_R = 370 MPa, G_{LT} = G_{LR} = 600 MPa, G_{RT} = 62 MPa. The Poisson ratios used are ν_{LT} = 0.48, ν_{LR} = 0.42, and ν_{RT} = 0.28. These resulted in an average error of the five computed and measured eigenfrequencies of less than 1%. The obtained parameters are assumed to be practically representative for the for CLT panel also for higher frequencies.

3.3 *Material properties of concrete*

The isotropic material properties used for concrete were gathered from Eurocodes 1 (EN1991) and 2 (EN1992), respectively, and found to be: Young's modulus 31 MPa, Poisson ratio 0.2, and density 2 400 kg/m^3. Here, the same damping value as for timber was used.

4 EFFECTS OF CONCRETE LAMELLAE ON THE VIBRATION RESPONSE OF THE PANEL

The vibration reduction in cross-laminated timber panels achieved by using individual concrete lamellae was investigated for two panel sizes: a long 9 m × 2.4 m panel, and a shorter 5 m × 2.4 m panel. The larger panel represents a long-span floor slab, which is currently not common in buildings. With future developments, such a panel may be of interest, especially if floating floors and other add-on secondary structures could be avoided. The shorter panel represents a typical floor slab. The panel sizes are adopted from Jonasson *et al.* (2024). They were designed according to the European building code (EN1995) using spruce of strength class C24 (EN338). The 5 m long panel has five layers of 30 mm thick and 120 mm wide boards (except for the two outer lamellae in the length direction, which are 160 mm wide in each layer) where the outermost layer on each surface is oriented in the span direction. The 9 m long panel has seven layers of 45 mm thick boards with a width of 200 mm, where the two outermost layers at each surface are oriented in the span direction.

The primary focus of the study was the large 9 m long panel, with additional analyses on the small 5 m long panel to assess whether its dimensions and/or layups affected the conclusions drawn from the large-panel analyses. For the large panel,

more than 70 different configurations of using various numbers of concrete lamellae in the panel were investigated. The paper is limited to solely including results that make the conclusions drawn plausible. As a reference value that can be used to interpret the obtained reduction levels, changing the whole panel to concrete results in a 90% reduction of the accelerance compared to a pure spruce CLT panel.

4.1 *Accelerance reduction for the 9 m long panel*

4.1.1 *Layup ID1*

This configuration, herein referred to as ID1, is of particular practical relevance. Two thinner CLT panels may be merged with a layer of concrete in between, see Figure 3. With 14% of the volume being concrete, a 40% reduction in the accelerance was found. Moreover, changing the top-layer to concrete provides a reduction of 35%, while changing the second layer gives a 29% reduction. Thus, the results indicate that the reduction in accelerance is higher for having concrete in the mid-layer in comparison to having a concrete layer closer to the panel's surface.

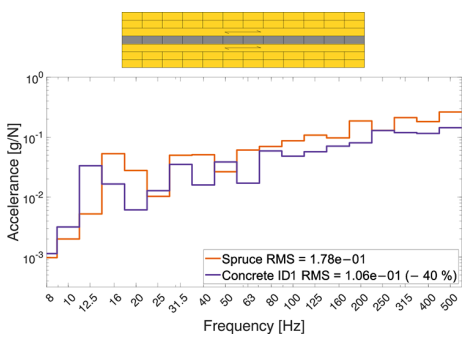

Figure 3. (top) Cross-section of layup ID1 with concrete lamellae as gray color. (bottom) Accelerance of reference spruce panel and ID1 panel.

4.1.2 *Layup ID2*

By only changing two longitudinal lamellae, see Figure 4, which corresponds to 2% of the total volume, the accelerance is reduced by 64%. In particular, this reduction is greater than changing the entire layer to concrete (cf. Figure 3). However, it must be noted that the load and observation points in the present analyses are placed on the top surface and at the diagonally opposite corners of the panel. This may favor a replacement of the wood boards by concrete lamellae along the edges. Less reduction may be observed for other configurations of the load and observation points, but no such conclusion can be supported by the data presented in this paper.

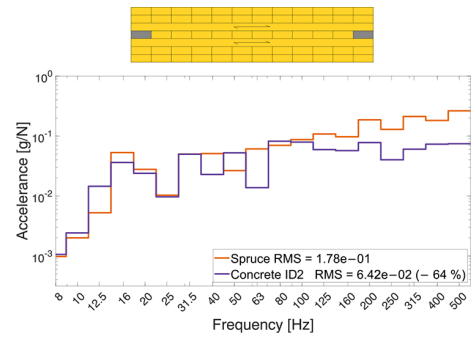

Figure 4. (top) Cross-section of layup ID2 with concrete lamellae as gray color. (bottom) Accelerance of reference spruce panel and ID2 panel.

4.1.3 *Layup ID3*

The results from ID2 indicated that a concrete frame around the perimeter of the panel was beneficial. It is further investigated here to introduce two, instead of one, layers. See Figure 5 for the layup and accelerance. This configuration corresponds to 4% of the volume being concrete, resulting in 75% reduction of the accelerance. Moreover, this reduction is greater than changing the two entire layers to concrete, which gave 61% reduction for 29% concrete.

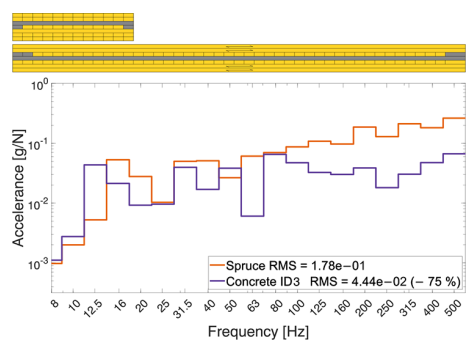

Figure 5. (top) Cross-sections of layup ID3 with concrete lamellae as gray color. (bottom) Accelerance of reference spruce panel and ID3 panel.

4.1.4 *Layup ID4*

Following the idea of utilizing a stiff and heavy concrete frame along the perimeter of the panels, configurations by changing lamellae in three of the seven layers were also studied, see Figure 6. Now, a reduction of 79% was obtained by only using 5% concrete.

4.1.5 *Layup ID5*

With this configuration, the aim was to test if amplification of the accelerance occurs when the perimeter remains as spruce, but the interior is

changed to concrete lamellae, see Figure 7. The volume share of concrete in this configuration is 38%. Indeed, a significant amplification of 48% occurs for this configuration.

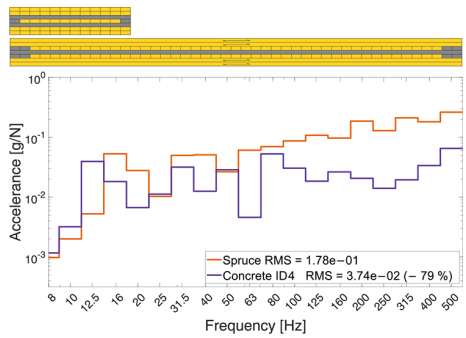

Figure 6. (top) Cross-sections of layup ID4 with concrete lamellae as gray color. (bottom) Accelerance of reference spruce panel and ID4 panel.

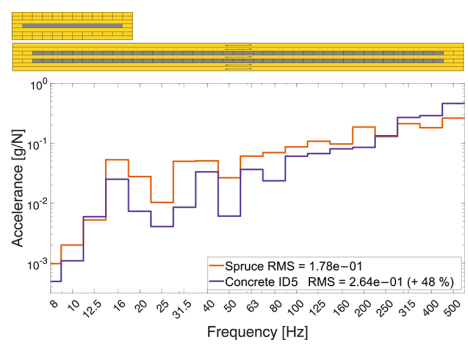

Figure 7. (top) Cross-sections of layup ID5 with concrete lamellae as gray color. (bottom) Accelerance of reference spruce panel and ID5 panel.

4.2 *Accelerance reduction for the 5 m long panel*

The corresponding results for the more common 5 m long panel had similar indications. Thus, a concrete frame placed in the mid-layers of the CLT layup around the perimeter of the panel was beneficial, whilst placing concrete lamellae in the interior may amplify the accelerance significantly.

4.3 *Summary of presented results*

In Table 1, a summary of the results for the 9 m long panel is presented. The table includes calculated RMS-values of the accelerance levels for each configuration together with the volume ratio of concrete. As seen, anything from an appreciable reduction to an amplification can be seen, depending on the position of the concrete lamellae in the CLT panel.

Table 1. Reduction in RMS-values of accelerance and volume ratios of concrete, for the configurations ID1–5.

ID	Reduction [%]	Volume ratio [%]
1	−40	14
2	−64	2
3	−75	4
4	−79	5
5	48	38

5 DISCUSSION

The most significant reduction in the accelerance takes place at the higher frequencies, approximately for one-third octave bands with center frequencies of 125–500 Hz. These frequencies are important for sound radiation from CLT panels, especially since the frequency range often includes the coincidence frequency. However, for the one-third octave band of 12.5 Hz, a vast majority of the tested configurations resulted in an amplified vibration response, which may be troublesome for floor vibration due to footfalls.

It should be noted that occasional shifts of resonance frequencies may significantly affect the response in a specific third octave band. Moreover, a consequence of using a fixed frequency range of interest, may be that the vibration level can be amplified if more resonance frequencies are located in the fixed range for a specific configuration in comparison to a different configuration, even though the peaks are not higher.

Placing the concrete lamellae around the perimeter of the panel is seen to be advantageous. However, for some support conditions (i.e. displacement boundary conditions), e.g. a four-sided simply supported panel, this effect would probably not have been seen. This needs to be further investigated in future work.

It was observed that the positions of the concrete lamellae must be carefully designed. In particular, a few percent of concrete could significantly reduce the accelerance. However, changing almost half of the lamellae to concrete may considerably amplify the accelerance if not designed properly. This highlights the need for further detailed FE analyses using realistic loading as well as support conditions to determine the optimal placement of the concrete lamellae, which is likely to be case dependent, i.e. depending on the present boundary conditions.

6 CONCLUDING REMARKS

In the paper, the vibration reduction in cross-laminated timber panels achieved by using individual concrete lamellae has been investigated

by employing calibrated finite element models. The following main conclusions can be drawn:

- Almost an 80% reduction in accelerance is achieved by changing five percent of the spruce lamellae to concrete. For comparison, a pure concrete panel results in a 90% reduction.
- An amplification of the accelerance may occur if concrete lamellae are only used in the center of the panel.
- The results are shown primarily for a 9 m long panel. However, the conclusions also hold for a regular 5 m long panel.
- Future analyses of realistic loading and support conditions are needed to determine practically achievable values of the reduction in vibration response and sound radiation.

ACKNOWLEDGEMENTS

The ÅForsk Foundation, The Önnesjö Foundation, The Södra Foundation for Research, Development and Education, and Vinnova are gratefully acknowledged for their financial support.

REFERENCES

Andersen, L., Mangliar L., Hudert M., Flodén O., and Persson P. (2022a). Early assessment of the vibroacoustic performance of large lightweight buildings. In *Current Perspectives and New Directions in Mechanics, Modelling and Design of Structural Systems, Proceedings of SEMC 2022*, Cape Town, South Africa.

Andersen, L., Mangliar L., Hudert M., Flodén O., and Persson P. (2022b). Vibroacoustic performance of multistorey buildings: A comparison og lightweight and heavy structures in the early design phase. In *Current Perspectives and New Directions in Mechanics, Modelling and Design of Structural Systems, Proceedings of SEMC 2022*, Cape Town, South Africa.

Antoniou A. and W. S. Lu (2007). *Practical Optimization – Algorithms and Engineering Applications.* New York, NY: Springer.

Bohman, A., Andersson L., Persson K., and Persson P. (2025). Vibration reduction in cross-laminated timber panels by using integrated elastomer layers. In *Proceedings of SEMC 2025*, Cape Town, South Africa.

Brandner, R. (2013, May). Production and technology of cross laminated timber (clt): A state-of-the-art report. In *Focus Solid Timber Solutions – European Conference on Cross Laminated Timber (CLT)*, Graz, Austria.

Dassault-Systemes (2023). *Abaqus Version 2023*.

EN1991 (2009). European Standard EN 1991-1-1/AC:2009. *Eurocode 1: Actions on structures – Part 1-1: General actions – Densities, self-weight, imposed loads for buildings.*

EN1992 (2005). *European Standard EN 1992-1-1:2005. Eurocode 2: Design of concrete structures – Part 1-1: General rules and rules for buildings.*

EN1995 (2004). *European Standard EN 1995-1-1:2004. Eurocode 5: Design of timber structures – Part 1-1: General – Common rules and rules for buildings.*

EN338 (2016). *European Standard EN 338:2016. Structural timber – Strength classes.*

Gibson, B., Nguyen T., Sinaie S., Heath D., and Ngo T. (2022). The low frequency structure-borne sound problem in multi-storey timber buildings and potential of acoustic metamaterials: A review. *Building and Environment 224*, 109531.

Johansson, S. and Ung K. A. (2024). Impact of different lamellae materials on vibrations in clt panels – a numerical study of concrete, air or elastomer materials. Technical Report TVSM 5270, Lund University.

Jonasson, J., Persson P., and Danielsson H. (2024). Mitigating footfall-induced vibrations in cross-laminated timber floor-panels by using beech or birch. *Journal of Building Engineering 86*, 108751.

Ljunggren, F. (2023). Innovative solutions to improved sound insulation of clt floors. *Developments in the Built Environment 13*, 100117.

Persson, P., Flodén O., Danielsson H., Peplow A., and Andersen L. V. (2021). Improved low-frequency performance of cross-laminated timber floor panels by informed material selection. *Applied Acoustics 179*, 108017.

Yeoh, D., Fragiacomo M., Franceschi M. D., and Boon K. H. (2011). State of the art on timber–concrete composite structures: Literature review. *Journal of Structural Engineering 137*, 1085–1095.

Paper B

Engineering Materials, Structures, Systems and Methods for a More Sustainable Future – Zingoni (Ed.)

Vibration reduction in cross-laminated timber panels by using integrated elastomer layers

A. Bohman, L. Andersson, K. Persson & P. Persson
Department of Construction Sciences, Lund University, Sweden

ABSTRACT: Construction with timber is becoming increasingly popular, partially due to its environmental benefits in comparison to steel and concrete. This is especially true for cross-laminated timber (CLT) panels – an engineered wood product consisting of stacked timber lamellae oriented perpendicularly to each other. CLT panels have high stiffness in comparison to its mass, which leads to a sensitivity to dynamic loads, such as footfall loading, and is thus prone to vibro-acoustic problems. Enhancing the design of these panels is therefore of importance in order to mitigate low-frequency vibrations and structure-borne noise. This study aims at numerically investigating the possibility of mitigating the vibration response of CLT panels by introducing elastomer layers in-between the timber layers, as well as by exchanging the timber material from the typical spruce to oak. Numerical simulations of the panels were performed by use of the finite element method. Frequency-dependent material properties were used for the elastomer layers. It was shown that by changing the wood species and integrating elastomer layers in CLT panels, the vibration response can be reduced in the frequency range 1–120 Hz.

1 INTRODUCTION

The use of cross-laminated timber (CLT) has increased the popularity of timber construction, partly due to its potential environmental benefits in comparison to concrete and steel. However, timber buildings have showcased problems with acoustic insulation, especially for low frequencies (20–120 Hz), for which propagating vibrations lead to the transmission of structure-borne sound. Existing sound insulation techniques, such as floating floors or mounted ceilings, are expensive and may be inadequate for solving these problems (Gibson *et al.* 2022).

CLT panels are typically manufactured using softwoods such as spruce or pine, however, research has shown that the use of hardwoods, such as birch or beech, can significantly reduce the vibration levels (Jonasson *et al.* 2024, Persson *et al.* 2021). In these studies, oak has not been included in the analyses, however, as it has similar material properties to beech, with high stiffnesses and density compared to spruce and pine, it is predicted to lead to significant vibration reduction compared to softwood CLT panels. Moreover, studies have shown that oak, in comparison to beech, shows a more robust behaviour in a changing climate (Dolos *et al.* 2016). Additionally, it has been shown that separate lamellae in CLT panels can be exchanged for other materials, such as concrete (Ung *et al.* 2025), leading to a vibration reduction.

Research has also been conducted showing that integrating an elastomer layer into the CLT panel leads to reduced vibration levels (Ljunggren 2023). Elastomers are commonly used in connections of structural elements in multi-storey timber buildings (Negreira *et al.* 2014, Flodén *et al.* 2015), to reduce the vibration transmission; however, CLT panels with integrated elastomer layers are not used in building designs today.

The present study numerically investigates vibration reduction in CLT panels using elastomer layers of various thicknesses. Moreover, spruce and oak, as well as a combination of both species were used for the panels. The investigated frequency range is 1–120 Hz.

2 MODELLING

2.1 *Geometry*

The dimensions, layup, load case and elastomer position of the analysed CLT panels are shown in Figure 1. The panels are built up by 5 layers, with a layer thickness of 30 mm. The elastomer is positioned between the top two layers. A unit load was applied in one corner of the panel, on top of the surface, and the response was evaluated in the corner diagonally opposite, on top of the surface, to determine the accelerance frequency response functions (FRFs). The out-of-plane response was considered.

Three timber configurations were investigated for the CLT panels. Firstly, using spruce for the whole panel, secondly, using oak for the whole

DOI: 10.1201/9781003677895-16

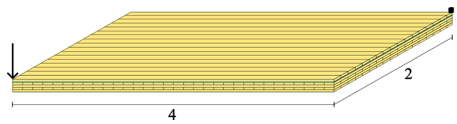

Figure 1. The investigated CLT panel. The yellow colour shows the timber, and the blue colour shows the elastomer layer. The load position is indicated by the arrow, and the evaluation point is indicated by the cylinder. The dimensions are in m.

panel, and thirdly, combining both spruce and oak for the panel. For the latter configuration, the outmost layers, i.e., the ones seen from above and below, were made of oak, and the three middle layers were made of spruce. This configuration will henceforth be referred to as spruce–oak.

The elastomer layer was analysed for three different thicknesses, 1, 5 and 10 mm, and compared to a reference case without an elastomer layer. This was done for the three timber configurations previously described, resulting in a total of 12 configurations.

2.2 *Material properties*

The timber was modelled using a rectangular coordinate system, in which the longitudinal (L), radial (R) and transversal (T) directions were considered. However, due to the uncertainness of the positioning of the growth rings, the radial and transversal direction were assumed to have the same properties, thus leading to the material being modelled as transversely isotropic. Due to the analyses being conducted in the serviceability limit state, with low vibration amplitudes, the timber was modelled as linear elastic.

For spruce, Young's moduli, E, the shear moduli, $G_{LR} = G_{LT}$, and the density, ρ, were obtained from SS338, and the rolling shear modulus, G_{RT}, from Dahl (2009). For oak, the corresponding values were obtained from Volkmer *et al.* (2014), for which the average value was calculated between the radial and transversal direction. Poisson's ratios, ν, were obtained from Persson *et al.* (2021), with the average value calculated between the longitudinal-radial and longitudinal-transversal directions. The loss factor, η, was obtained from EN 1995-1-1 (2003) for both materials. All timber material properties are presented in Table 1.

The material of the elastomer layer was Sylodyn NE (Getzner Werkstoffe 2025). The elastomer was modelled using a homogenous, isotropic, viscoelastic material model, with frequency-dependent stiffnesses and damping, using the method presented in Negreira *et al.* (2014). The results were extrapolated to include the frequency span 1–120 Hz. The material properties calibrated in Negreira *et al.* (2014) were used in this paper, in which the static Young's modulus is $E = 3.25$ MPa, Poisson's ratio is $\nu = 0.42$ and the density is $\rho = 750$ kg/m^3.

2.3 *Finite element modelling*

The panels were evaluated using finite element (FE) models, using the commercial FE software Abaqus (Dassault Systémes SIMULIA 2023). All layers in the panels were assumed to have full interaction with each other. The panels were modelled using free–free displacement boundary conditions. Eight-node solid shell elements of size 0.05 m, with one element in the thickness direction, were used for the timber, and the elastomer was modelled using eight-node hybrid elements of size 0.05 m, with one element in the thickness direction.

Steady-state analyses were conducted using frequency increments of 0.25 Hz. The damping of the timber was applied as a loss factor, resulting in rate-independent damping. The dynamic stiffness matrix can thus be expressed as

$$\mathbf{D} = -\omega^2\mathbf{M} + \mathbf{K}(1 + \mathrm{i}\eta), \tag{1}$$

where ω is the angular frequency, $\mathbf{M}$ is the mass matrix, $\mathbf{K}$ is the stiffness matrix, i is the imaginary unit and η is the loss factor.

Frequency dependent FRFs can be expressed based on acceleration,

$$\widehat{\mathbf{a}} = -\omega^2\mathbf{D}^{-1}\widehat{\mathbf{f}} = \mathbf{H_a}\widehat{\mathbf{f}}, \tag{2}$$

where $\widehat{\mathbf{f}}$ is the force amplitude, and $\mathbf{H_a}$ contains the acceleration FRFs.

The results were evaluated as accelerance, using the magnitude of the complex amplitude. The reference value for the calculations of the dB-levels was $a_{ref} = 1$ m/s^2.

2.4 *Evaluation metrics*

For evaluating the results with a single number rating, the root mean square (RMS) value was

Table 1. Material properties for spruce and oak. All elastic moduli, E and G, are in MPa, Poisson's ratios, ν, are dimensionless, the density, ρ, is in kg/m^3, and the loss factor, η, is dimensionless.

	E_L	E_R	E_T	G_{LR}	G_{LT}	G_{RT}	ν_{LR}	ν_{LT}	ν_{RT}	ρ	η
Spruce	11 000	370	370	690	690	49	0.45	0.45	0.28	420	0.02
Oak	13 988	732.5	732.5	1 392	1 392	460	0.45	0.45	0.28	637	0.02

used, expressed as

$$a_{RMS} = \sqrt{\frac{1}{N}\sum_{j=1}^{N} \widehat{a}_j^2}, \quad (3)$$

in which N is the number of frequency increments, j is the frequency increment in question and $\widehat{a}_j$ is the accelerance magnitude of increment j.

To compare the resonance frequencies of the various configurations, a normalised relative frequency difference (NRFD) was used, defined as

$$\text{NRFD} = \frac{f_{m,A} - f_{m,B}}{f_{m,B}}, \quad (4)$$

in which $f_{m,A}$ and $f_{m,B}$ are eigenfrequencies number m for configurations A and B.

To ensure that the frequencies corresponding to the same operational deflection shapes were compared, the modal assurance criterion (MAC) (Allemang and Brown 1982) was used, defined as

$$\text{MAC} = \frac{|(\Phi_{m,A})^T(\Phi_{n,B})|^2}{(\Phi_{m,A})^T(\Phi_{m,A})(\Phi_{n,B})^T(\Phi_{n,B})}, \quad (5)$$

where $\Phi_{m,A}$ and $\Phi_{n,B}$ are the mode shapes of numbers m and n of configurations A and B, respectively.

3 RESULTS

3.1 *CLT panels of spruce, oak and spruce–oak*

To compare the effect of the timber configurations, i.e., spruce, oak and spruce–oak, on the vibration response of the CLT panels, analyses were first conducted without elastomer layers. The accelerance FRFs are presented in Figure 2.

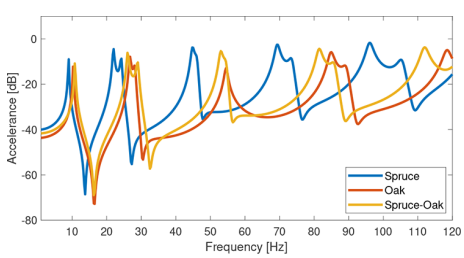

Figure 2. Accelerance FRFs for CLT panels of spruce, oak and spruce–oak without an elastomer layer.

The modes appear in the same order for all timber configurations. This order is Bending 1, Torsion 1, Bending 2, Torsion 2, Bending 3, Torsion 3, Bending 4, Torsion 4 and Bending 5. For oak and spruce–oak, the last mode under 120 Hz is Torsion 4; hence, spruce has an additional mode in the frequency range. The mode shapes are presented in Figure 3. Note that Torsion 2 and Bending 3, at approximately 45–55 Hz, are very close in frequency, and thus, can be difficult to distinguish from each other. In Figure 2, this can be observed especially for the oak accelerance FRF, where the difference in frequency between these modes is 0.1 Hz, and thus, the resonance peaks merge.

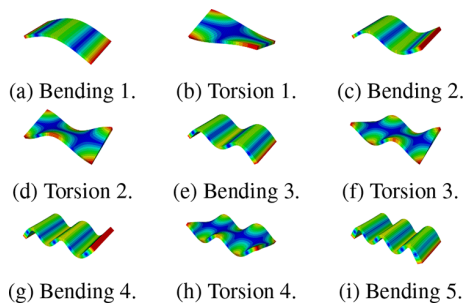

Figure 3. The mode shapes appearing in the frequency range 1–120 Hz.

The oak and spruce–oak CLT panels have higher resonance frequencies than the spruce panels for all identified resonance frequencies, which follows from the values of the material properties, where the increase for oak compared to spruce is 50% for the density, 30% for E_L, 100% for $E_R = E_T$ and $G_{LR} = G_{LT}$ and 800% for G_{RT}. The oak and spruce–oak panels have essentially identical resonance frequencies until approximately 80 Hz, above which the oak panel has higher resonance frequencies. For oak, the NRFD value is generally increasing with frequency, with the torsion modes more affected than the bending modes. For Bending mode 1, the NRFD value is 14%, while for Bending mode 5, it is 25%. The difference in resonance amplitude is generally increasing with increasing frequency, with the largest difference for Bending mode 4, with a decrease of 4 dB. The smallest decrease is 1.3 dB for Bending mode 1. For spruce–oak, however, the NRFD value is only slightly decreasing with increased frequency. Additionally, the difference in resonance amplitudes are relatively constant, especially for the first five modes. The largest difference is for Bending mode 4, with a decrease of 2.6 dB. The smallest decrease is 1.3 dB for Bending mode 3.

The RMS accelerance values for the oak and spruce–oak CLT panels, normalised against the RMS value of the spruce panel, are −4.0 and −1.6 dB, respectively, i.e., the total vibration response is decreased using both oak and spruce–oak as compared to spruce.

3.2 *CLT panels with elastomer layers*

Accelerance FRFs for spruce, oak and spruce–oak CLT panels with elastomer layers of thickness 1, 5 and 10 mm are presented in Figure 4. Generally, adding the elastomer layer to the panels leads to decreased resonance frequencies and decreased resonance amplitudes in comparison to the panel without an elastomer layer. For all cases, the torsion modes are more affected by the integration of the elastomer layer than the bending modes; the torsion modes generally have both higher absolute NRFD values, and larger differences at the peaks. The mode that is affected the most, for all timber configurations, in the studied frequency range is Torsion mode 4. Integrating the elastomer layer into the CLT panels does not change the order of the modes.

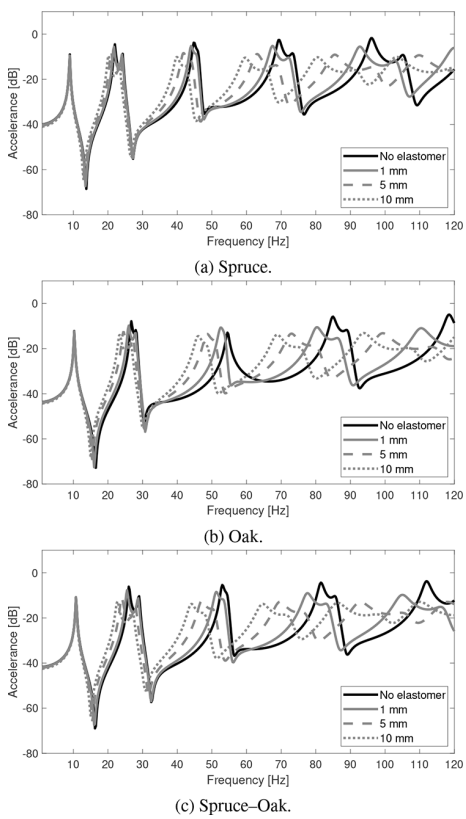

(a) Spruce.

(b) Oak.

(c) Spruce–Oak.

Figure 4. Accelerance FRFs for CLT panels of spruce, oak and spruce–oak with an elastomer of thickness 1, 5 or 10 mm, compared to the configurations without an elastomer.

In Figure 4a, it can be observed that since the resonance frequencies for the spruce panels are decreased by the elastomer layer, additional modes show up in the studied frequency span. Using a 5 mm elastomer layer adds Torsion mode 5, and a 10 mm elastomer layer in addition adds Bending mode 6. Furthermore, the results indicate that with increasing elastomer thickness, the resonance frequencies and resonance amplitudes are increasingly reduced. The average decrease of resonance frequency is 1.7%, 6.0% and 9.4% for panels with a 1, 5 and 10 mm elastomer layer, respectively. As for the resonance amplitudes, the average reduction is 1.8, 4.7 and 6.3 dB, respectively.

For the oak panels presented in Figure 4b, the resonance amplitudes of Torsion mode 2 and Bending mode 3 could not be distinguished from each other. Thus, even though both amplitudes could be identified by inserting the elastomer layer, it cannot be determined how the resonance amplitude is affected as compared to the panel without an elastomer. As for the spruce panels, the resonance frequencies are decreased by adding the elastomer layer, and thus, using a 5 and 10 mm elastomer layer, Bending mode 5 appears in the investigated frequency span. The average reduction of resonance frequencies is 3.2%, 8.8% and 12.6% for panels with a 1, 5 and 10 mm elastomer layer, compared to a panel without an elastomer. The resonance amplitudes are, on average, reduced with 3.3, 5.6 and 6.5 dB, for each respective thickness.

For the spruce–oak panels shown in Figure 4c, the same trends are shown as for the spruce and oak panels, in which the resonance frequencies are decreased by integrating the elastomer layer. A 1 mm elastomer layer leads to Bending mode 5 appearing in the investigated frequency span, and by using a 5 mm elastomer layer, also Torsion mode 5 appears. The average resonance frequency reduction is 2.7%, 9.0% and 13.5% for panels with elastomer layers of thickness 1, 5 and 10 mm, respectively, as compared to a panel without an elastomer. The resonance amplitudes are on average reduced by 2.8, 6.0 and 7.3 dB, respectively.

The accelerance RMS values of all investigated CLT panels from Figure 4 are presented in Table 2. Here, the values are normalised against the RMS value of a spruce panel without an elastomer layer. A negative value indicates a reduction.

Table 2. Accelerance RMS values for spruce, oak and spruce–oak CLT panels with elastomer layers of various thicknesses, normalised against the RMS value for a spruce panel without an elastomer layer.

	Spruce	Oak	Spruce–Oak
No layer	ref.	−4.0	−1.6
1 mm	−0.8	−5.7	−3.8
5 mm	−2.2	−7.1	−5.2
10 mm	−3.0	−7.3	−5.5

From this table, it can be observed that integrating the elastomer layer into the panels results in lowered accelerance RMS values for all cases. For the spruce panels, the reduction when comparing 1 and 5 mm to 5 and 10 mm, is 0.8 and 1.4 dB, respectively. For oak and spruce–oak, the largest reduction of RMS value is obtained by adding a 1 mm elastomer layer, as compared to a panel without an elastomer layer, with a reduction of 1.7 and 2.2 dB, respectively. The reduction between 1 and 5 mm is 1.4 dB for both oak and spruce–oak, but between 5 and 10 mm, the reduction is only 0.2 and 0.3 dB, respectively.

4 DISCUSSION

Free–free displacement boundary conditions and a unit load positioned in one panel corner have been considered when determining the accelerance FRFs in this study. FRFs give insight into the dynamic behaviour of the studied panels. Moreover, further studies are needed where realistic boundary conditions, realistic floor dimensions with multiple CLT panels connected, and realistic loading situations are considered. Implementing this, also a weighing filter corresponding to the human sensitivity to vibrations could be added, where the lowest frequencies have the most impact.

In this study, CLT panels made of a combination of spruce and oak have been analysed numerically. Today, in practice, these panels would be difficult to manufacture, due to the sawmills being specialised on certain wood species. However, if these types of CLT panels could be manufactured, aesthetically they could be used without add-ons, such as floating floors or mounted ceilings, for floor and ceiling.

Comparing the accelerance RMS values of the CLT panels with 5 and 10 mm elastomer layers, it can be noted that there is no significant reduction by using 10 instead of 5 mm. Adding the elastomer layer to the panel leads to decreased resonance frequencies, i.e., a thicker elastomer layer leads to lower resonance frequencies. Thus, a larger amount of resonances appear in the investigated frequency span, but the damping of the elastomer also leads to reduced amplitudes. It is plausible that the reason for a panel with a 10 mm elastomer layer not showing significant mitigation of vibration response as compared to a panel with a 5 mm elastomer layer is due to there being more resonances in the studied frequency span. Even if the amplitudes are reduced, there are more amplitudes that affect the vibration response, as evaluated in terms of a RMS value. This is a result of using a fixed frequency interval. If instead a certain amount of modes were included in the analyses, the results would show that a 10 mm elastomer layer leads to an even higher vibration reduction than a 5 mm elastomer layer for CLT panels.

The normalised accelerance RMS value of a spruce CLT panel with a 10 mm integrated elastomer layer is −3.0 dB. For an oak CLT panel without an elastomer layer, the corresponding value is −4.0 dB, meaning that changing the timber material from spruce to oak leads to a larger vibration reduction than using a 10 mm elastomer layer in a spruce panel. These values can be compared to the spruce–oak panel without an elastomer layer, that leads to −1.6 dB normalised accelerance RMS value, i.e., a larger reduction than using a 1 mm elastomer layer in a spruce panel, which leads to a value of −0.8 dB.

5 CONCLUSIONS

In the study, a numerical investigation of the vibration response of cross-laminated timber (CLT) panels constructed with spruce, oak and a combination of both, where the top and bottom layers were oak and the middle ones were spruce, was conducted. Additionally, the effect of integrating elastomer layers of various thicknesses into the CLT panels was studied, evaluating the vibration response. The results indicate that, in the frequency span 1–120 Hz, the vibration response, evaluated as accelerance frequency response functions, can be significantly reduced both by changing the timber type, and by integrating an elastomer layer into the CLT panel. The main conclusions are presented below.

- By constructing CLT panels with oak instead of spruce, the vibration levels can be reduced, with a reduction of accelerance root mean square (RMS) value of 4.0 dB, as compared to a spruce panel.
- By exchanging the top and bottom layers of a CLT panel with oak instead of spruce, the vibration levels can be reduced, with a reduction of accelerance RMS value of 1.6 dB, as compared to a spruce panel.
- By integrating an elastomer layer into a CLT panel, the vibration levels can be reduced as compared to panels without an elastomer layer. The accelerance RMS values were decreased by 3.0, 3.3 and 3.9 dB for spruce, oak and spruce–oak, respectively, using a 10 mm elastomer.

ACKNOWLEDGEMENTS

ÅForsk foundation, Önnesjö foundation, Södra foundation, Vinnova and Erik Stenström foundation are gratefully acknowledged for their financial support.

REFERENCES

Allemang, R. J. and Brown D. L. (1982). A Correlation Coefficient for Modal Vector Analysis. In *Proceedings of the 1st International Modal Analysis Conference (IMAC I)*, pp. 110–116.

Dahl, K. B. (2009). *Mechanical properties of clear wood from Norway spruce*. Ph. D. thesis, Norwegian University of Science and Technology.

Dassault Systémes SIMULIA (2023). *Abaqus*. Dassault Systémes SIMULIA.

Dolos, K., Mette T., and Wellstein C. (2016). Silvicultural climatic turning point for European beech and sessile oak in Western Europe derived from national forest inventories. *Forest Ecology and Management 373*, 128–137.

EN 1995-1-1 (2009). *Eurocode 5: Design of timber structures – Part 1-1: General – Common rules and rules for buildings*.

EN 338 (2016). *Structural timber – Strength classes*.

Flodén, O., Persson K., and Sandberg G. (2015). Numerical Investigation of Vibration Reduction in Multi-storey Lightweight Buildings. In *Conference Proceedings of the Society for Experimental Mechanics Series*, pp. 443–453.

Getzner Werkstoffe (2025). Austria: Getzner Werkstoffe.

Gibson, B., Nguyen T., Sinaie S., Heath D., and Ngo T. (2022). The low frequency structure-borne sound problem in multi-storey timber buildings and potential of acoustic metamaterials: A review. *Building and Environment 224*, 109531.

Jonasson, J., Persson P., and Danielsson H. (2024). Mitigating footfall-induced vibrations in cross-laminated timber floor-panels by using beech or birch. *Journal of Building Engineering 86*, 108751.

Ljunggren, F. (2023). Innovative solutions to improved sound insulation of CLT floors. *Developments in the Built Environment 13*, 100117.

Negreira, J., Austrell P.-E., Flodén O., and Bard D. (2014). Characterisation of an Elastomer for Noise and Vibration Insulation in Lightweight Timber Buildings. *Building Acoustics 21*(*4*), 251–276.

Persson, P., Flodén O., Danielsson H., Peplow A., and Vabbersgaard Andersen L. (2021). Improved low-frequency performance of cross-laminated timber floor panels by informed material selection. *Applied Acoustics 179*, 108017.

Ung, K. A., Bohman A., Andersson L., Johansson S., Vabbersgaard Andersen L., and Persson P. (2025). Vibration reduction in cross-laminated timber panels by using individual concrete lamellae. In *Proceedings of the SEMC 2025 International Conference*.

Volkmer, T., Lorenz T., Hass P., and Niemz P. (2014). Influence of heat pressure steaming (HPS) on the mechanical and physical properties of common oak wood. *European Journal of Wood and Wood Products 72*, 249–259.

Paper C

Journal of Building Engineering 118 (2026) 115037

Contents lists available at ScienceDirect

Journal of Building Engineering

journal homepage: www.elsevier.com/locate/jobe

Full length article

Vibration reduction in cross-laminated timber panels using various lamination materials and integrated elastomer layers

Annie Bohman [a,*], Linus Andersson [a], Kent Persson [a], Fredrik Ljunggren [b], Peter Persson [a]

[a] Department of Construction Sciences, Lund University, Lund, 221 00, Sweden
[b] Department of Civil, Environmental and Natural Resources Engineering, Luleå University of Technology, Luleå, 971 87, Sweden

ARTICLE INFO

Keywords:
Cross-laminated timber
Experimental modal analysis
Numerical vibration analysis
Lamination materials
Elastomer layer

ABSTRACT

Cross-laminated timber (CLT) is increasingly used for construction of multi-storey buildings. However, ensuring satisfactory vibro-acoustic performance, particularly in the low-frequency range (typically below 200 Hz), remains a significant challenge, often necessitating add-on solutions such as floating floors. In this study, the aim was to investigate how vibration levels for CLT panels can be reduced by using various lamination materials as well as integrated elastomer layers. Finite element (FE) models were developed, calibrated and validated based on experimental modal analysis of CLT panels with and without elastomer layers. Specifically, elastic moduli of spruce, birch and compressed spruce were calibrated to experimentally obtained eigenfrequencies and mode shapes. Moreover, calibrated FE models of selected panels were used to determine and calibrate a viscoelastic material model for the elastomer layer using frequency-dependent stiffnesses and damping. Using the material model for the numerical simulations, the deviations in accelerance root mean square values were less than 1 dB compared to the experimental data. Finally, it was shown that by using birch or compressed spruce instead of spruce the vibration response could be reduced by 30% and 50%, respectively, for a realistic floor panel size. By integrating a 12 mm elastomer layer into the panels, the vibration response could be reduced by an additional 40%, compared to a panel without an elastomer layer.

1. Introduction

Achieving a satisfactory acoustic insulation for timber buildings is challenging and has been a subject of research for many years [1,2]. Particularly in the lower frequency range (20–200 Hz), insufficient acoustic insulation presents a significant challenge for timber buildings compared to conventional concrete buildings [2], mainly due to timber's low mass in comparison to concrete. This can lead to discomfort for occupants, even when the building complies with regulations. Vibrations transmitted through structural building elements, known as structure-borne sound, are a significant concern for residents [2]. The most common source of annoyance at low frequencies is the sound generated by people walking, referred to as impact sounds [3]. Nevertheless, timber construction remains desirable due to its potential as a sustainable construction material.

The acoustic responses in the lower frequency range is particularly relevant in the study of timber buildings, since it strongly correlates with impact sounds [4,5]. Historically, building codes have excluded frequencies below 100 Hz because they are generally

* Corresponding author.
E-mail address: annie.bohman@construction.lth.se (A. Bohman).

https://doi.org/10.1016/j.jobe.2025.115037
Received 3 October 2025; Received in revised form 4 December 2025; Accepted 18 December 2025
Available online 18 December 2025

not significant for the acoustic performance of concrete buildings [2]. This omission leads to discrepancies between calculated sound transmission ratings and occupant perceptions in timber buildings. Research from [5,6] has indicated that the correlation between single-number ratings and occupant perceptions of impact sounds is higher when frequencies down to 25 Hz are included in the evaluation.

The development of cross-laminated timber (CLT) systems, and their widespread acceptance in the building code has facilitated the increase of timber construction in multi-storey buildings [2]. CLT is an engineered wood product built up of several layers of wood, glued together with each layer oriented perpendicular to its adjacent layers [7]. Each layer is composed of several lamellae. Prefabricated CLT panels can be cut to the required dimensions, including openings, and transported to construction sites. Furthermore, CLT exhibits high in-plane strength, rendering it beneficial for long-span floors. However, long-span CLT floors are particularly susceptible to vibro-acoustic problems such as impact sound transmission and vibrations propagating through the structure [3]. In [8], a case study was conducted, investigating the reason for unexpectedly high acceleration levels in CLT floors. Here, it was found that partition walls, which are not taken into consideration in the design phase, had a significant impact on the response of the floors. Moreover, CLT walls can lead to problems with air-borne sound transmission and flanking transmission through the junctions between structural elements [9,10]. Thus, effective vibro-acoustic design and analysis of CLT panels is essential for mitigating occupant discomfort.

Examples of existing technologies for improving acoustic insulation in buildings include floating floors and mounted ceiling systems. Floating floor systems can mitigate impact sound levels above approximately 120 Hz [11], whereas mounted ceiling systems reduce impact sound levels above 60 Hz [12]. Another method for improving the acoustic performance is to use a timber-concrete-composite system in which a concrete layer is cast onto the timber. In [13], the timber-concrete-composite system was shown to be effective at frequencies greater than 100 Hz. Taking this into account, effective solutions are typically unavailable for frequencies lower than 60 Hz. Moreover, using these methods requires additional steps in the construction process compared to using the CLT panels as-is.

One approach for improving a CLT panel's acoustic performance and reduce its vibration response is to change lamination material. Typically, softwoods such as spruce or pine are used for CLT panels; however, the use of hardwoods, which have increased density and stiffness compared to spruce, has been shown to reduce the vibration levels [14–16]. In addition, the use of compressed wood in CLT panels has been investigated [17,18], where compressed lamellae were used to construct CLT panels. Wood can be compressed by various methods. Either the entire specimen is compressed, in a process called bulk densification, or only the surface is compressed through surface densification. Wood compression is often performed radially [19] using a combination of heat, moisture, and pressure [20]. Although compressed wood is not common for structural elements in buildings, as mentioned in [21], it shows potential to create high-quality construction products using compressed low-density softwoods.

Timber exhibits significant variations in material properties, even within the same species [22–24]. To investigate the vibration response of CLT panels, it is therefore often necessary to utilise a combination of measurements and numerical methods to accurately capture the behaviour. Doing this, the measurement data can, e.g., be used to calibrate material properties for the numerical models, or for validating the numerical results. For studies where both measurements and use of numerical finite element (FE) models were utilised, e.g., see [15,25,26].

To mitigate the impact sound transmission in timber buildings, elastomers are commonly introduced at element connections [27]. In [28], a study was conducted in which two two-storey mock-ups – one with screwed connections, and the other with elastomers in-between elements – were compared using experiments and numerical models. It was found that, by using elastomers, the eigenfrequencies decreased, while the mode shapes stayed unaffected. Studies evaluating the effectiveness of elastomers have yielded mixed results [29]. One study [29] compared two full-scale wooden mock-ups differing only in their element connections: one with elastomer strips between the elements and the other with screwed connections, featuring no interlayers. Results showed that for low frequencies, damping was high for modes with large deformations near the elastomer. For frequencies above approximately 70 Hz, the mean vibration levels were significantly reduced using elastomers compared to screwed connections. Conversely, below 70 Hz, the impact sound could increase by using elastomers.

A method for modelling the material properties of viscoelastic elastomers using frequency-dependent material properties was presented in [30]. This approach combined experimental data, manufacturer data sheets, and FE simulations to validate an elastomer material model. The material model was also implemented in [31], where the numerical model was successfully validated against measurement data.

In [32], experimental modal analysis (EMA) was conducted on lab-sized CLT panels, with the objective of improving the sound insulation using two methods; increasing the mass and stiffness by changing the lamination material from the typical spruce to birch or compressed spruce, and by increasing the damping by integrating an elastomer layer into the panel. The results indicated that by utilising birch or compressed spruce instead of spruce, the mobility levels, presented in one-third octave bands for the frequency range 20–125 Hz, could be decreased significantly. Additionally, for the same frequency range, by integrating an elastomer layer into the lab-sized CLT panels, the mobility levels could be substantially reduced compared to a panel without an elastomer layer.

In the present study, additional measured data from the campaign in [32] is evaluated and presented as narrow band accelerance FRFs. The experiments are, moreover, in the present paper, presented in the frequency span 10–200 Hz to extend the important low-frequency acoustic range. The FRFs were used to extract eigenfrequencies, modal damping ratios and mode shapes for the CLT panels of spruce, birch and compressed spruce. These, as well as the narrow band accelerance FRFs, were used to calibrate accurate numerical models of the various panels. The calibrated models were then utilised to develop a viscoelastic material model for the elastomer layer, calibrated to measured accelerance FRFs. Furthermore, the calibrated material properties were used to determine

the effects of using various lamination materials as well as an integrated elastomer layer on the vibration levels in CLT panels, analysed for both lab-sized panels and realistic panel sizes.

The paper is organised as follows. Section 2 describes the measurements and presents previously unpublished results from the EMA and spatially averaged narrow band accelerance FRFs between 10–200 Hz, both partially reported in [32]. In Section 3, the numerical modelling and dynamic analysis methods are introduced. In Section 4, the calibration of material properties to the measured data for CLT panels, and the development of a material model for the elastomer are presented. In Section 5, a case study is presented analysing the vibration levels of lab-sized and realistically sized five-layer CLT panels for various lamination materials. In Section 6, the impact of integrating an elastomer layer to the lab-sized and five-layer CLT panels of various lamination materials is investigated. Finally, Section 7 presents the main conclusions.

2. Experimental testing of cross-laminated timber panels

In this section, the additional measurements not previously published and a more detailed description of the experimental campaign previously reported in [32] is presented. The analysis is a re-evaluation of the raw data, without using any results obtained in [32]. In the present paper, eigenfrequencies, mode shapes, modal damping ratios and narrow band accelerance FRFs from 10–200 Hz were determined for 25 separate panels. In [32], only the lowest five eigenfrequencies, mode shapes and modal damping ratios were presented for all panels, while mobility FRFs were presented in the one-third octave bands 20–125 Hz for solely 8 panels.

Modal analysis was conducted on 22 lab-sized single panels (cf. Fig. 1(a)), 2 lab-sized double panels with elastomer layers (cf. Fig. 1(b)) and 1 double panel without an elastomer layer (cf. Fig. 1(b), $t = 0$). The single panels were three-layer panels with a layer thickness of 20 mm. These included 16 spruce panels, 4 birch panels, and 2 compressed spruce panels; the spruce and birch panels were manufactured in a factory, and the compressed spruce panels in the laboratory. The single panels are identified as Spruce #1–16, Birch #1–4, and Compressed spruce #1–2. Panels with integrated elastomer layers, referred to as double panels, were constructed in the laboratory using two single spruce panels, glued together with the elastomer in between. Two elastomer thicknesses were considered: 2 and 12 mm. The width of all panels was 0.5 m. The length of the spruce and birch panels was 4 m, whereas the length of the compressed spruce panels was 2.4 m due to manufacturing limitations. The CLT panels made of compressed spruce were manufactured with spruce lamellae measuring 0.5 m in length, which were separately heated and mechanically pressed to a compression ratio of approximately 55% in the thickness direction. These lamellae were then used to construct the CLT panels. Throughout the preparation and execution of the experimental campaign, all panels were kept in a stationary indoor environment.

The material used for the elastomer layer was VS-10, manufactured by Swedac Acoustic [33]. The composition of VS-10 is: 35% carbon black, 25% butyl polymer, 15% EDPM polymer, 10% mineral oils, 10% fillers, and 5% additives [33]. This material is used to dampen resonant vibrations in structures. The standard thickness of VS-10 is 1 mm, but the manufacturer provided the option to merge multiple layers, enabling the use of various thicknesses. A photograph of VS-10 is presented in Fig. 2.

Note that 22 single panels were used for calibrating the timber material properties (16 spruce, wherein 4 were treated separately, 4 birch and 2 compressed spruce). This was deemed a sufficient number for the purpose of determining realistic material properties, and subsequently determining averaged moduli from this experimental campaign. For calibrating the material model for the elastomer layer, one double panel of each elastomer thickness (2 and 12 mm) was used. Preferably, there should be a larger number of double panels with elastomers, to further validate the results, however, it is believed that the number of panels is sufficient to present reliable results. Also to be noted is that the panels are lab-sized in dimensions, meaning that they are smaller than typical CLT panels; nevertheless, they are here regarded as sufficiently realistic for calibrating the material model. Additionally, CLT panels with dimensions commonly used in real-life applications are studied in Sections 5 and 6.

2.1. Experimental setup

To simulate free–free displacement boundary conditions, the panels were suspended from stiff sawhorses using rubber straps, as shown in Fig. 3. To excite the panels, an electromagnetic shaker (LDS V201) was placed underneath the position indicated by the red circle in Fig. 4. The experimental setup was chosen to adequately excite the low-frequency modes, without exciting the rigid

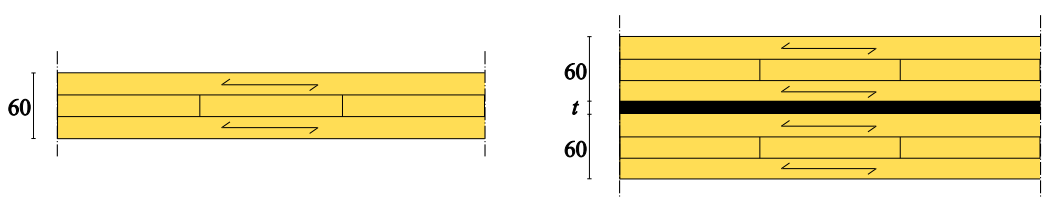

(a) Single panel. (b) Double panel.

Fig. 1. Schematics of cutouts of single and double CLT panels. The double panels were made from two single panels, glued together with an elastomer layer in between. The thickness of the elastomer is denoted by t. The dimensions are in mm.

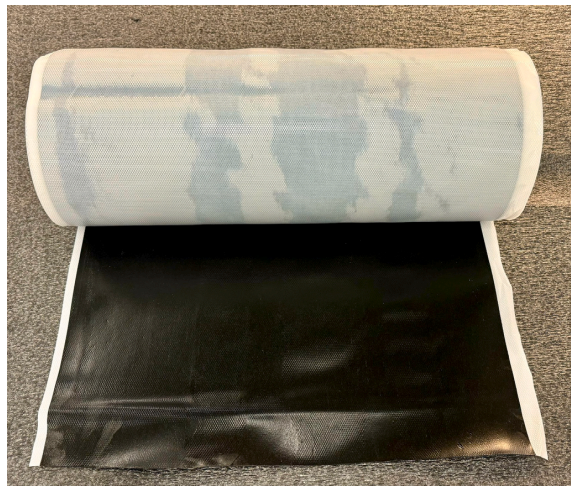

Fig. 2. Photograph of the elastomer VS-10 [33].

body modes redundantly. The out-of-plane acceleration was measured on top of the panels using uni-axial accelerometers (Brüel & Kjær 4508). For panels of length 4 m, a grid of 9 × 3 equally spaced accelerometers were used, whereas 7 × 3 were used for the 2.4 m panels, as shown in Fig. 4.

For each panel, EMA was conducted; FRFs were measured with each accelerometer, and these were used to determine the eigenfrequencies, modal damping ratios, and corresponding mode shapes. This analysis was conducted using the BK Connect software [34], using the rational fractional polynomial Z algorithm. The algorithm implements a least-squares approach to take the FRFs from all accelerometers into account when determining the sought properties [35].

The average density of each lamination material was determined by weighing panels: $\rho = 429$ kg/m^3 for spruce, $\rho = 608$ kg/m^3 for birch and $\rho = 787$ kg/m^3 for compressed spruce. No other material parameters were determined from the experimental campaign. However, for timber, the elastic moduli that affect the response were calibrated for each single panel using the measured eigenfrequencies and mode shapes (see Sections 4.1.2 and 5.1.2), and for the elastomer, the material model was calibrated using the measured accelerance FRFs (see Section 4.2).

2.2. Experimental modal analysis

Examples of FRFs for the panels of each lamination material – spatially averaged over all accelerometer positions – from the measurements are shown in Fig. 5, where the spatial averaging is given as

$$\hat{a} = \frac{1}{n}\sum_{j=1}^{n} \hat{a}_j, \tag{1}$$

where $\hat{a}$ is the spatially averaged accelerance magnitude, n is the number of accelerometers, and $\hat{a}_j$ is the accelerance magnitude of accelerometer j (cf. Eq. (4)). The accelerance reference value for the calculations of the dB levels was $a_{ref} = 1$ m/s^2 throughout this study.

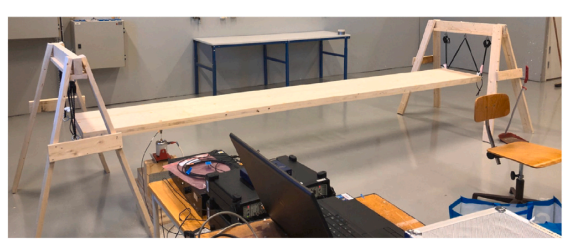

Fig. 3. CLT panel in the experimental setup; suspended using rubber straps and excited by the shaker [32].

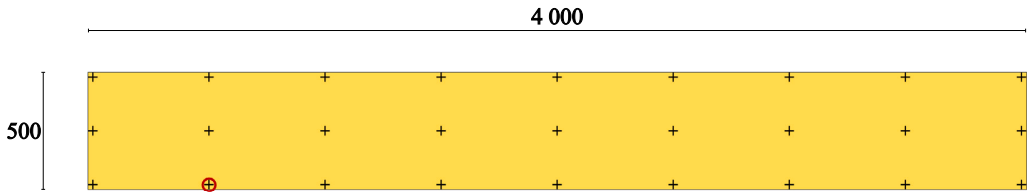

(a) 4 m panel, for spruce and birch.

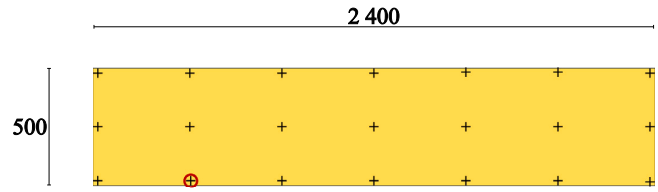

(b) 2.4 m panel, for compressed spruce.

Fig. 4. Accelerometer- and shaker placement on the CLT panels. The accelerometers were equally spaced over the panel surface. Black plus signs indicate accelerometer positions, and the red circle indicates the shaker position. The dimensions are in mm.

For the 4 m spruce and birch panels, 10 resonance frequencies were identified below 230 Hz. For the 2.4 m compressed spruce panels, 5 resonance frequencies were identified within the same frequency range. Note that for the 4 m panels, two resonance frequencies were observed in the range of 145–160 Hz, corresponding to the fourth bending and torsion modes, occasionally merging into a single peak. The same phenomenon occurs at approximately 200–230 Hz, where the resonance frequencies of the fifth torsion and bending modes occasionally merge into one peak. For the 4 m panels, the position of the shaker was close to the node line of bending modes 2 and 3 (approximately 50 and 90–110 Hz, respectively); thus, the responses of these modes were low, and consequently, could not be identified for some panels. The averaged measured eigenfrequencies of the single panels of each lamination material are presented in Table 1, corresponding to the mode shape order in Fig. 7. In Appendix A, spatially averaged narrow band accelerance FRFs are presented for all single panels, showing a comparison of the measured and computed results, using the calibrated material parameters.

The distribution of eigenfrequencies and modal damping ratios for all single panels are presented in Fig. 6. For the spruce and birch panels, the modes appearing in the frequency range 10–230 Hz are shown in Fig. 7, determined using the FRF in Fig. 5(a). For the compressed spruce panels, only the first 5 modes shown in Fig. 7 were identified for this frequency range, owing to the shorter length of the panels. Of the 10 modes, there are 5 bending and 5 torsion modes for the 4 m panels, whereas for the 2.4 m panels, there are 3 bending and 2 torsion modes. Analysing Figs. 6 and 7 together, it can be observed that for the first four modes, the bending modes (modes 1 and 3) have lower damping compared to the torsion modes (modes 2 and 4). This pattern was not observed for higher-order modes, however.

3. Finite element modelling

The numerical analyses utilised the FE method, e.g., see [36] for further details on the FE method. The CLT panels and elastomer layers were studied using the commercial FE software Abaqus [37]. Steady-state analyses of harmonic loading in the frequency domain, with frequency increments of 0.25 Hz, were considered. The frequency increments were chosen to obtain a sufficient resolution of resonance peaks.

For the purpose of studying comfort vibrations, timber can be modelled as a homogeneous orthotropic material using a rectangular coordinate system, e.g, see. [10,15,22,25,26], even if timber follows a cylindrical coordinate system due to its growth rings. For modelling of timber, the orthotropy simplification is reasonable because, otherwise, the placement and radius of the growth rings would need to be known or assumed for each lamella, which is generally not feasible. The three directions of the

Table 1
Averaged measured eigenfrequencies below 230 Hz for the spruce-, birch- and compressed spruce panels.

	f_1	f_2	f_3	f_4	f_5	f_6	f_7	f_8	f_9	f_{10}
Spruce	19.7	32.4	52.1	66.8	98.7	108	155	157	210	221
Birch	18.8	33.2	49.3	69.3	94.5	111	152	158	214	221
Compressed spruce	43.4	68.9	111	138	203	–	–	–	–	–

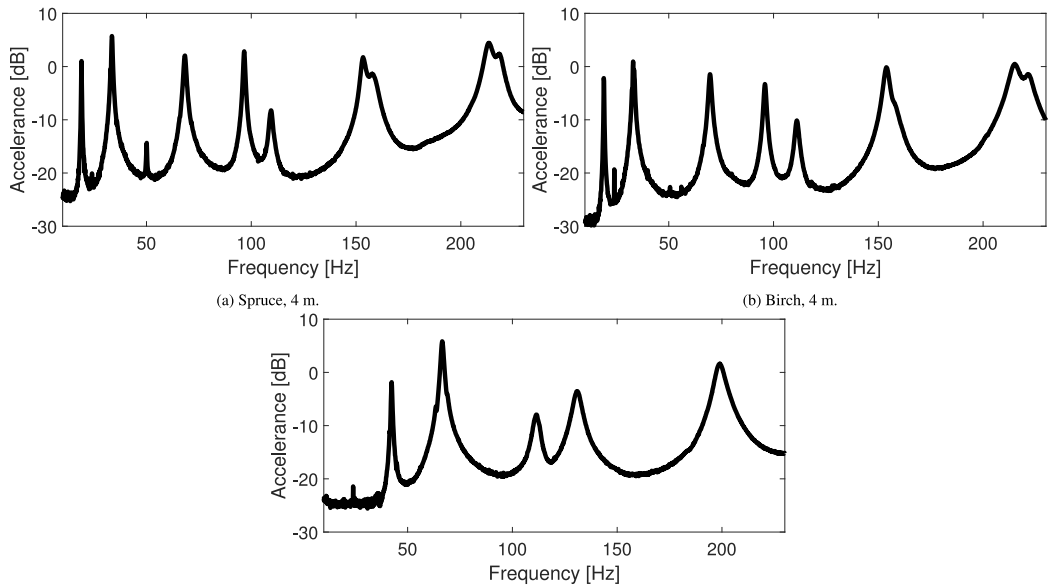

(a) Spruce, 4 m.

(b) Birch, 4 m.

(c) Compressed spruce, 2.4 m.

Fig. 5. Examples of experimentally obtained spatially averaged accelerance FRFs between 10 and 230 Hz for spruce, birch and compressed spruce CLT panels.

coordinate system are the longitudinal (L), radial (R), and transversal (T) directions. The longitudinal direction is parallel with the fibre direction, the radial direction is perpendicular to the growth rings, and the tangential direction is parallel with the growth rings. Using a rectangular coordinate system with the defined directions, it is assumed that the lamellae were sawn far from the pith. In Fig. 8, a lamella is shown with the rectangular coordinate system used for the numerical analyses.

Because the study concerns comfort vibrations where the amplitudes of load and strain are low, timber can be modelled as linear elastic, e.g., see [14,15,22,25,26]. The elastomer was modelled with an isotropic viscoelastic material model. Because the vibration amplitudes are low, the elastomer layer experiences only small strains; hence, amplitude-dependent behaviour was not included, as was also assumed in e.g. [30].

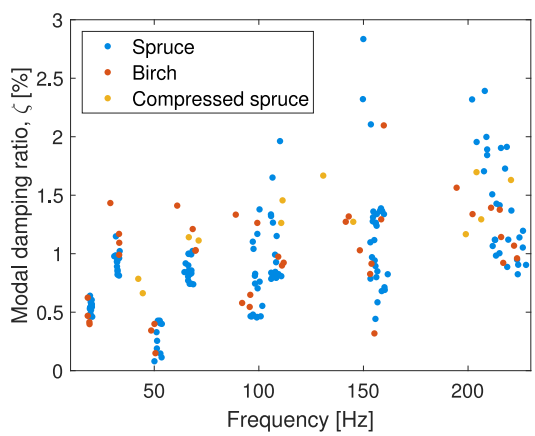

Fig. 6. Experimentally obtained eigenfrequencies and modal damping ratios, ζ, for all single panels.

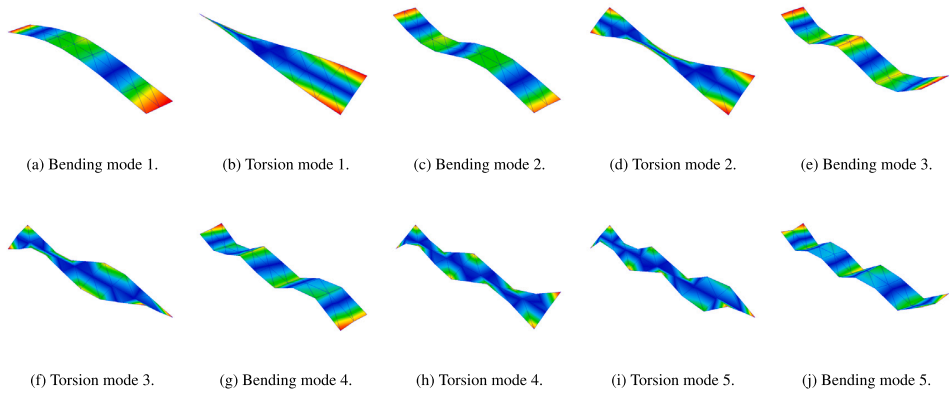

(a) Bending mode 1. (b) Torsion mode 1. (c) Bending mode 2. (d) Torsion mode 2. (e) Bending mode 3.

(f) Torsion mode 3. (g) Bending mode 4. (h) Torsion mode 4. (i) Torsion mode 5. (j) Bending mode 5.

Fig. 7. Experimentally obtained mode shapes for a 4 m panel.

3.1. Modelling of panels

For the timber, 8–node solid-shell elements with a length of 25 mm in the longitudinal and transverse directions, with one element in the thickness direction of each layer, were used. Solid-shell elements only have displacement degrees of freedom and have been shown to provide accurate vibration predictions in FE analyses of timber panels [38]. For the elastomer, hybrid 8–node elements of size 25 mm were used, with one element in the thickness direction. Here, hybrid elements were used to ensure satisfactory results for the elastomer, which is close to incompressible. Specifically, hybrid elements include an additional degree of freedom that represents the pressure stress.

The element sizes were selected to ensure sufficient accuracy for eigenfrequencies, mode shapes and accelerance FRFs up to 230 Hz. The chosen element sizes amounts to more than 30 nodes per half-sine for the highest order mode shape evaluated in this study. The chosen element size amounts to more than 30 nodes per half-sine for the highest order mode shape evaluated in this study. The chosen element types were validated by comparing the results to that of a model finely meshed with 20–node solid brick elements. In Fig. 9, a meshed lab-sized- and five-layer CLT panel is presented. For the lab-sized model, 19 200 solid shell elements and 3 200 hybrid elements were used, while 120 000 solid shell elements and 24 000 hybrid elements were used for the five-layer panel.

The surface nodes of the elastomer layer were tied to those of the CLT panels. Thus, a full interaction between the timber panels and elastomer layer is assumed, e.g., see [30].

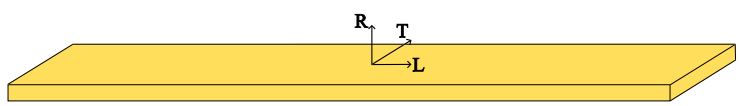

Fig. 8. Material orientation for one lamella using the rectangular coordinate system.

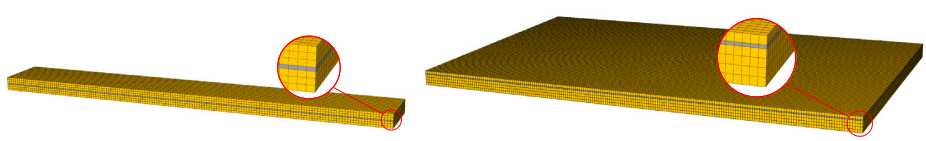

(a) Lab-sized panel, $4\ \mathrm{m} \times 0.5\ \mathrm{m}$. (b) Five-layer panel, $5\ \mathrm{m} \times 3\ \mathrm{m}$.

Fig. 9. Meshed CLT panels. The yellow and grey colours indicate timber and elastomer layer, respectively.

3.2. Vibration response to harmonic loading

This section describes the governing theory for the numerical dynamic analyses, e.g., see [39] for further details. The linear elastic equation of motion in the time domain can be written as

$$\mathbf{M}(t)\ddot{\mathbf{u}} + \mathbf{C}(t)\dot{\mathbf{u}} + \mathbf{K}(t)\mathbf{u} = \mathbf{f}(t), \tag{2}$$

where $\mathbf{M}$, $\mathbf{C}$ and $\mathbf{K}$ are the mass, damping and stiffness matrices, respectively, t is the time, $\mathbf{u}$ is the displacement vector, $\dot{\mathbf{u}}$ is the velocity vector, $\ddot{\mathbf{u}}$ is the acceleration vector and $\mathbf{f}$ is the external load vector.

Assuming harmonic loading, $\mathbf{f} = \hat{\mathbf{f}}\exp(\mathrm{i}\omega t)$, and implementing the damping as a loss factor, η, which can be determined as $\eta = 2\zeta$, where ζ is the damping ratio [40], the equation of motion can be written in the frequency domain to obtain the steady-state response, i.e.,

$$(-\omega^2\mathbf{M} + \mathbf{K}(1 + \mathrm{i}\eta))\hat{\mathbf{u}} = \hat{\mathbf{f}}, \tag{3}$$

where ω is the angular frequency, i is the imaginary unit, $\hat{\mathbf{u}}$ is the displacement amplitude and $\hat{\mathbf{f}}$ is the force amplitude. Implementing the damping as a loss factor for timber is a common approach, e.g., see [15,25].

Frequency domain transfer functions can be expressed as frequency-dependent FRFs based on displacements and accelerations,

$$\hat{\mathbf{u}} = (-\omega^2\mathbf{M} + \mathbf{K}(1 + \mathrm{i}\eta))^{-1}\hat{\mathbf{f}} = \mathbf{H_u}\hat{\mathbf{f}} \quad \text{and} \quad \hat{\mathbf{a}} = -\omega^2\mathbf{H_u}\hat{\mathbf{f}} = \mathbf{H_a}\hat{\mathbf{f}}, \tag{4}$$

where $\mathbf{H_u}$ contains the FRFs based on displacement, known as compliance, and $\mathbf{H_a}$ contains the FRFs based on acceleration, known as accelerance.

The measurements were conducted using accelerometers; thus, the raw data were accelerance FRFs. Hence, to compare the simulation and measurement FRFs directly, accelerance was used in this study. For all FRFs, the magnitude of the complex amplitude was considered in the evaluation.

4. Material model for elastomer layer

A realistic elastomer material model is required to further analyse how the elastomer layer influences the vibration response of the CLT panels. The material model was developed using the measurement data of the double panel with a 12 mm elastomer layer. The double panel with a 2 mm elastomer layer was used to validate the material model and determined material properties.

4.1. Material properties for cross-laminated timber panels

Prior to determining the material properties of the elastomer layer, the elastic moduli of the single panels without elastomer layers were calibrated. The single panels assembled with the 12 mm elastomer layer were Spruce #1 and #2, whereas Spruce #3 and #4 were used for the 2 mm elastomer layer. The purpose of calibrating the spruce material properties of the single panels was to, as accurately as possible, capture the behaviour of the single panels, such that reliable material properties could be obtained for the material model of the elastomer layer.

Because the material parameters were calibrated to the measured eigenfrequencies, gluing, possible imperfections, and growth ring orientations were implicitly considered when determining the elastic moduli. The same principle applies to damping. Because damping is a measure of the energy loss of a structure, any discrepancies in gluing or inconsistencies in manufacturing are considered in the calibrated values.

4.1.1. Sensitivity analysis

To determine which timber material parameters affect the eigenfrequencies and eigenmodes of the CLT panels, a sensitivity analysis was conducted. This was performed by varying one material parameter at a time, while the others were kept constant. The parameters were varied between the lower- and upper limits, see Table 2, using five equally spaced steps. The lower and upper limits were determined as seemingly reasonable variations in the spruce moduli. The elastic moduli varied in the sensitivity analysis were the longitudinal, radial, and transversal Young's moduli, E_L, E_R and E_T, respectively, as well as the shear moduli G_{LR} and G_{LT} and the rolling shear modulus, G_{RT}. As the average densities of the panels were known, this parameter was not varied in the sensitivity analysis. It was found that changing the values of Poisson's ratios did not influence the results, which was also demonstrated in [14,41]. Therefore, Poisson's ratios were set to $\nu_{LR} = 0.42$, $\nu_{LT} = 0.48$ and $\nu_{RT} = 0.28$, as in [14].

If, instead, the reference material parameters in Table 2 were used, the measured spatially averaged FRF for Spruce #1 and the spatially averaged FRF computed using the reference values are shown in Fig. 10. It can be observed that the computed curve does not correspond sufficiently well to the measured, especially at resonance frequencies. This illustrates the need for calibrating material properties for the panels.

The sensitivity analysis was evaluated by comparing the eigenfrequencies and mode shapes with a reference model, for which the parameters in Table 2 were used. The 10 modes identified for the 4 m panels were considered. In order to compare the eigenfrequencies, a normalised relative frequency difference (NRFD) was used, defined as

$$\mathrm{NRFD} = \frac{f_{i,A} - f_{i,B}}{f_{i,B}}, \tag{5}$$

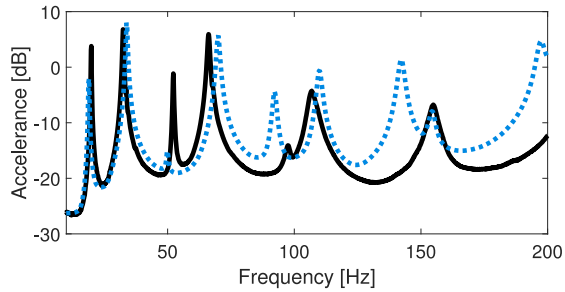

Fig. 10. Measured spatially averaged FRF for Spruce #1 (black line), compared to the computed spatially averaged FRF using the reference values (dotted blue line).

Table 2
Lower and upper limits, as well as reference values used for the sensitivity analysis for spruce. Reference values for G_{RT} from [23] and the remainder of the moduli from [42]. The moduli are in MPa.

	E_L	E_R	E_T	G_{LR}	G_{LT}	G_{RT}
Lower limit	7 000	200	200	400	400	30
Upper limit	16 000	600	600	1 000	1 000	100
Reference	11 000	370	370	690	690	49

in which $f_{i,A}$ and $f_{i,B}$ are eigenfrequencies number i for models A and B, where model B uses the reference values.

To ensure that the compared frequencies correspond to the same mode shapes, the modal assurance criterion (MAC) [43] was used, which is given by

$$\mathrm{MAC} = \frac{|(\boldsymbol{\Phi}_{i,A})^T(\boldsymbol{\Phi}_{j,B})|^2}{(\boldsymbol{\Phi}_{i,A})^T(\boldsymbol{\Phi}_{i,A})(\boldsymbol{\Phi}_{j,B})^T(\boldsymbol{\Phi}_{j,B})}, \tag{6}$$

where $\boldsymbol{\Phi}_{i,A}$ and $\boldsymbol{\Phi}_{j,B}$ are the mode shapes of numbers i and j of models A and B, respectively.

The sensitivity analysis showed that the elastic moduli that affect the eigenfrequencies and mode shapes are E_L, G_{LT} and G_{RT}, as shown in Fig. 11. The other moduli, E_R, E_T and G_{RT}, had negligible effects on the eigenfrequencies and mode shapes and will thus not be mentioned further. Subsequently, E_L, G_{LT} and G_{RT} were the moduli that were calibrated.

In Fig. 11, the NRFD plot shows how the eigenfrequencies corresponding to the matching mode shapes change with the material parameters. In this figure, it can be observed that E_L affects the bending modes but not the torsion modes, whereas varying G_{LT} results in the opposite effect. It was also found that G_{RT} affects all modes, and the effect increases with increasing frequency, which aligns with [14,15]. The MAC values showed that some modes change order when the material parameters are varied, while the same mode basis is obtained for all values. A comparison of the measured and computed mode shapes is presented in Appendix B.

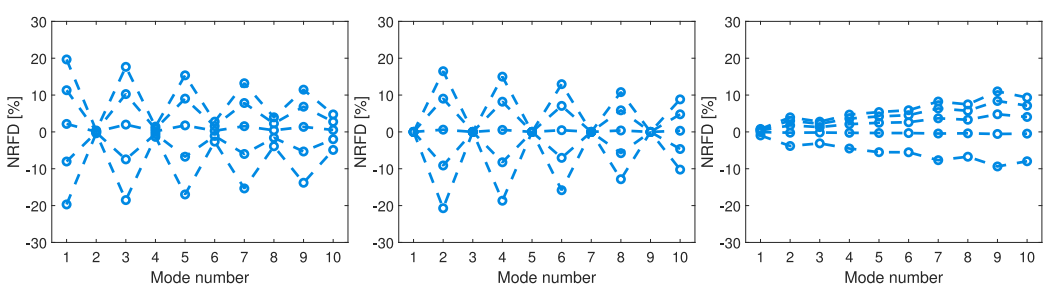

(a) Young's modulus, E_L. (b) Shear modulus, G_{LT}. (c) Shear modulus, G_{RT}.

Fig. 11. The effect of material parameters on the eigenfrequencies of spruce CLT panels, showed for the five values used in the sensitivity analysis.

4.1.2. Elastic moduli and damping

The elastic moduli E_L, G_{LT} and G_{RT} were calibrated against the measured eigenfrequencies of the four single panels using Newton optimisation. The MAC values were used to ensure that the eigenfrequencies of the same modes were compared. For further information on Newton optimisation, e.g., see [44]. The function that was minimised was the sum of the squared NRFD values of all the considered eigenfrequencies, given as

$$g = \sum_{i=1}^{N} \left(\frac{f_{calc.,i} - f_{exp.,i}}{f_{exp.,i}} \right)^2, \tag{7}$$

where $f_{calc.,i}$ and $f_{exp.,i}$ are the calculated and measured eigenfrequencies, respectively.

For the calibration, the reference values in Table 2 were used as the initial guess for each panel. The calibrated elastic moduli are presented in Table 3. The other material properties, E_R, E_T and G_{LR}, which do not affect the eigenfrequencies, were set to the reference values in Table 2. The calibrations were verified using an average absolute NRFD value,

$$\mathrm{NRFD}_{avg} = \frac{1}{n} \sum_{k=1}^{n} |\mathrm{NRFD}|_k, \tag{8}$$

where n is the number of modes and k is the mode number. This led to an average difference of 0.9%, 1%, 0.8% and 1% for Spruce #1–4, respectively.

Since Spruce #1–4 were used to construct the double panels with 12 and 2 mm elastomer layer, a minimal difference was desired between the computed and measured spatially averaged FRFs for the separate panels. Thus, the initiation of the calibration of the elastomer layer would begin with sources of error kept to a minimum. Due to this, the loss factors of Spruce #1–4 were calibrated using the difference in accelerance root mean square (RMS) value. The accelerance RMS is given by

$$a_{RMS} = \sqrt{\frac{1}{N} \sum_{k=1}^{N} \hat{a}_k^2}, \tag{9}$$

where N is the number of frequency increments and $\hat{a}_k$ is the spatially averaged accelerance of frequency increment k (cf. Eq. (1)). Furthermore, a criterion for the calibrated loss factor was that it should be within the experimentally obtained minimum and maximum (modal) loss factors presented in Table 4. The average loss factor from the measurement and the calibrated value of the loss factor are presented in the table. None of the calibrated loss factors significantly differed from the measured average values. The calibration resulted in the accelerance RMS difference between computed and measured results being 0.02, 0.03, 0.04 and 0.03 dB for Spruce #1–4, respectively. In Fig. 12, the spatially averaged FRFs are shown for Spruce #1–4, showing both the measured values and computed results using the calibrated material properties.

4.2. Calibrating material model for elastomer layer

The known material properties of the elastomer (from the manufacturer) are the density $\rho = 1150\ \mathrm{kg/m^3}$ and the shear modulus, which varies linearly between $G(100\ \mathrm{Hz}) = 6.8$ MPa and $G(200\ \mathrm{Hz}) = 10.0$ MPa [45], see Fig. 13(a). By extrapolation, the static shear modulus was determined as $G_0 = 3.8$ MPa (note that Fig. 13(a) begins at 10 Hz). Assuming that Poisson's ratio is $\nu = 0.43$, the static Young's modulus and bulk modulus were determined as $E_0 = 10.7$ MPa and $K_0 = 25.5$ MPa, respectively. From the EMA of the double panels with integrated elastomer layers, it can be observed that the damping of the entire panel generally increases with frequency, as shown in Fig. 13(b). Thus, a frequency-dependent linearly varying damping was employed.

Table 3
Calibrated elastic moduli for Spruce #1–4, needed for the calibration of the elastomer material model. The moduli are in MPa.

	E_L	G_{LT}	G_{RT}
Spruce #1	12 144	582.1	63.7
Spruce #2	12 267	601.2	69.0
Spruce #3	12 843	582.6	66.4
Spruce #4	11 697	542.1	70.4

Table 4
Loss factors for the modes of Spruce #1–4 from measurements (minimum, maximum and average) and from calibration, needed for the calibration of the elastomer material model. The loss factors are in percent.

	$\eta_{min.}$	$\eta_{max.}$	$\eta_{avg.}$	$\eta_{cali.}$
Spruce #1	0.83	3.8	2.1	3.0
Spruce #2	0.84	5.7	2.4	3.0
Spruce #3	0.80	4.8	2.4	3.4
Spruce #4	0.85	4.6	2.7	2.8

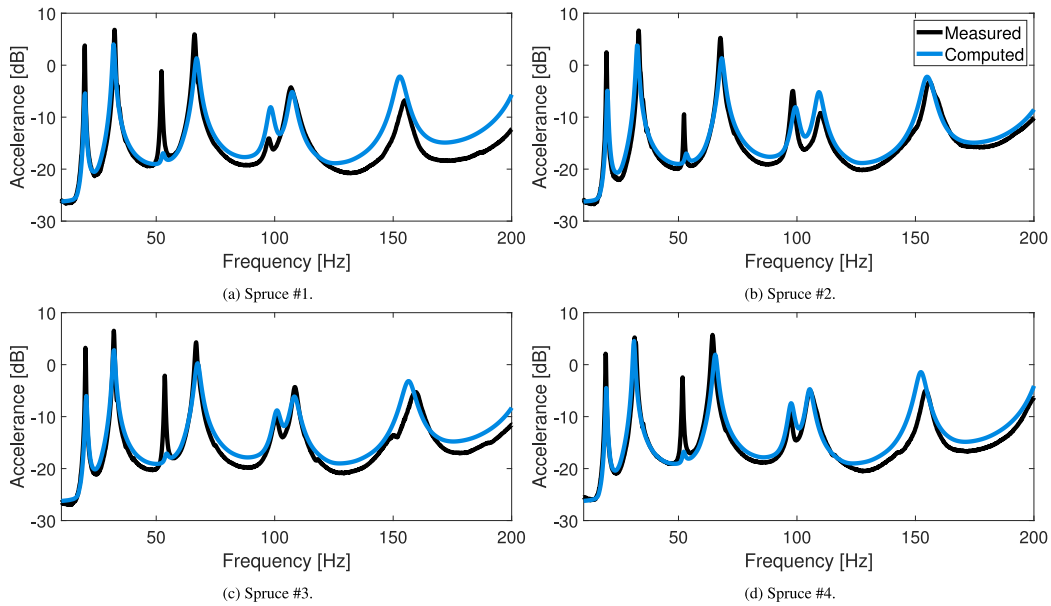

(a) Spruce #1. (b) Spruce #2.

(c) Spruce #3. (d) Spruce #4.

Fig. 12. Measured and computed spatially averaged accelerance FRFs for Spruce #1–4. The legend is valid for all subplots.

To develop a material model for the elastomer layer with frequency-dependent elastic moduli and damping, the procedure outlined in [30] was adopted. Here, the unknown material parameter is the damping, which was therefore calibrated.

For the material modelling, the frequency-dependent shear, G, and bulk moduli, K, were required. These can, in complex rectangular form, be expressed as

$$G_{dyn} = G_s + \mathrm{i}G_l \quad \text{and} \quad K_{dyn} = K_s + \mathrm{i}K_l, \tag{10}$$

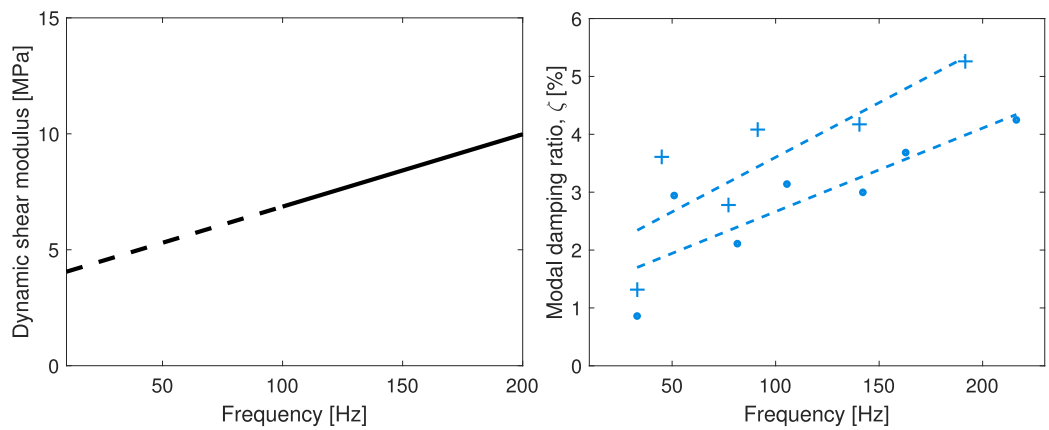

(a) Dynamic shear modulus for the elastomer. Solid line is from the manufacturer data sheet [45], dashed line is extrapolated.

(b) Measured modal damping ratios, ζ, for the panels with a 2 mm elastomer (circles) and 12 mm (plus signs), each with a linear regression curve (dashed lines). The coefficients of determination $R^2 = 0.72$ and $R^2 = 0.70$, respectively.

Fig. 13. Frequency-dependent shear modulus, G_{dyn}, and modal damping ratio, ζ.

where subscripts s and l denote the storage and loss moduli, respectively. The storage modulus is a measure of the amount of energy that the material can store elastically, whereas the loss modulus is related to its ability to dissipate energy.

In the modelling of the material, a frequency-dependent scaling factor, $\alpha(f)$, is introduced, given as

$$\alpha(f) = \frac{G_{dyn}(f)}{G_0}, \tag{11}$$

and, thus the frequency-dependent moduli can be calculated as

$$G_{dyn} = \alpha G_0 \quad \text{and} \quad K_{dyn} = \alpha K_0. \tag{12}$$

In FE modelling, the storage and loss moduli need to be known, which can be achieved by applying the trigonometric principles of

$$\begin{aligned} G_s &= G_{dyn}\cos\delta, \quad G_l = G_{dyn}\sin\delta, \\ K_s &= K_{dyn}\cos\delta, \quad K_l = K_{dyn}\sin\delta, \end{aligned} \tag{13}$$

where δ is the loss angle defined as $\delta = \arctan(\eta)$. However, for small angles, this can be simplified to $\arctan(\eta) \approx \eta$. Therefore, the loss factor, η, can be used for this purpose.

In the calibration, nine separate frequency dependencies of the loss factor were evaluated and compared. To evaluate the loss factors, the difference in accelerance RMS levels was used to compare the total vibration responses of the computed and measured spatially averaged accelerance FRFs over the frequency interval. To ensure that the resonance frequencies of the same operational deflection shapes (ODSs) were compared, the NRFD (cf. Eq. (5)) and MAC (cf. Eq. (6)) values were checked. Additionally, the error between the measured and computed FRFs, as well as the difference in resonance amplitudes were considered in the evaluation. The calibration of the linearly varying loss factor resulted in $\eta(10\text{ Hz}) = 0.15$ and $\eta(200\text{ Hz}) = 0.40$, shown in Fig. 14(a). Thus, the storage and loss parts of the shear and bulk moduli could be determined with Eq. (13), using the known frequency dependence of the shear modulus, and consequently, the frequency dependence of the bulk modulus. These are presented in Figs. 14(b)–14(e).

Usage of this viscoelastic material model for the elastomer layer (cf. Fig. 14) resulted in the accelerance FRF of the double CLT panel with a 12 mm elastomer layer shown in Fig. 15. The difference in accelerance RMS level between the measured and computed FRFs is 0.7 dB, with the measured RMS level being the lowest. The order of the identified modes is the same as in Fig. 7, except that bending mode 3 is missing from the measured FRF. It can be observed that bending mode 2 only faintly can be seen, particularly in the numerical results. When introducing the elastomer layer, the resonance peaks are lowered, and thus the ODSs and modes become less distinct. Consequently, some of them became difficult to identify. For the evaluated frequency span, the average absolute NRFD value was 5%, and the maximum NRFD value was 9% for bending mode 4.

4.3. Validation of material model for elastomer layer

The measured FRFs of the double CLT panel with a 2 mm elastomer layer were used to validate the material model and the calibrated stiffness and damping values. The computed and measured FRFs are shown in Fig. 16. For this case, the difference in RMS is 0.9 dB, with the measured value being the lowest. The modes appear in the same order as for the double panel with a 12 mm layer, but for this case, all modes can be identified both for the measurements and computations. The average absolute NRFD value for the identified modes was 3% and the largest value was 4% for torsion mode 3. Because the elastomer layer has both lower stiffness and larger mass than the timber, the resonance frequencies will decrease. Thus, for the double panel with a 2 mm elastomer, six resonance frequencies were identified in the frequency interval of interest, whereas seven resonance frequencies were identified for the double panel with a 12 mm elastomer.

5. Effects of changing lamination material

To investigate how the vibration response is affected by exchanging spruce with birch and compressed spruce, both for lab-sized and more realistically sized panels, first, the material parameters of the remaining single panels were calibrated. The purpose of this calibration was to determine realistic elastic moduli for spruce, birch and compressed spruce. The elastic moduli in the FE models were calibrated to the experimentally obtained resonance frequencies and their corresponding mode shapes for 12 spruce, 4 birch and 2 compressed spruce panels. The four spruce panels previously used in the calibration of the elastomer material model were not included in this part.

5.1. Material properties for cross-laminated timber panels

5.1.1. Sensitivity analysis

To determine the parameters of interest to calibrate for birch and compressed spruce, a sensitivity analysis was conducted in the same manner as for spruce (cf. Section 4.1.1). For birch, the lower, upper and reference values are based on [16,46–48] and compiled in [15]. For compressed spruce, the reference values were determined by increasing the reference values for spruce with the ratio of density increase for compressed spruce compared to the (non-compressed) spruce. The lower, upper and reference moduli for birch and compressed spruce are presented in Appendix C.

The results were evaluated in the same manner as for spruce using NRFD and MAC values. For birch, the same mode shapes as those of spruce were identified in the frequency range of interest, whereas the higher-order modes were different for compressed

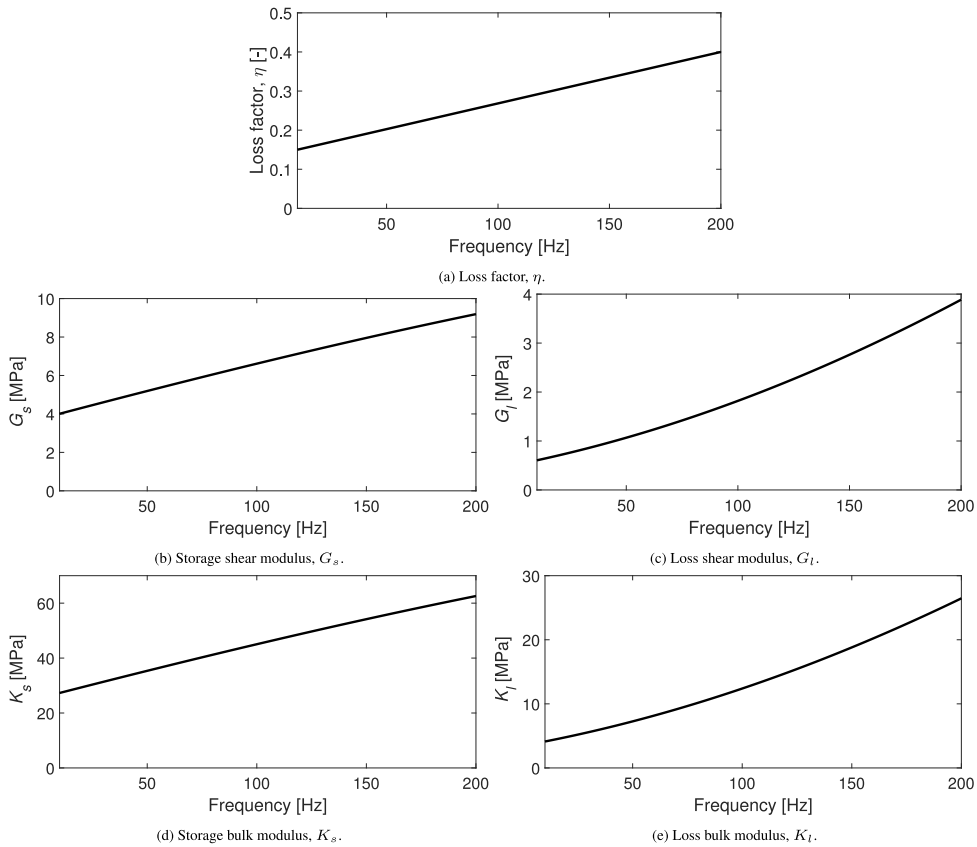

(a) Loss factor, η.

(b) Storage shear modulus, G_s.

(c) Loss shear modulus, G_l.

(d) Storage bulk modulus, K_s.

(e) Loss bulk modulus, K_l.

Fig. 14. The loss factor as well as the shear and bulk moduli of the elastomer separated into storage and loss components.

spruce. As for spruce, the modes switched order when certain material properties were varied, which was accounted for when calculating the NRFDs. The results of the sensitivity analyses for birch and compressed spruce showed that the elastic moduli that affected the eigenfrequencies in the investigated frequency range were E_L, G_{LT} and G_{RT}, that is, the same moduli as for spruce. The NRFD plots for birch and compressed spruce are presented in Appendix C.

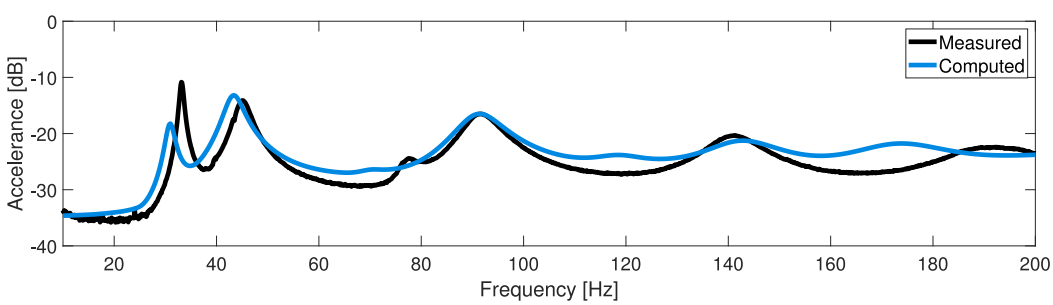

Fig. 15. Measured and computed spatially averaged accelerance FRFs for the double panel with a 12 mm elastomer layer.

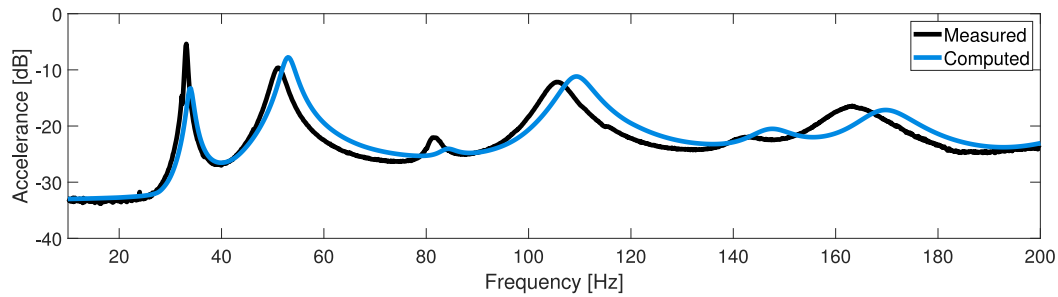

Fig. 16. Measured and computed spatially averaged accelerance FRFs for the double panel with a 2 mm elastomer layer.

5.1.2. Elastic moduli and damping

The calibration procedure described in Section 4.1.2 was followed for all remaining single panels, due to a discrepancy in response observed when comparing the measured and computed spatially averaged FRFs employing the reference values for each respective lamination material. The reference parameters from Tables 2, C.9 and C.10 were used as the initial guesses for spruce, birch and compressed spruce, respectively. The damping was determined as the average of the modal damping ratios from the measurements of each panel, translated into loss factors. In Fig. 17, E_L, G_{LT}, G_{RT} and loss factor, η, for each single panel are presented. The calibration was evaluated by comparing all resonance frequencies and mode shapes. For spruce, the average absolute NRFD value for all modes and panels was 1%. For birch and compressed spruce this value was 0.8% and 1%, respectively. The maximum individual absolute NRFD values were 3%, 2% and 3% for spruce, birch and compressed spruce, respectively.

For the spruce and birch panels, 10 modes were identified under 230 Hz. However, due to the panels of compressed spruce spanning 2.4 m instead of 4 m, the eigenfrequencies were higher, and thus 5 modes were identified in the frequency range. Consequently, the material properties were calibrated using these 5 eigenfrequencies. A convergence analysis was conducted evaluating how the material properties varied depending on how many eigenfrequencies were included in the calibration. It was found that by using 5 modes, the resulting material parameters were not significantly different compared to those determined from using 10 modes. Thus, the calibration of material properties for the compressed spruce panels was considered sufficient. Note that the 2.4 m lab-sized panels were only used for the calibration of compressed spruce properties.

For spruce, the calibrated material parameters were similar to the reference parameters listed in Table 2. For E_L, the value was generally higher than the reference, with a difference of approximately 20% between the highest and lowest calibrated values. The value of G_{LT} for each spruce panel is essentially constant, whereas G_{RT} exhibits a difference of approximately 75% between the lowest and highest. This modulus is known to vary appreciably between test specimens of the same species and strength class [16,23]. For G_{RT}, the calibrated value was markedly higher than the reference value for all spruce panels, which aligns with previous studies [16,49].

The calibrated elastic moduli of birch are generally close to the reference moduli. For E_L, two panels have a value of approximately 14 000 MPa, whereas the other two have a value of approximately 15 000 MPa. As for the spruce panels, the calibrated values of G_{LT} for the four birch panels are similar to each other. The most significant difference between the panels is for G_{RT}, where one panel has a value of approximately 100 MPa, whereas the others have a value of approximately 170 MPa. This result is reasonable because this panel, Birch #4, shows lower eigenfrequencies than the other birch panels, as can be seen in Appendix A. All the values correspond well to the measured moduli in [47,48].

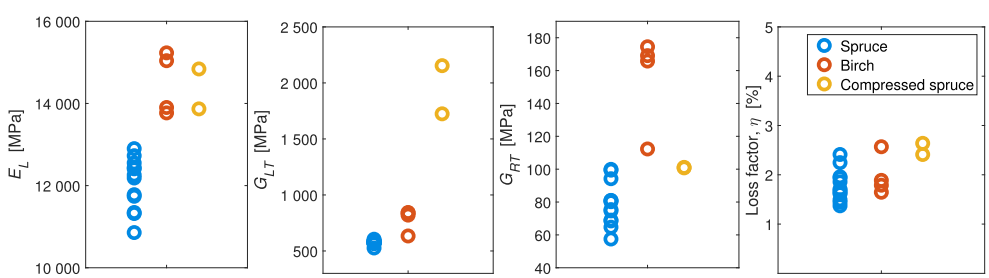

(a) Young's modulus, E_L. (b) Shear modulus, G_{LT}. (c) Shear modulus, G_{RT}. (d) Loss factor, η.

Fig. 17. Calibrated elastic moduli, E_L, G_{LT}, G_{RT} and experimentally obtained average loss factor, η, for each panel. The legend is valid for all subplots.

For the compressed spruce panels, the calibration of E_L resulted in significantly lower moduli than the reference value used as the initial guess. This is a reasonable result for compressed spruce compared to [50] for a compression ratio of approximately 50%. The value of G_{LT} is significantly higher than the calibrated moduli of both spruce and birch, which also agrees with the results in [50]. The G_{RT} values for the two panels are essentially the same, with the value being the same as a high spruce value. The accelerance FRFs of all the single panels, comparing the measured and computed results, can be found in Appendix A.

For each lamination material, the average values of the calibrated elastic moduli in Fig. 17 were used for the case studies, as listed in Table 5 (note that the spruce moduli in Table 3 are not considered in this average). This was done to obtain reasonable values based on the calibrations of material properties for each lamination material. For the non-calibrated moduli, the reference values in Tables 2, C.9 and C.10 were assigned, since these do not influence the response. The densities given in Section 2 were assigned to each lamination material.

5.2. Lab-sized cross-laminated timber panels of various lamination materials

Firstly, the calibrated material parameters were used to evaluate the response of lab-sized double panels. Both single panels used for the double panel were assigned the same material parameters. All panels were modelled with a length of 4 m and width of 0.5 m. Accelerance FRFs were calculated for these panels. The resulting spatially averaged accelerance FRFs are shown in Fig. 18. Spruce and birch show similar resonance frequencies and the same mode order; however, birch generally results in a lower accelerance. For compressed spruce, the resonance frequencies of the bending modes are lower than that of spruce and birch, whereas all torsion modes are higher in frequency. Additionally, the mode order is not the same as for spruce and birch, with torsion mode 2 and bending mode 3 switching positions and torsion mode 3 appearing above the frequency interval of interest. Instead, the resonance frequency of bending mode 4 is reduced, such that it appears in the frequency interval. For the compressed spruce panel, all bending modes occur at lower frequencies, while all torsion modes occur at higher frequencies. This behaviour reflects the material parameters: the density is approximately 80% higher, whereas E_L increases by only 20% and G_{LT} by approximately 240%. The accelerance RMS values for the lab-sized panels are presented in Table 6, normalised against spruce.

5.3. Realistic cross-laminated timber panels of various lamination materials

The vibration response of realistically sized five-layer panels was also evaluated for exchanging the spruce with birch or compressed spruce, using the material parameters in Table 5. These panels measured $5\ \text{m} \times 3\ \text{m}$ and were composed of five layers (cf. Fig. 9(b)), each 30 mm thick and oriented perpendicular to the adjacent ones. The surface layers were oriented in the 5 m direction. The displacement boundary conditions were free–free as for the lab-sized panels, and the panels were excited with a unit load in one corner, on the surface closest to the elastomer layer. The accelerance response was evaluated on the whole surface on the opposite side of the load.

In Fig. 19, the spatially averaged spruce, birch and compressed spruce accelerance FRFs are presented. Due to the increased mass of the five-layer panels, the resonance frequencies are reduced. Thus, below 200 Hz there are 22 resonances for the spruce and birch panels and 24 for the compressed spruce panel. As for the lab-sized panels, spruce and birch show similar resonance

Table 5
Moduli and loss factors used for the case studies in Sections 5.2, 5.3, 6.1 and 6.2. The moduli are in MPa and the loss factor is in percent.

	E_L	E_R	E_T	G_{LR}	G_{LT}	G_{RT}	η
Spruce	12 043	370	370	690	575.9	78.8	1.8
Birch	14 486	1185	640	850	784.2	155.4	2.0
Compressed spruce	14 354	679	679	1267	1939.1	101.0	2.5

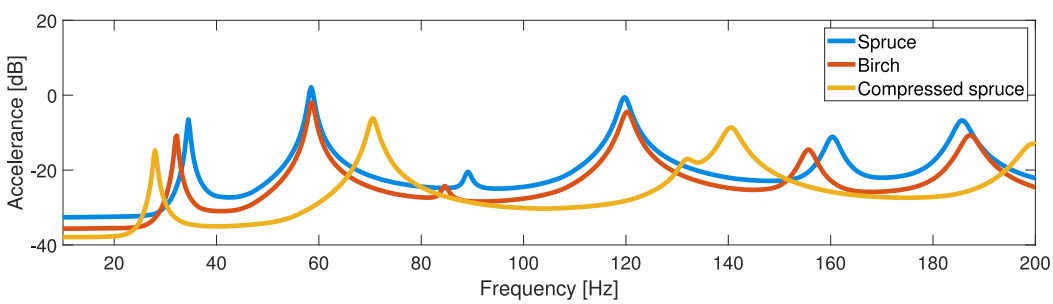

Fig. 18. Computed spatially averaged accelerance FRFs of lab-sized double panels of spruce, birch and compressed spruce without an elastomer layer.

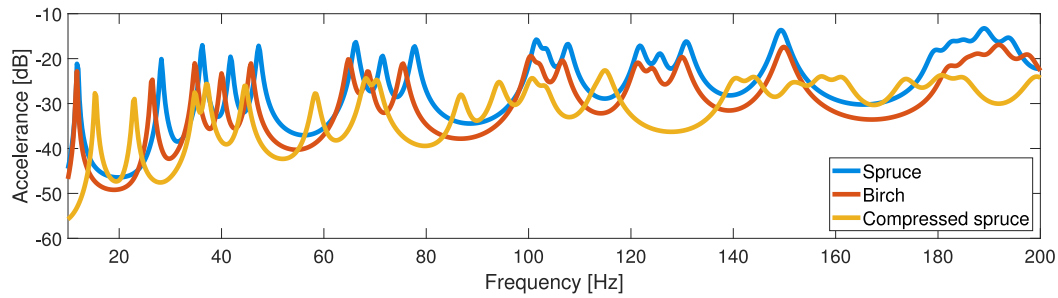

Fig. 19. Computed spatially averaged accelerance FRFs for the spruce, birch and compressed spruce five-layer panels without an elastomer layer.

Table 6
Reduction in accelerance RMS values for the lab-sized and five-layer panels of spruce, birch and compressed spruce, normalised against spruce of each dimension. The values are in dB and percent. The reductions in percent are calculated as $1 - a_{RMS}/a_{RMS,ref}$.

	Birch		Compressed spruce	
	dB	%	dB	%
Lab-sized	3.5	33	6.4	52
Five-layer	3.4	32	6.9	55

frequencies and overall behaviour, with all modes appearing in the same order, however the response is generally lower for birch. In contrast, for the compressed spruce panels, the resonance frequencies of the bending modes are lower in frequency, while the torsion modes are higher than both spruce and birch; as for the lab-sized panels. Note that unlike the lab-sized panels, the first mode in the investigated frequency range in Fig. 19 is torsion 1 for all panels, owing to the change of dimensions.

The accelerance RMS values for the five-layer panels are presented in Table 6, normalised against spruce. From Table 6 it can be observed that the effect of exchanging the spruce to birch or compressed spruce seems to be the same for the tested panel dimensions. By utilising birch, the RMS values are approximately lowered by 30% compared to spruce. By exchanging the spruce for compressed spruce the RMS values are approximately halved. This was an expected result because birch has been shown to reduce the vibration levels of CLT panels [14,15]. The use of compressed spruce also leads to increased density and elastic moduli, and is thus also expected to lead to decreased vibration levels.

6. Effects of integrated elastomer layers

The effect of integrating an elastomer layer into the CLT panels was investigated, both for the lab-sized panels, as well as the five-layer panels previously analysed in Section 5. For both panel dimensions, elastomer thicknesses of 2 and 12 mm were utilised.

6.1. Lab-sized cross-laminated timber panels with elastomer layer

In Fig. 20(a), the computed accelerance FRFs for lab-sized double panels of spruce with 2 and 12 mm elastomers, as well as the reference case with no elastomer layer are shown. Additionally, the measured accelerance FRFs are shown in Fig. 20(b). Note that for the computations, the same material parameters were assigned to all spruce panels (cf. Table 5), and these are thus identical, and the influence of the elastomer layer can be evaluated. For the measured FRFs, however, different single panels with slightly varying material properties were used. Thus, the computed and measured results cannot be compared in detail. The measured FRFs are shown as a means of verifying the validity of the computed FRFs.

By adding the elastomer, the thickness of the panel is increased, which in turn leads to an increased stiffness. To verify that it is the elastomer that affects the response of the panel, models were developed in which the timber thickness was increased by 2 and 12 mm, by increasing the thickness of the various timber layers. For each lamination material, this resulted in slightly increased resonance frequencies, however the peaks were not affected significantly.

In Table 7, the RMS values of the accelerance FRFs for each panel normalised against the RMS value for spruce without an elastomer are shown. For each lamination material, the RMS level was reduced by adding an elastomer and the response decreased more with 12 mm layer compared to 2 mm layer thickness.

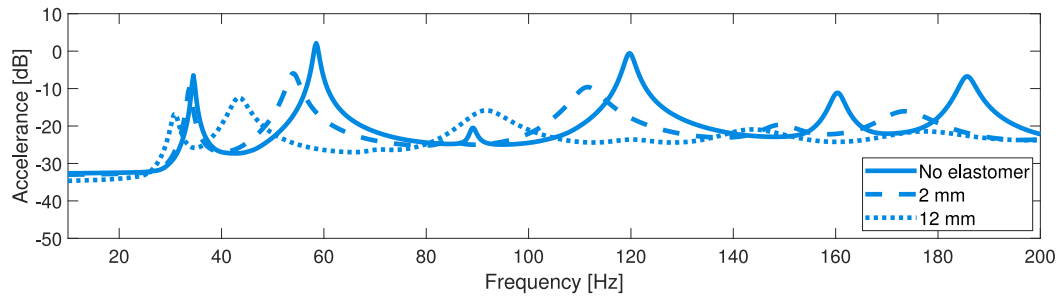

(a) Spruce, computed.

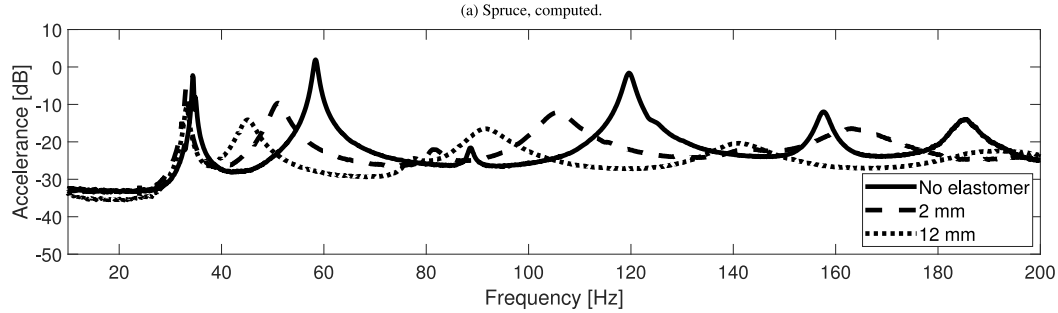

(b) Spruce, experimental.

Fig. 20. Spatially averaged accelerance FRFs showing the response of the lab-sized spruce panels with 2 and 12 mm elastomer layer, compared to without an elastomer layer.

Table 7
Reduction in accelerance RMS values for all lab-sized panels, normalised against spruce without an elastomer layer. The values are in dB and percent. The reductions in percent are calculated as $1 - a_{RMS}/a_{RMS,ref}$.

	Spruce		Birch		Compressed spruce	
	dB	%	dB	%	dB	%
2 mm	4.5	41	8.1	61	10.7	71
12 mm	8.4	62	11.0	72	12.5	76

6.2. Realistically sized cross-laminated timber panels with elastomer layer

In Fig. 21, spatially averaged FRFs are presented for spruce, birch and compressed spruce panels with 2 and 12 mm elastomer layer, compared to the panels without an elastomer layer. As for the lab-sized panels, the response is generally reduced by inserting the elastomer layer. Due to the decreased stiffness and higher mass, the resonance frequencies are also lowered.

In Table 8, the accelerance RMS values are presented, normalised against spruce without an elastomer layer. Comparing this table to Table 7, it can be observed that the reduction of accelerance RMS value is less for the five-layer panels than the lab-sized panels, which is reasonable, due to the elastomer layer occupying a smaller percentage of the total panel volume for the larger panel. Still, the same trends can be observed, with the reduction in response being larger the thicker the elastomer layer is, and the combination of changing lamination material and integrating the elastomer layer leads to the largest reductions of accelerance RMS values.

To quantify the results, the insertion loss was calculated for the investigated frequency range as $IL = L_{ref.} - L_{mod.}$, where L is the accelerance RMS level. The subscripts $ref.$ and $mod.$ denote the responses of the reference panel and the modified panels, respectively. A positive value indicates a reduction in response for the modified panel in comparison to the reference.

A summarisation of the calculated insertion losses for the five-layer panels are presented in Fig. 22. $L_{ref.}$ is the spruce panel with no elastomer. In the figure, “No ela.” represents the insertion loss for using birch or compressed spruce instead of spruce, while “2 mm” and “12 mm” represents the additional insertion loss gained from inserting an elastomer layer into the panels. It can be observed that, using dB, the reduction in response from changing the spruce to compressed spruce is approximately double the reduction of using birch. Also to be noted is that by integrating a 12 mm elastomer layer, the reduction is approximately doubled compared to integrating a 2 mm elastomer layer, for panels of each lamination materials.

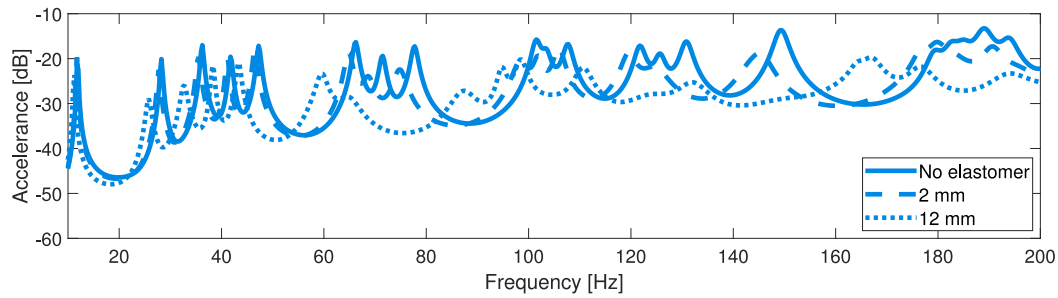

(a) Spruce.

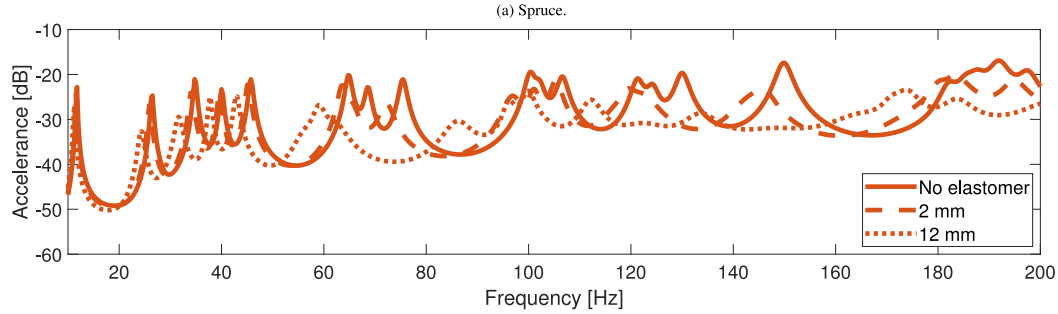

(b) Birch.

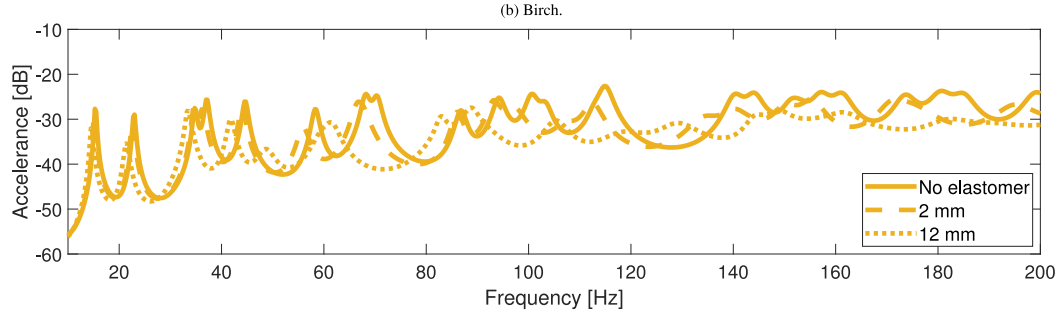

(c) Compressed spruce.

Fig. 21. Spatially averaged accelerance FRFs showing the response of the five-layer spruce, birch and compressed spruce panels with 2 and 12 mm elastomer layer, compared to without an elastomer layer.

Table 8
Reduction in accelerance RMS values for all five-layer panels, normalised against spruce without an elastomer layer. The values are in dB and percent. The reductions in percent are calculated as $1 - a_{RMS}/a_{RMS,ref}$.

	Spruce		Birch		Compressed spruce	
	dB	%	dB	%	dB	%
2 mm	2.0	21	5.6	48	8.8	64
12 mm	5.0	43	8.1	61	10.8	71

7. Concluding remarks

The study demonstrates the effect of using various lamination materials and an integrated elastomer layer on the vibration response of cross-laminated timber (CLT) panels through experimental and numerical investigations in the frequency range 10–200 Hz. A viscoelastic material model was developed for the elastomer layer based on experimental data. Finite element models of CLT panels made of spruce, birch and compressed spruce were calibrated to a series of experimentally obtained accelerance frequency

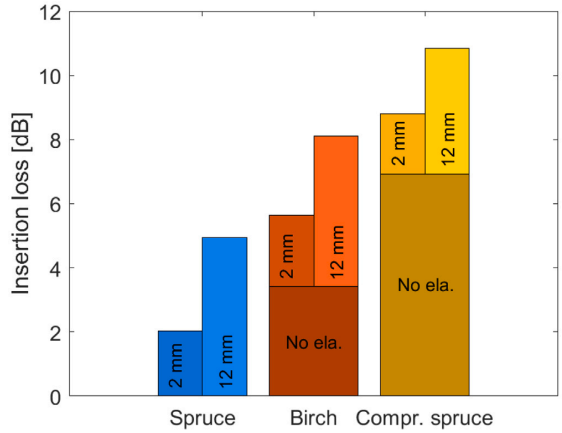

Fig. 22. Summarisation of insertion losses for the five-layer panels. The reference is the spruce panel without an elastomer.

response functions (FRFs). Additionally, the calibrated material properties were used to investigate how the vibration response is affected when exchanging the standard spruce for birch or compressed spruce, as well as for integrating an elastomer layer into the panel. This was evaluated both for lab-sized panels, and realistically sized five-layer panels. The main conclusions from this study are presented below.

- Frequency-independent elastic moduli and loss factors were calibrated for 22 separate single CLT panels; 16 spruce, 4 birch and 2 compressed spruce. It was found that the computed FRFs corresponded closely with the measured FRFs.
- By exchanging the typical spruce to birch or compressed spruce with higher density and stiffness, the accelerance RMS value can be reduced with 30% and 50%, respectively.
- An accurate frequency-dependent viscoelastic material model was developed for an elastomer layer, on the basis of experimental data. The model provides frequency-dependent stiffnesses and damping, and computed FRFs were found to correspond well with measured FRFs.
- By integrating an elastomer layer into a CLT panel, the vibration response can be reduced compared to a panel with no elastomer layer. With a 12 mm elastomer layer, the response can be reduced approximately 40% for spruce, birch and compressed spruce panels.
- The results indicate that a thicker elastomer layer leads to increasingly reduced vibration levels. For spruce, the increased reduction in accelerance RMS for a 12 mm elastomer layer compared to a 2 mm was approximately 30%. For birch and compressed spruce the reduction was 25% and 20%, respectively.

While this study adds valuable insights on the vibrational behaviour of CLT panels of spruce, birch and compressed spruce with integrated elastomer layers, it also identifies areas where further research would be beneficial. To strengthen the connection to the practical engineering application of CLT, the effect of various displacement boundary conditions on the vibration performance could be studied. In addition, realistic load scenarios could be studied. Furthermore, the vibrational behaviour of alternative configurations of CLT panels with integrated resilient layers could be evaluated.

CRediT authorship contribution statement

Annie Bohman: Writing – original draft, Visualization, Validation, Software, Methodology, Investigation, Formal analysis, Conceptualization. **Linus Andersson:** Writing – review & editing, Validation, Supervision, Formal analysis. **Kent Persson:** Writing – review & editing, Validation, Supervision, Investigation, Formal analysis. **Fredrik Ljunggren:** Writing – review & editing, Validation, Methodology, Investigation, Formal analysis, Conceptualization. **Peter Persson:** Writing – review & editing, Visualization, Validation, Supervision, Methodology, Funding acquisition, Formal analysis, Conceptualization.

Declaration of competing interest

The authors declare that they have no known competing financial interests or personal relationships that could have appeared to influence the work reported in this paper.

Acknowledgements

Formas – a Swedish Research Council for Sustainable Development, ÅForsk foundation, the Södra Foundation for Research, Development and Education, Vinnova – Sweden's Innovation Agency and Önnesjö foundation are gratefully acknowledged for their financial support.

Appendix A. Measured and computed frequency response functions for all single panels

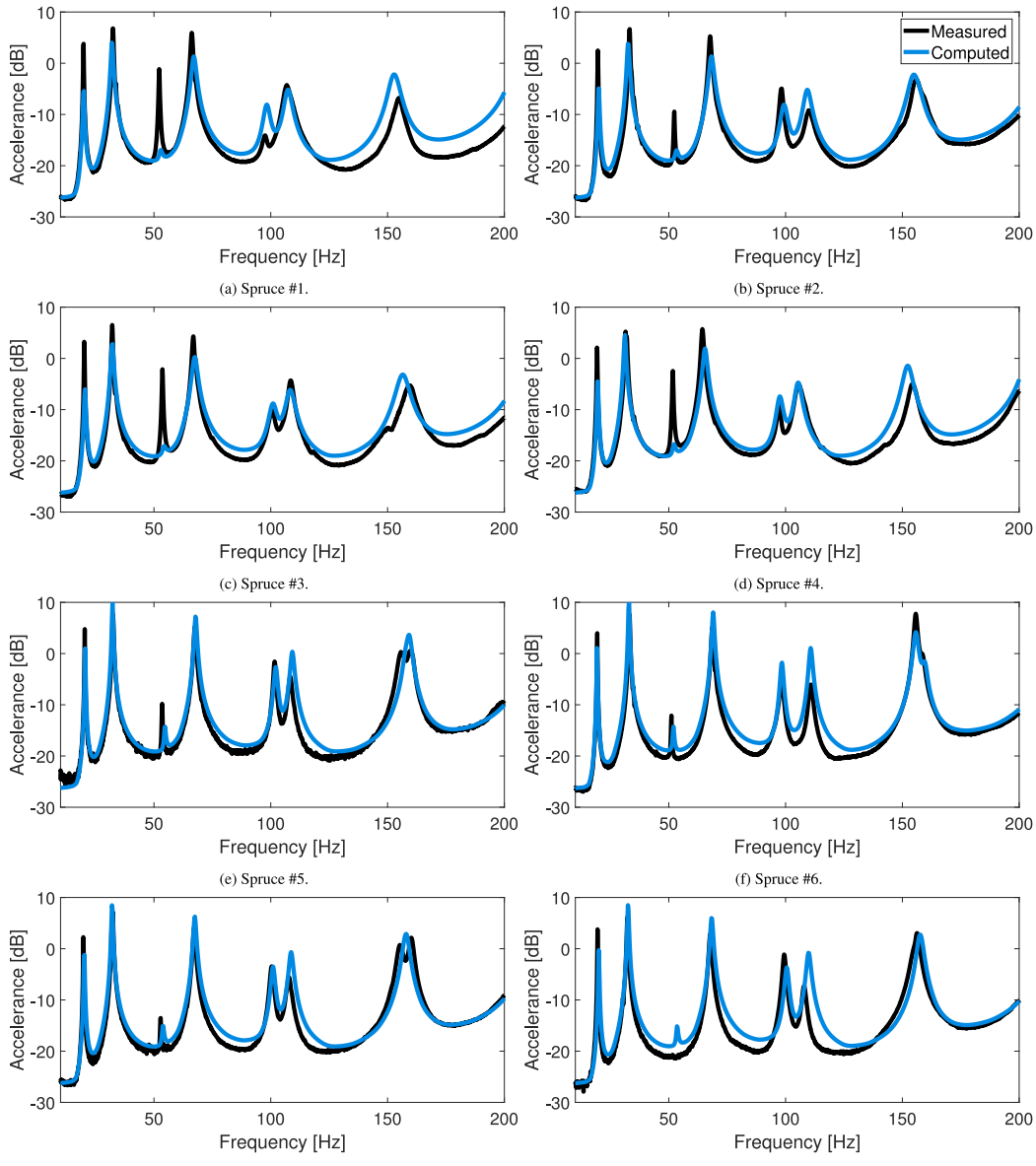

(a) Spruce #1.

(b) Spruce #2.

(c) Spruce #3.

(d) Spruce #4.

(e) Spruce #5.

(f) Spruce #6.

(g) Spruce #7.

(h) Spruce #8.

Fig. A.23. Measured (black) and computed (blue, red or yellow) spatially averaged accelerance FRFs for all single panels. The legend is valid for all subplots.

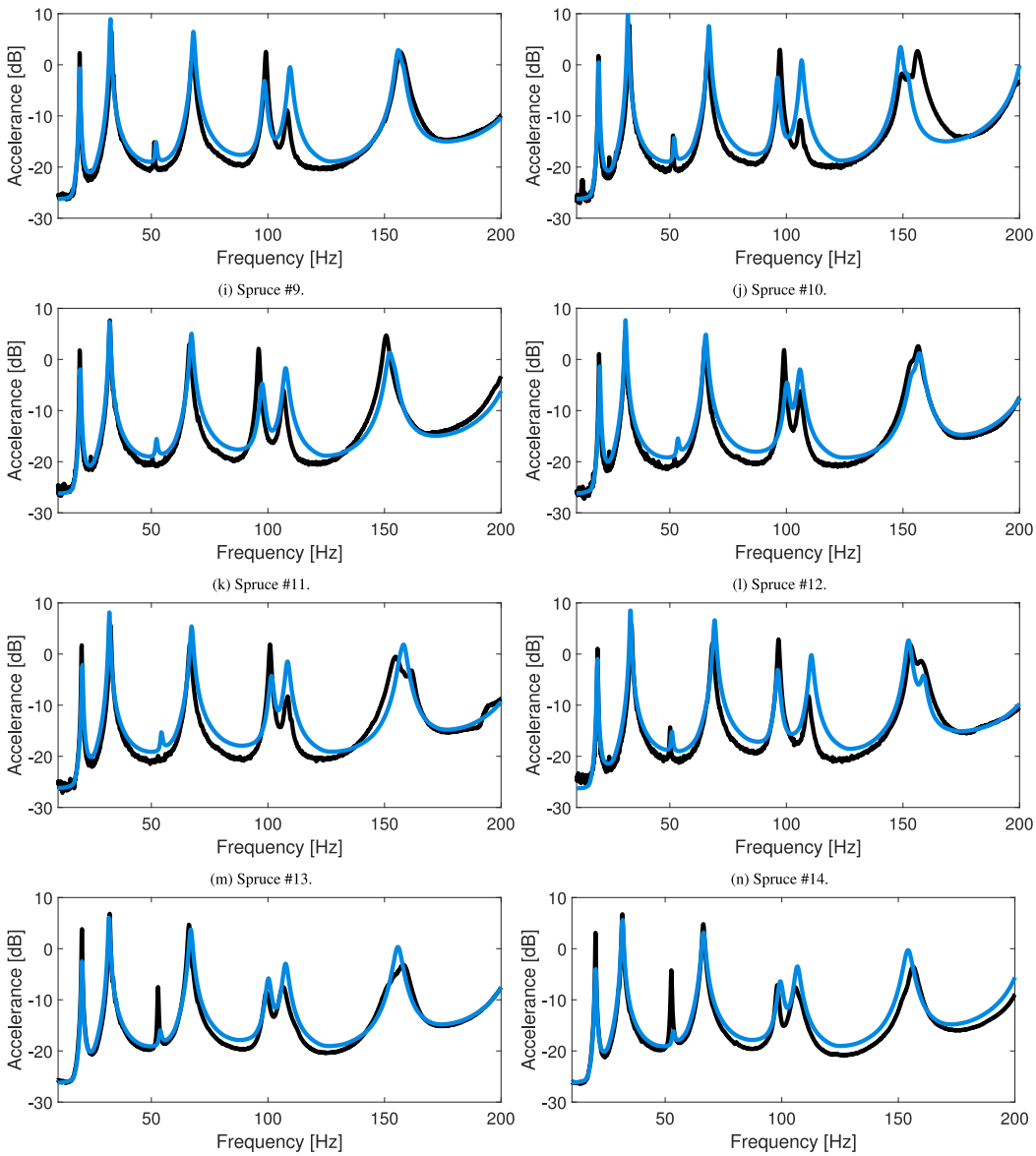

(i) Spruce #9.

(j) Spruce #10.

(k) Spruce #11.

(l) Spruce #12.

(m) Spruce #13.

(n) Spruce #14.

(o) Spruce #15.

(p) Spruce #16.

Fig. A.23. (*continued*).

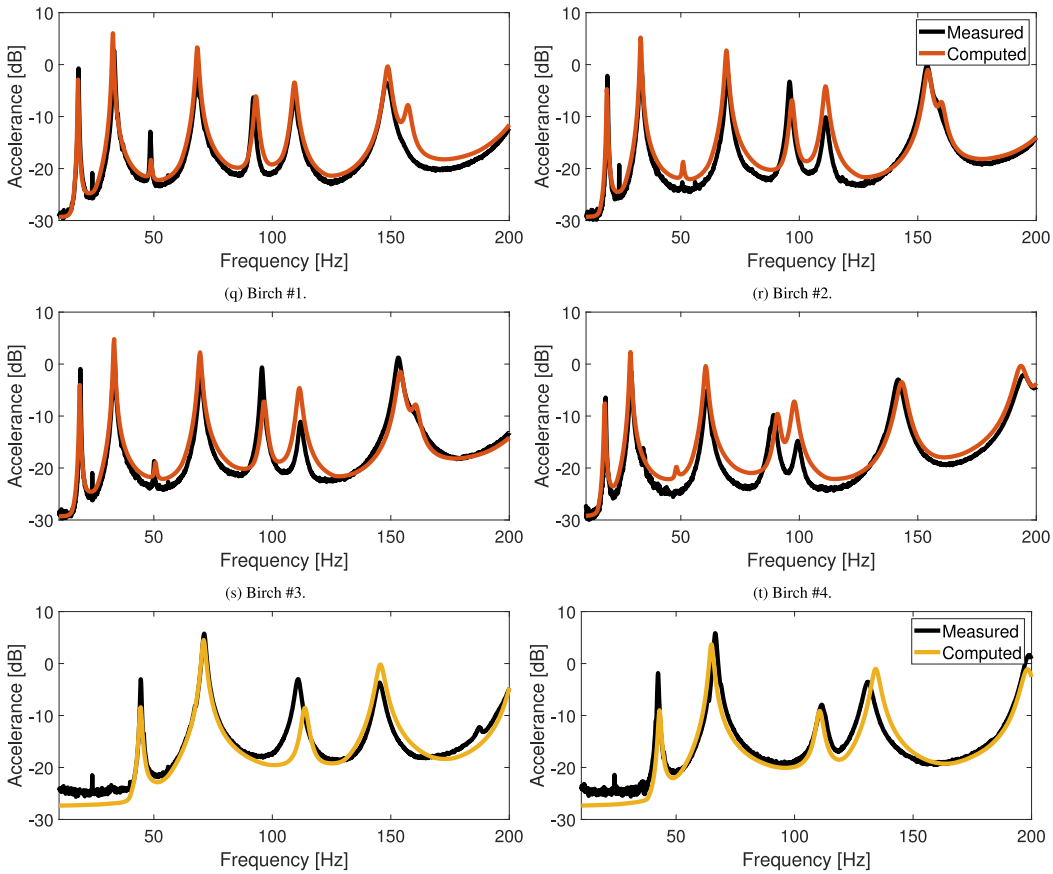

(q) Birch #1.

(r) Birch #2.

(s) Birch #3.

(t) Birch #4.

(u) Compressed spruce #1.

(v) Compressed spruce #2.

Fig. A.23. (*continued*).

Appendix B. Measured and computed mode shapes for a single panel

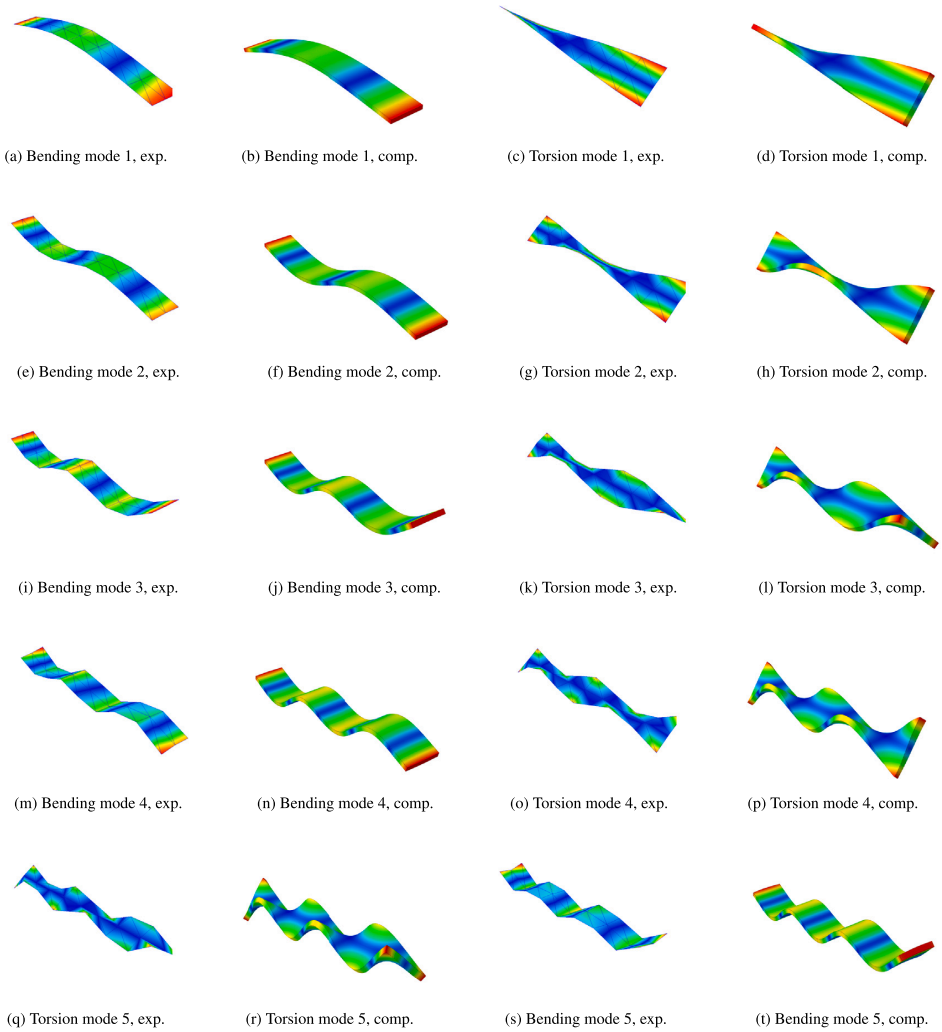

(a) Bending mode 1, exp. (b) Bending mode 1, comp. (c) Torsion mode 1, exp. (d) Torsion mode 1, comp.

(e) Bending mode 2, exp. (f) Bending mode 2, comp. (g) Torsion mode 2, exp. (h) Torsion mode 2, comp.

(i) Bending mode 3, exp. (j) Bending mode 3, comp. (k) Torsion mode 3, exp. (l) Torsion mode 3, comp.

(m) Bending mode 4, exp. (n) Bending mode 4, comp. (o) Torsion mode 4, exp. (p) Torsion mode 4, comp.

(q) Torsion mode 5, exp. (r) Torsion mode 5, comp. (s) Bending mode 5, exp. (t) Bending mode 5, comp.

Fig. B.24. Comparison of experimentally obtained mode shapes (exp.) and computed mode shapes (comp.).

Appendix C. Sensitivity analysis for single panels of birch and compressed spruce

Table C.9
Lower and upper limits, as well as reference values used for the sensitivity analysis for birch. The moduli are in MPa.

	E_L	E_R	E_T	G_{LR}	G_{LT}	G_{RT}
Lower limit	13 000	600	600	700	700	140
Upper limit	17 000	1 300	1 300	1 200	1 200	250
Reference	15 000	1 185	640	850	850	175

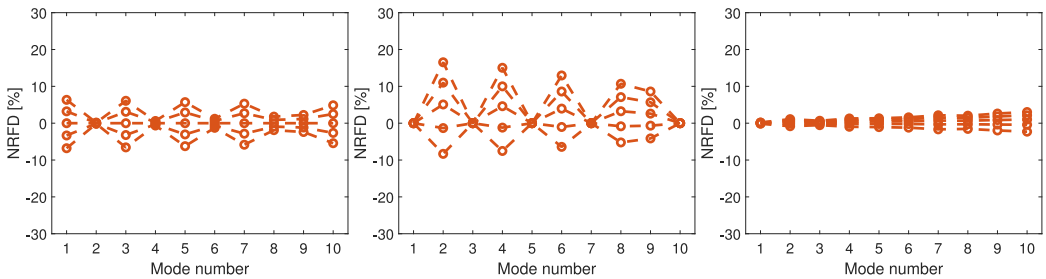

(a) E_L. (b) G_{LT}. (c) G_{RT}.

Fig. C.25. The effect of material parameters on the eigenfrequencies of birch CLT panels, showed for the five values used in the sensitivity analysis.

Table C.10
Lower and upper limits, as well as reference values used for the sensitivity analysis for compressed spruce. The moduli are in MPa.

	E_L	E_R	E_T	G_{LR}	G_{LT}	G_{RT}
Lower limit	11 000	400	400	800	800	50
Upper limit	25 000	1 000	1 000	2 000	2 000	130
Reference	20 200	679	679	1 267	1 267	90

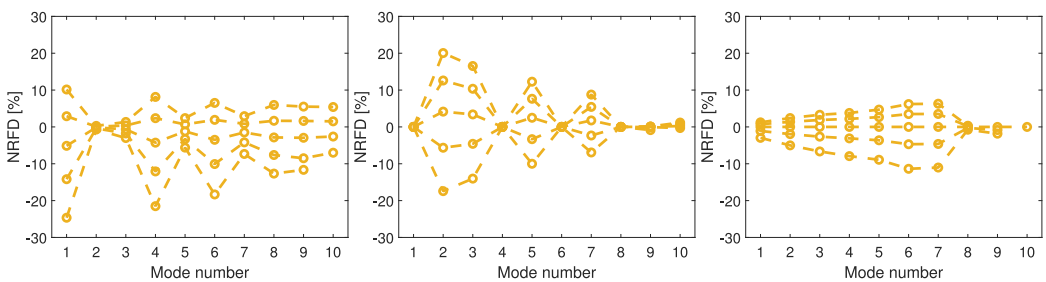

(a) E_L. (b) G_{LT}. (c) G_{RT}.

Fig. C.26. The effect of material parameters on the eigenfrequencies of compressed spruce CLT panels, showed for the five values used in the sensitivity analysis.

Data availability

Data will be made available on request.

References

[1] K. Bodlund, Alternative reference curves for evaluation of the impact sound insulation between dwellings, J. Sound Vib. 102 (3) (1985) 381–402, http://dx.doi.org/10.1016/S0022-460X(85)80149-8.

[2] B. Gibson, T. Nguyen, S. Sinaie, D. Heath, T. Ngo, The low frequency structure-borne sound problem in multi-storey timber buildings and potential of acoustic metamaterials: A review, Build. Environ. 224 (2022) 109531, http://dx.doi.org/10.1016/j.buildenv.2022.109531.

[3] J. Forssén, W. Kropp, J. Brunskog, S. Ljunggren, D. Bard, G. Sandberg, F. Ljunggren, A. Ågren, O. Hallström, H. Dybro, K. Larsson, K. Tillberg, K. Jarnerö, L.-G. Sjökvist, B. Östman, K. Hagberg, Å. Bolmsvik, A. Olsson, C.-G. Ekstrand, M. Johansson, Acoustics in Wooden Buildings: State of the Art 2008, SP Technical Research Institute of Sweden, 2008.

[4] R. Öqvist, F. Ljunggren, R. Johnsson, Walking sound annoyance vs. impact sound insulation from 20 Hz, Appl. Acoust. 135 (2018) 1–7, http://dx.doi.org/10.1016/j.apacoust.2018.01.019.

[5] F. Ljunggren, C. Simmons, Correlation between sound insulation and occupants' perception – Proposal of alternative single number rating of impact sound, Part III, Appl. Acoust. 197 (2022) 108955, http://dx.doi.org/10.1016/j.apacoust.2022.108955.

[6] F. Ljunggren, C. Simmons, K. Hagberg, Correlation between sound insulation and occupants' perception – Proposal of alternative single number rating of impact sound, Appl. Acoust. 85 (2014) 57–68, http://dx.doi.org/10.1016/j.apacoust.2014.04.003.

[7] G. Schickhofer, Starrer und nachgiebiger Verbund bei geschichteten, flächenhaften Holzstrukturen (Ph.D. thesis), TU Graz, Austria, 1994.

[8] E. Ussher, A. Aloisio, D.P. Pasca, S. Lysebo Hansen, R. Tomasi, Effect of partition walls on the vibration serviceability of cross-laminated timber floors, J. Build. Eng. 95 (2024) 110001, http://dx.doi.org/10.1016/j.jobe.2024.110001.

[9] S. Schoenwald, B. Zeitler, I. Sabourin, F. King, Sound insulation performance of cross laminated timber building systems, in: 42nd International Congress and Exposition on Noise Control Engineering: Inter-Noise 2013 (18 September 2013), 2013.

[10] S. Moons, R. Lanoye, E.P. Reynders, Prediction of flanking sound transmission through cross-laminated timber junctions with resilient interlayers, Appl. Acoust. 228 (2025) 110317, http://dx.doi.org/10.1016/j.apacoust.2024.110317.

[11] M. Caniato, F. Bettarello, P. Fausti, A. Ferluga, L. Marsich, C. Schmid, Impact sound of timber floors in sustainable buildings, Build. Environ. 120 (2017) 110–122, http://dx.doi.org/10.1016/j.buildenv.2017.05.015.

[12] P. Sipari, Sound insulation of multi-storey houses — A summary of finnish impact sound insulation results, Build. Acoust. 7 (1) (2000) 15–30, http://dx.doi.org/10.1260/1351010001501471.

[13] D. Yeoh, M. Fragiacomo, M. De Franceschi, K.H. Boon, State of the art on timber-concrete composite structures: Literature review, J. Struct. Eng. 137 (10) (2011) 1085–1095, http://dx.doi.org/10.1061/(ASCE)ST.1943-541X.0000353.

[14] P. Persson, O. Flodén, H. Danielsson, A. Peplow, L. Vabbersgaard Andersen, Improved low-frequency performance of cross-laminated timber floor panels by informed material selection, Appl. Acoust. 179 (2021) 108017, http://dx.doi.org/10.1016/j.apacoust.2021.108017.

[15] J. Jonasson, P. Persson, H. Danielsson, Mitigating footfall-induced vibrations in cross-laminated timber floor-panels by using beech or birch, J. Build. Eng. 86 (2024) 108751, http://dx.doi.org/10.1016/j.jobe.2024.108751.

[16] T. Ehrhart, R. Brandner, Rolling shear: Test configurations and properties of some European soft- and hardwood species, Eng. Struct. 172 (2018) 554–572, http://dx.doi.org/10.1016/j.engstruct.2018.05.118.

[17] T.Y. Feng, L.K. Chiang, Effects of densification on low-density plantation species for cross-laminated timber, in: AIP Conference Proceedings, 2020, 020001.

[18] M. Schwarzkopf, M. Burnard, G. Martínez Pastur, L. Monelos, A. Kutnar, Performance of three-layer composites with densified surface layers of Nothofagus pumilio and N. antarctica from Southern Patagonian forests, Wood Mater. Sci. Eng. 13 (5) (2018) 305–315, http://dx.doi.org/10.1080/17480272.2017.1366945.

[19] J.P. Cabral, B. Kafle, M. Subhani, J. Reiner, M. Ashraf, Densification of timber: a review on the process, material properties and application, J. Wood Sci. 68 (2022) http://dx.doi.org/10.1186/s10086-022-02028-3.

[20] D. Sandberg, A. Kutnar, G. Mantanis, Wood modification technologies – a review, IForest - Biogeosciences For. 10 (6) (2017) 895–908, http://dx.doi.org/10.3832/ifor2380-010.

[21] A. Scharf, B. Neyses, D. Sandberg, Continuous densification of wood with a belt press: the process and properties of the surface-densified wood, Wood Mater. Sci. Eng. 18 (4) (2023) 1573–1586, http://dx.doi.org/10.1080/17480272.2023.2216660.

[22] P. Persson, O. Flodén, Effect of material parameter variability on vibroacoustic response in wood floors, Appl. Acoust. 146 (2019) 38–49, http://dx.doi.org/10.1016/j.apacoust.2018.10.034.

[23] K.B. Dahl, Mechanical Properties of Clear Wood From Norway Spruce (Ph.D. thesis), Norwegian University of Science and Technology, 2009.

[24] M. Milojević, V. Racic, M. Nefovska-Danilović, Uncertainty analysis of CLT floor vibrations due to inherent variability in structural properties, J. Build. Eng. 113 (2025) 113725, http://dx.doi.org/10.1016/j.jobe.2025.113725.

[25] E. Ussher, K. Arjomandi, J. Weckendorf, I. Smith, Prediction of motion responses of cross-laminated-timber slabs, Structures 11 (2017) 49–61, http://dx.doi.org/10.1016/j.istruc.2017.04.007.

[26] D. Casagrande, I. Giongo, F. Pederzolli, A. Franciosi, M. Piazza, Analytical, numerical and experimental assessment of vibration performance in timber floors, Eng. Struct. 168 (2018) 748–758, http://dx.doi.org/10.1016/j.engstruct.2018.05.020.

[27] Å. Bolmsvik, A. Linderholt, Damping elastomers for wooden constructions – Dynamic properties, Wood Mater. Sci. Eng. 10 (3) (2015) 245–255, http://dx.doi.org/10.1080/17480272.2015.1046920.

[28] M. Salvalaggio, F. Lorenzoni, M.R. Valluzzi, Impact of sound-insulated joints in the dynamic behavior of Cross-Laminated Timber structures, J. Build. Eng. 91 (2024) 109525, http://dx.doi.org/10.1016/j.jobe.2024.109525.

[29] Å. Bolmsvik, A. Brandt, Damping assessment of light wooden assembly with and without damping material, Eng. Struct. 49 (2013) 434–447, http://dx.doi.org/10.1016/j.engstruct.2012.11.026.

[30] J. Negreira, P.-E. Austrell, O. Flodén, D. Bard, Characterisation of an elastomer for noise and vibration insulation in lightweight timber buildings, Build. Acoust. 21 (4) (2014) 251–276, http://dx.doi.org/10.1260/1351-010X.21.4.251.

[31] A. Paolini, S. Kollmannsberger, C. Winter, M. Buchschmid, G. Müller, A. Rabold, S. Mecking, U. Schanda, E. Rank, A high-order finite element model for vibration analysis of cross-laminated timber assemblies, Build. Acoust. 24 (3) (2017) 135–158, http://dx.doi.org/10.1177/1351010X17727126.

[32] F. Ljunggren, Innovative solutions to improved sound insulation of CLT floors, Dev. the Built Environ. 13 (2023) 100117, http://dx.doi.org/10.1016/j.dibe.2022.100117.

[33] Swedac acoustic, Sweden, 2024.

[34] Hottinger Brüel & Kjær BK Connect, 2022.

[35] A. Fasana, Modal parameters estimation in the Z-domain, Mech. Syst. Signal Process. 21 (1) (2009) 217–225, http://dx.doi.org/10.1016/j.ymssp.2008.03.015.

[36] K.-J. Bathe, Finite Element Procedures, second ed., Prentice hall, New Jersey, 2014.
[37] Dassault Systèmes SIMULIA, Abaqus, 2023.
[38] J. Paroissien, M. Oudjene, P. Lardeur, Verification and validation of finite element models for laminated timber structures using solid, solid-beam and solid-shell approaches, Compos. Struct. 345 (2024) 118083, http://dx.doi.org/10.1016/j.compstruct.2024.118083.
[39] R.R. Craig, A.J. Kurdila, Fundamentals of Structural Dynamics, second ed., John Wiley & Sons, New Jersey, 2006.
[40] M. Géradin, D.J. Rixen, Mechanical Vibrations: Theory and Application to Structural Dynamics, third ed., John Wiley & Sons, New Jersey, 2015.
[41] O. Perret, A. Lebée, C. Douthe, K. Sab, Equivalent stiffness of timber used in CLT: closed-form estimates and numerical validation, Eur. J. Wood Wood Prod. 77 (2019) 367–379, http://dx.doi.org/10.1007/s00107-019-01395-x.
[42] EN 338, Structural timber – strength classes, 2016, URL https://www.sis.se/api/document/get/8019871.
[43] R.J. Allemang, D.L. Brown, A correlation coefficient for modal vector analysis, in: Proceedings of the 1st International Modal Analysis Conference (IMAC I), 1982, pp. 110–116.
[44] A. Antoniou, W.S. Lu, Practical Optimization: Algorithms and Engineering Applications, Springer, New York, 2007.
[45] Swedac acoustic, data sheet of VS-10 (Swedish), 2024.
[46] B. Bartolucci, A. De Rosa, C. Bertolin, F. Berto, F. Penta, A.M. Siani, Mechanical properties of the most common European woods: a literature review, Frat. Ed IntegritÀ Strutt. 54 (2020) 249–274, http://dx.doi.org/10.3221/IGF-ESIS.54.18.
[47] G. Jeitler, M. Augustin, G. Schickhofer, Mechanical properties of glued laminated timber and cross laminated timber produced with the wood species birch, in: WCTE 2016 - World Conference on Timber Engineering, 2016.
[48] H. Holmberg, D. Sandberg, Structure and Properties of Scandinavian Timber, HoS Grenarna HB, Stockholm, 1997.
[49] T. Ehrhart, R. Brandner, G. Schickhofer, A. Frangi, Rolling shear properties of some European timber species with focus on Cross Laminated Timber (CLT): Test configuration and parameter study, in: International Network on Timber Engineering Research: Proceedings of Meeting 48, 2015, pp. 61–76.
[50] H. Yoshihara, S. Tsunematsu, Bending and shear properties of compressed Sitka spruce, Wood Sci. Technol. 41 (2007) 117–131, http://dx.doi.org/10.1007/s00226-006-0091-8.